Evolution of the spin-orbit splitting from ^{16}O to ^{22}O and the role of tensor force

Antoine Barrière, Olivier Sorlin, Nikhil Mozumdar, and the R^{3}B Collaboration

GDR Resanet 2025

IJCLab Irène Joliot-Curie Laboratoire de Physique des 2 Infinis

GANIL R3B

Shell evolution and ISM

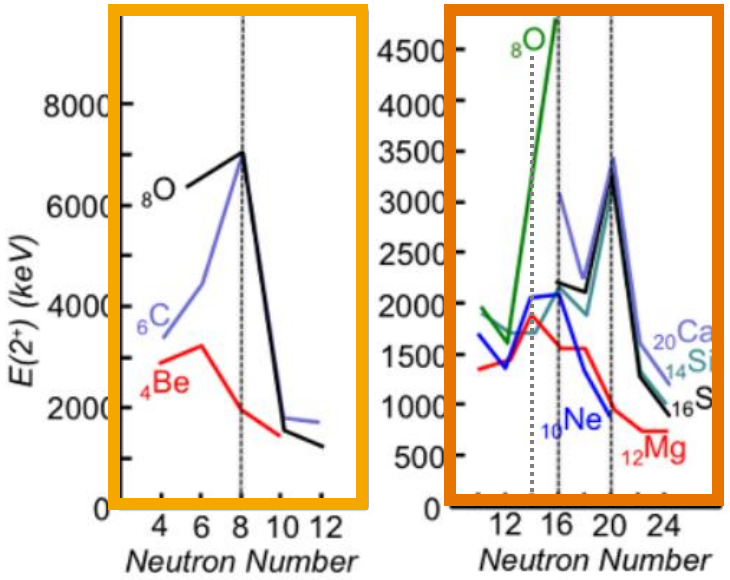

O. Sorlin. EPJ Web of Conferences (2014)

As gaps disappear, others appear !

Sudden breakdown of several shell closures:
residual interaction beyond the IPM model

⇨ **Interacting Shell Model (ISM)**

$$H = H_0 + H_{res} = H_0 + H_m + H_M$$

Mean field

Central
Spin-orbit
Tensor

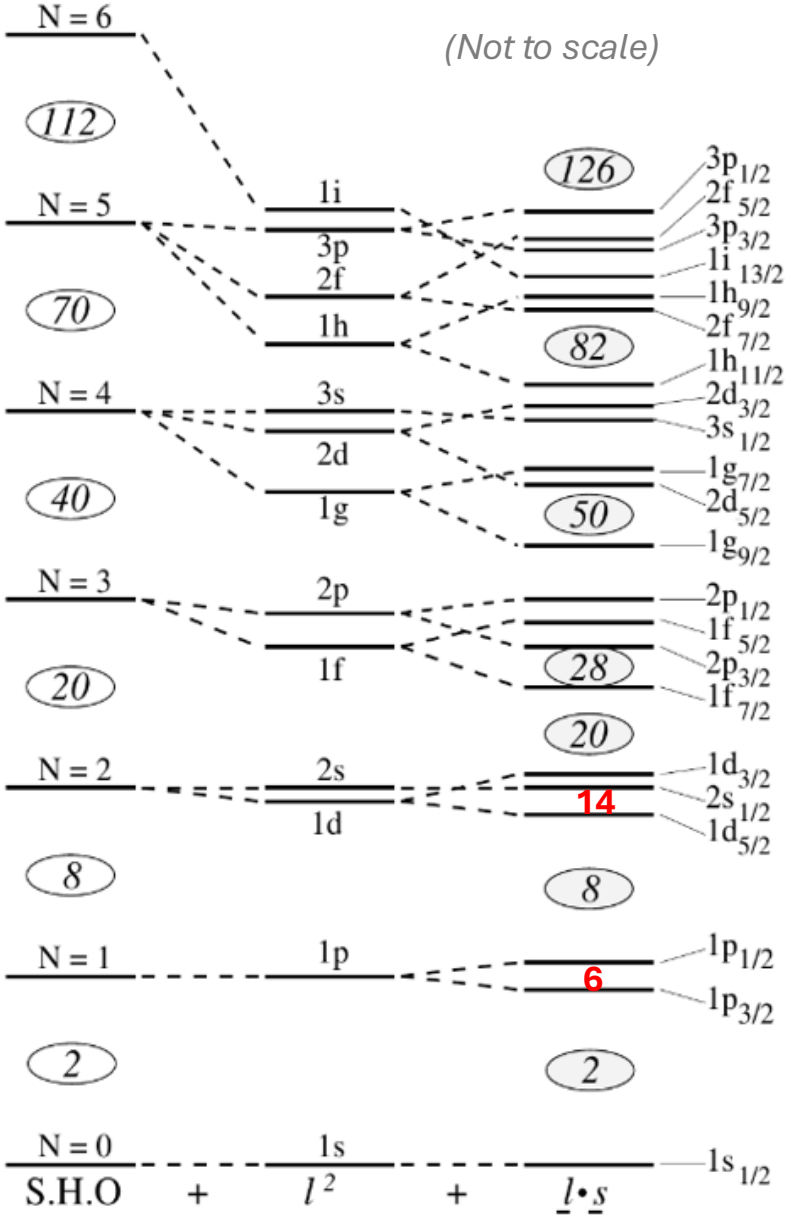

Shell evolution and ISM

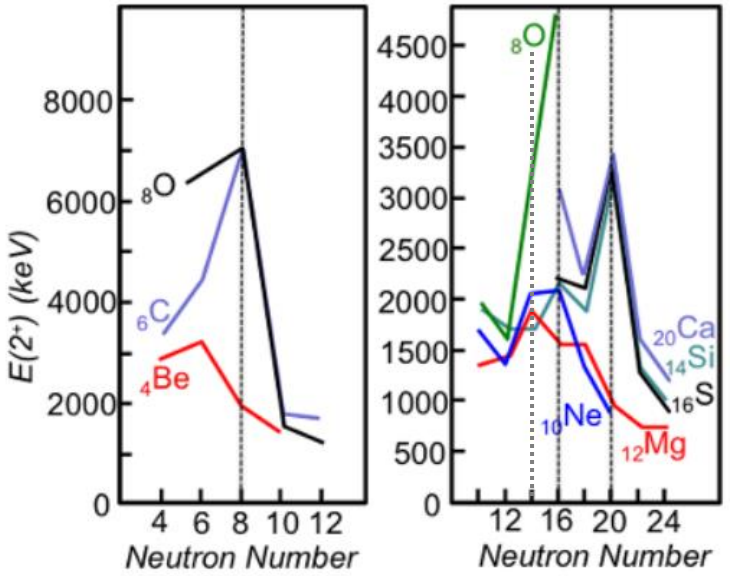

O. Sorlin. EPJ Web of Conferences (2014)

Sudden breakdown of several shell closures:
residual interaction beyond the IPM model

⇨ **Interacting Shell Model (ISM)**

$$H = H_0 + H_{res} = H_0 + H_m + H_M$$

Central
Spin-orbit
Tensor

Except if *l* or *l'* = 0

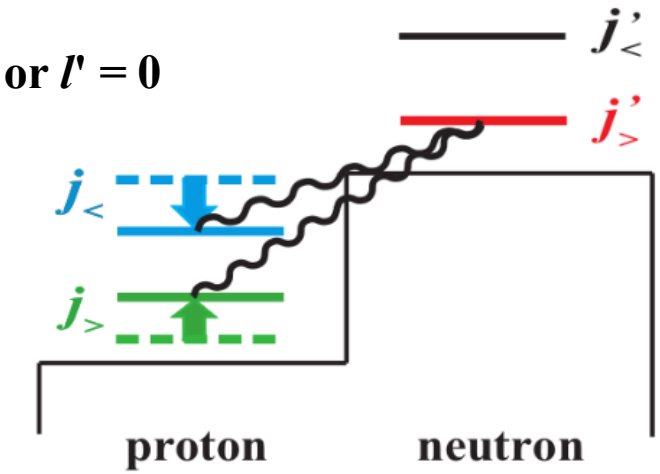

T.Otsuka, PRL (2005)

Attractive between orbitals with the **opposite spin projection**
Repulsive between orbitals with the **same spin projection**

This interaction can also **reduce** or **increase** the **SO splitting**.
It plays an important role in the breakdown of several shell closures

Shell evolution and ISM

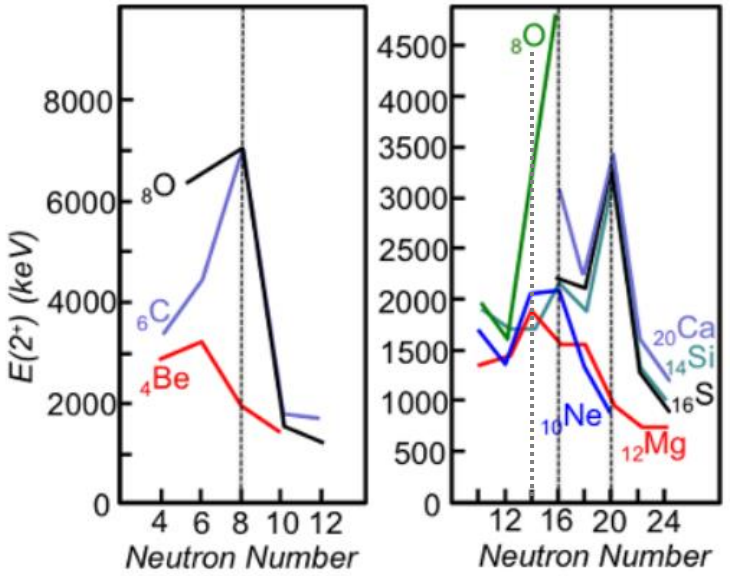

O. Sorlin. EPJ Web of Conferences (2014)

Sudden breakdown of several shell closures:
residual interaction beyond the IPM model

⇨ **Interacting Shell Model (ISM)**

$$H = H_0 + H_{res} = H_0 + H_m + H_M$$

Central
Spin-orbit
Tensor

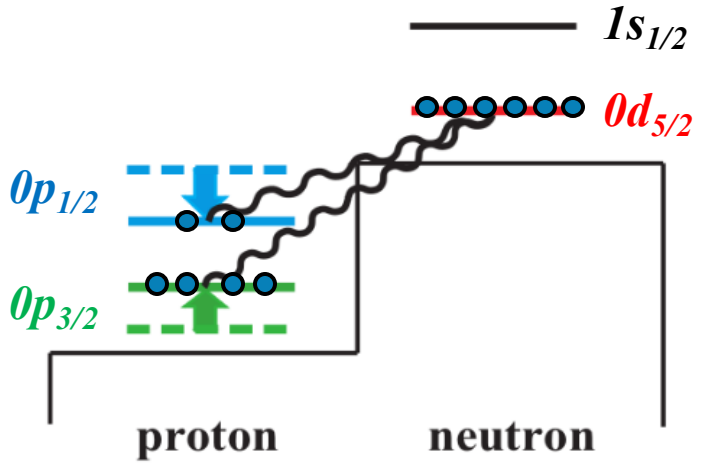

T.Otsuka, PRL (2005)

Attractive between π($0p_{1/2}$) and ν($0d_{5/2}$)
Repulsive between π($0p_{3/2}$) and ν($0d_{5/2}$)

This interaction should **reduce** the ***Z=6* SO splitting**, when the **ν($0d_{5/2}$) is filled** between ^{16}O and ^{22}O.

Filling of the *sd*-shell in O chain

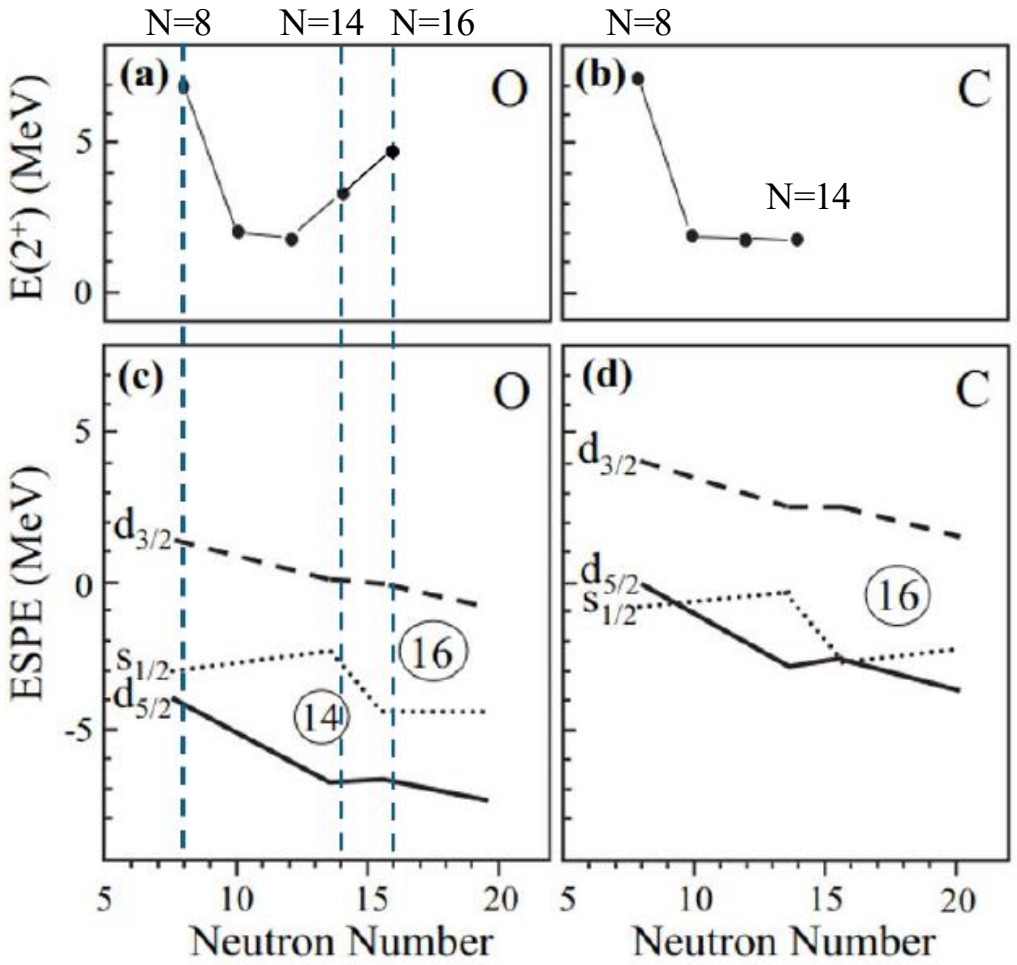

M. Stanoiu et al. Phys. Rev. C **78** (2008)

The occupancy of the *sd*-shell in ^{16}O is less than 10% , mostly in the $0d_{5/2}$.

J. L. Snelgrove and E. Kashy , Phys. Rev. **187** (1969)

While the $1s_{1/2}$ and $0d_{5/2}$ are almost degenerate in the C chain, a gap at ***N=14*** **is created in the O chain** at ^{22}O, contrary to ^{20}C.

Magic number *N=14*

Spectroscopic Factor : $\mathbf{SF = \sigma_{exp}/\sigma_{s.p.,th}}$

Neutron occupancy in the orbital *i* : **SF(*i*) / ΣSF**

^{22}O(*p*,*pn*)^{21}O

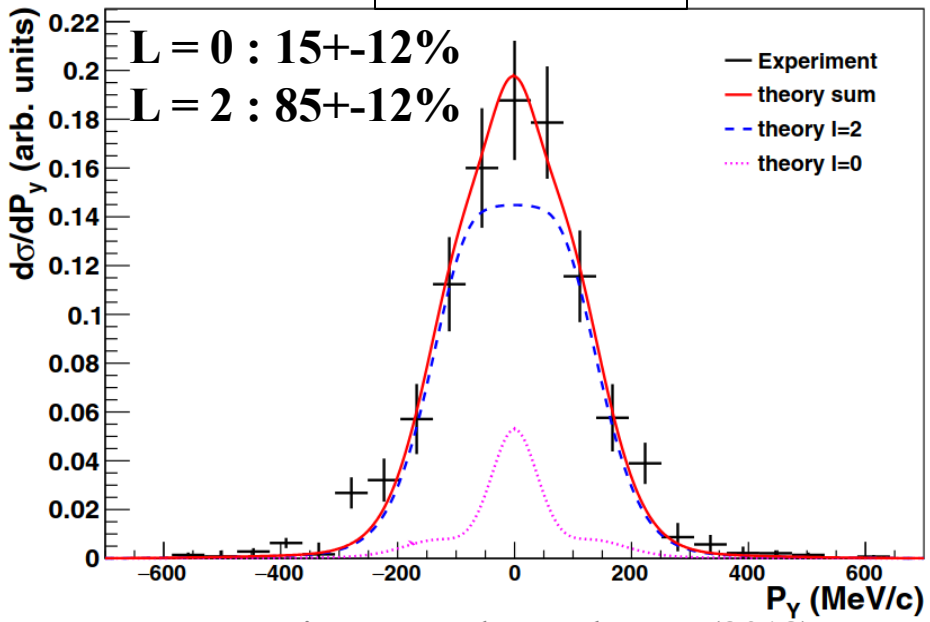

P. Diaz Fernandez et al, PRC (2018)

1σ range : 3 - 27 %

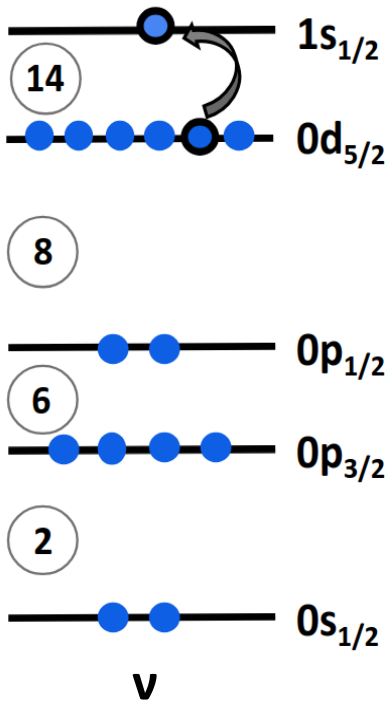

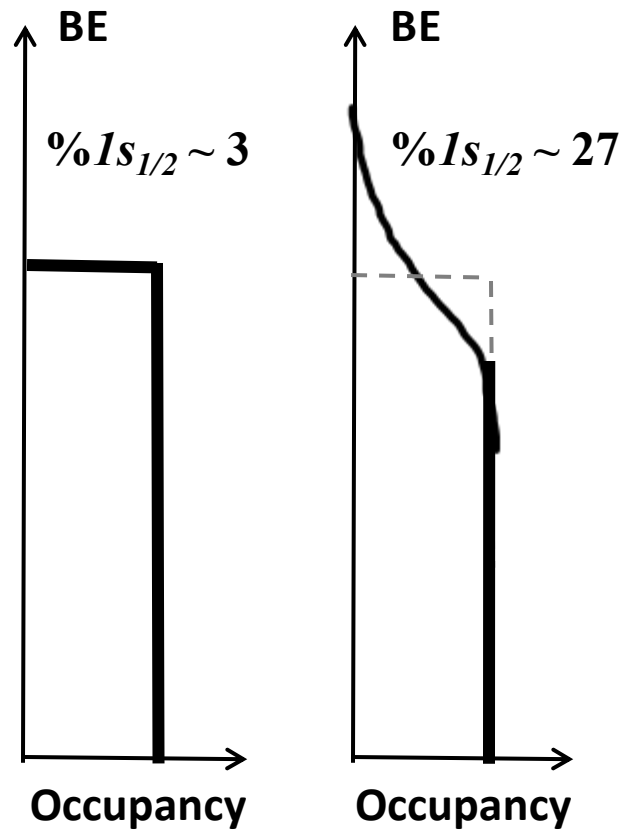

Probing the **Fermi surface** is also crucial for characterizing the **nuclei magicity**

These results are not precise enough to rule out correlations across the *N=14* gap.

Need for new measurement(s)

Evolution of the SO splitting

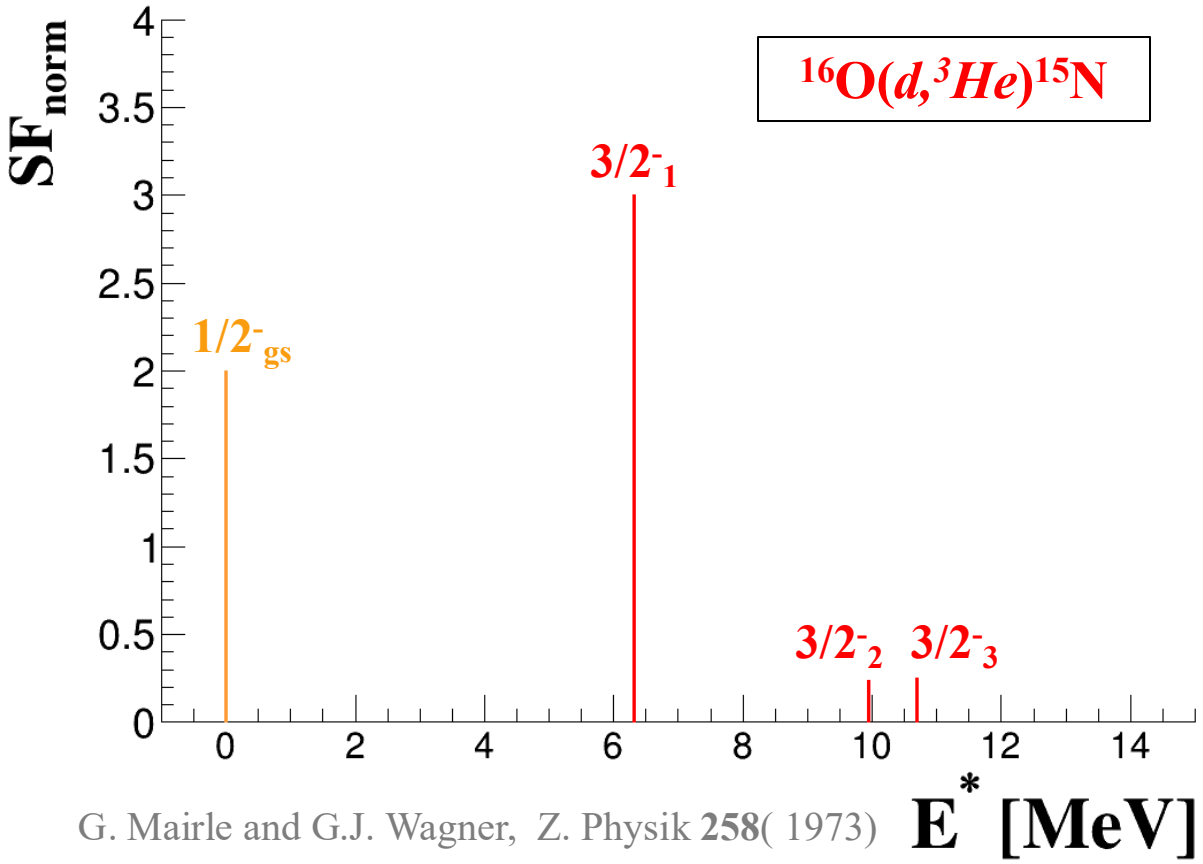

G. Mairle and G.J. Wagner, Z. Physik **258**(1973)

Measurement of most of the strength of the **1/2**$^-$ and **3/2**$^-$ hole states in ^{16}O

Evolution of the SO splitting

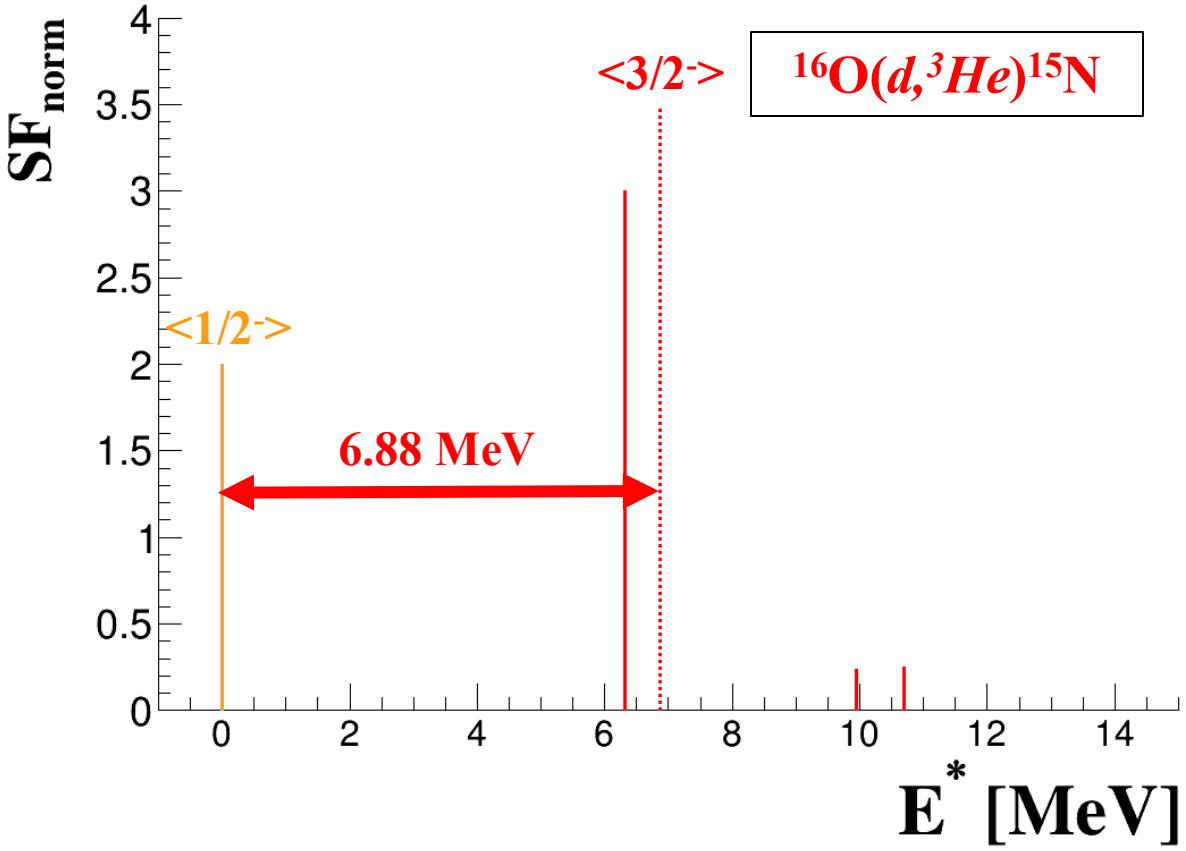

Energy centroid = $\Sigma(SF \cdot E^*) / \Sigma SF$

SO gap : difference between the centroids of SO partners

It will be interesting to determine it in ^{22}O

SO gap measured mostly in the stable nuclei or magic nuclei lying near the valley of stability:

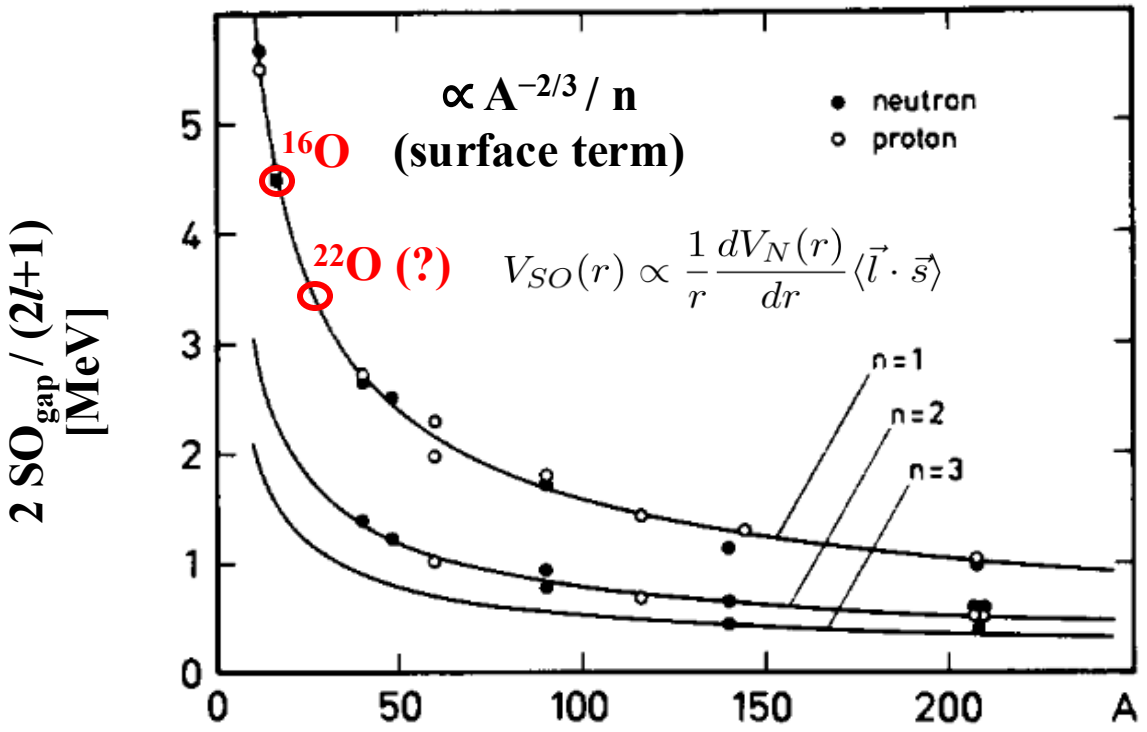

G. Mairle, PLB (1993)

The SO splitting decreases according to $A^{-2/3}$, which agrees with the surface-dependance of the SO interaction.

R³B-setup for the s509 experiment

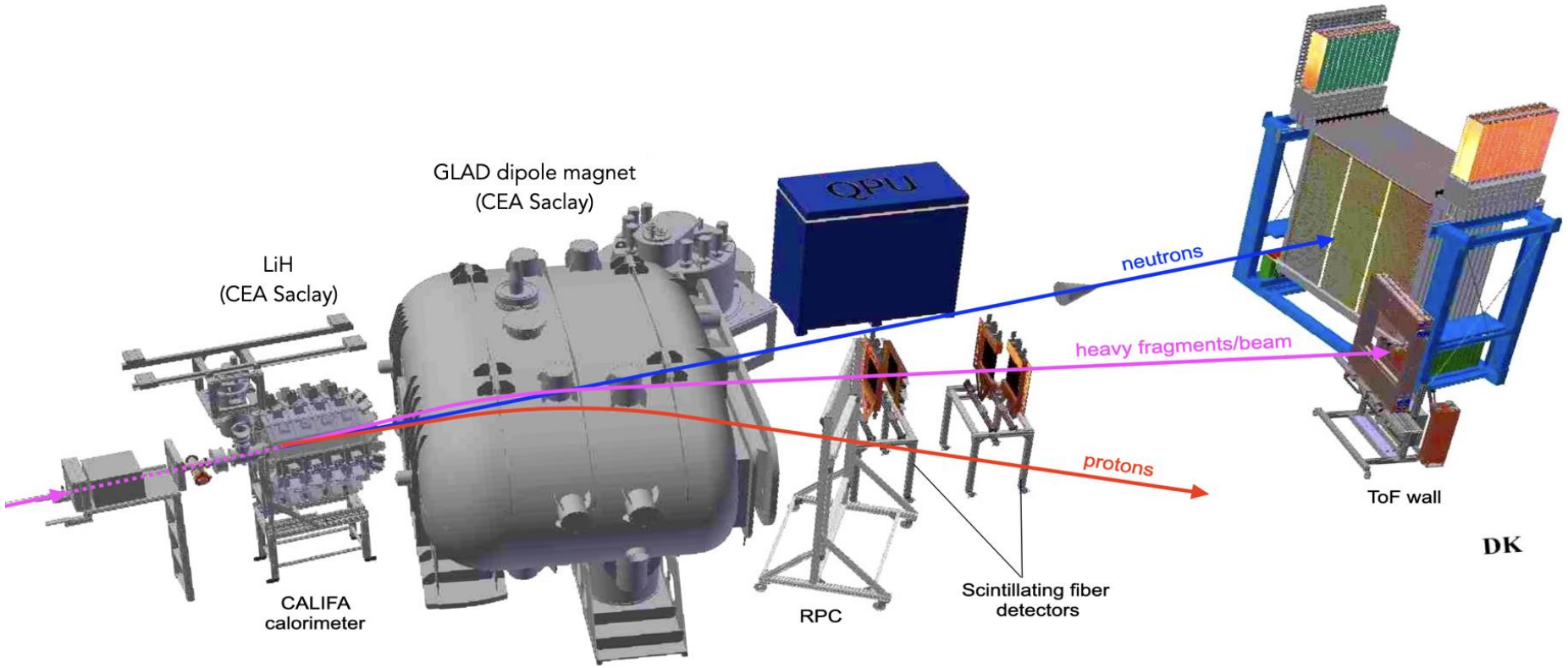

Radioactive cocktail beams

Cocktail beams from the FRagment Separator with E_{beam} ~ 550MeV/A

Cave C at the end of the R^3B line

2 beam settings: optimized for A/Z ~ 2.75 and A/Z ~ 3

About 140 pps for ^{22}O , 10% of the cocktail beam

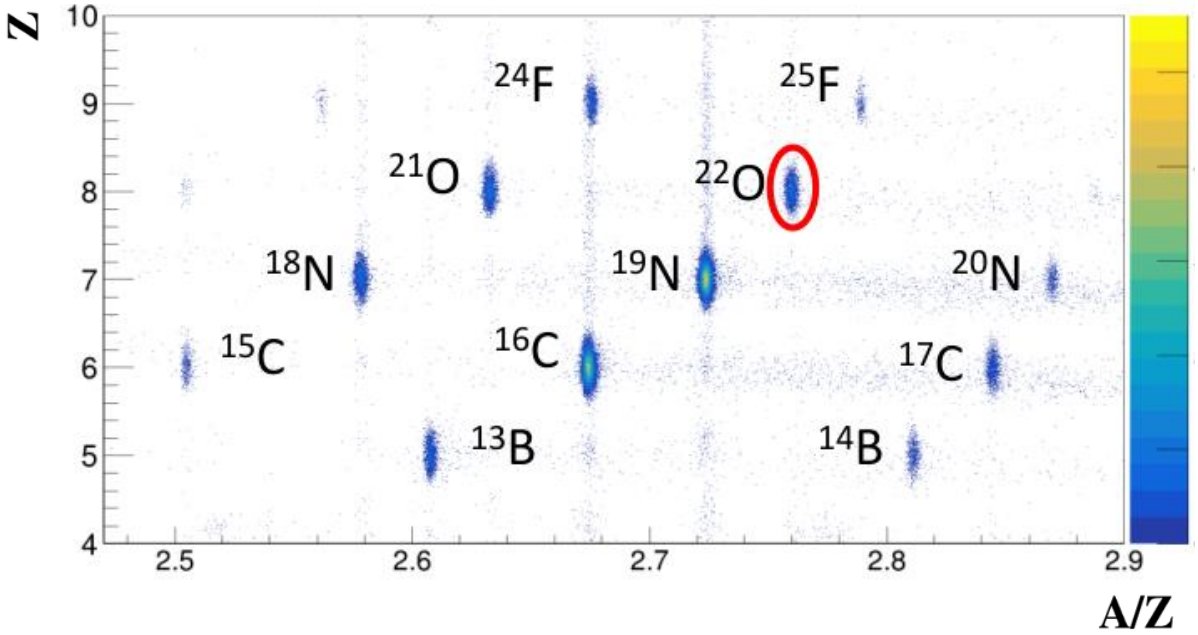

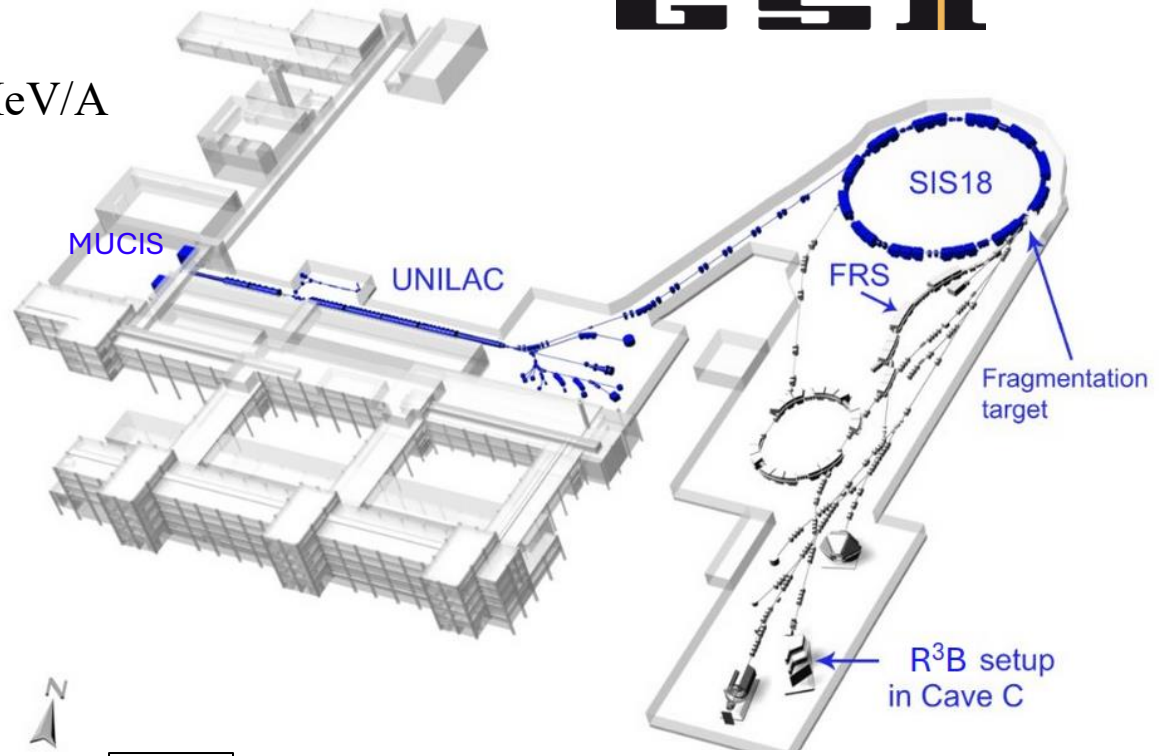

FRS

$B\rho$ - ΔE - $B\rho$

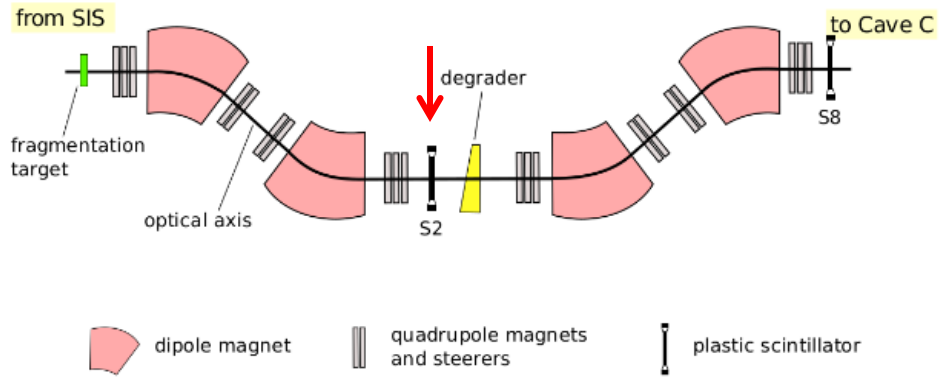

Incoming nuclei identification

QFS reaction e.g. (*p,pn*) and (*p,2p*) in LiH_2

Complete measurement in inverse kinematics (E,**p**):

- **Incoming nuclei**;

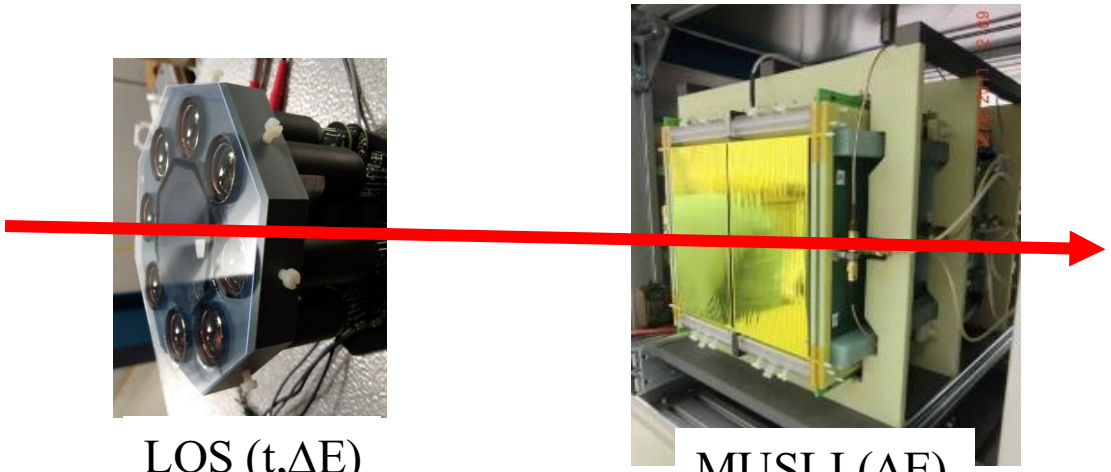

LOS (t,ΔE)

MUSLI (ΔE)

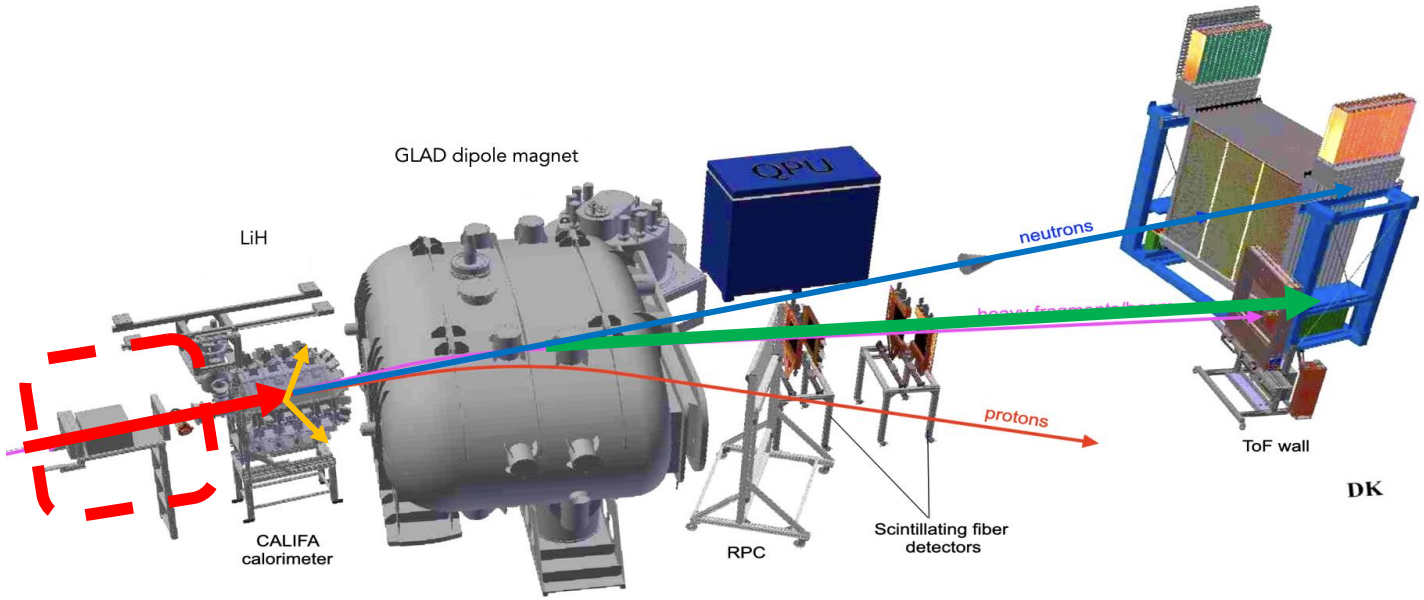

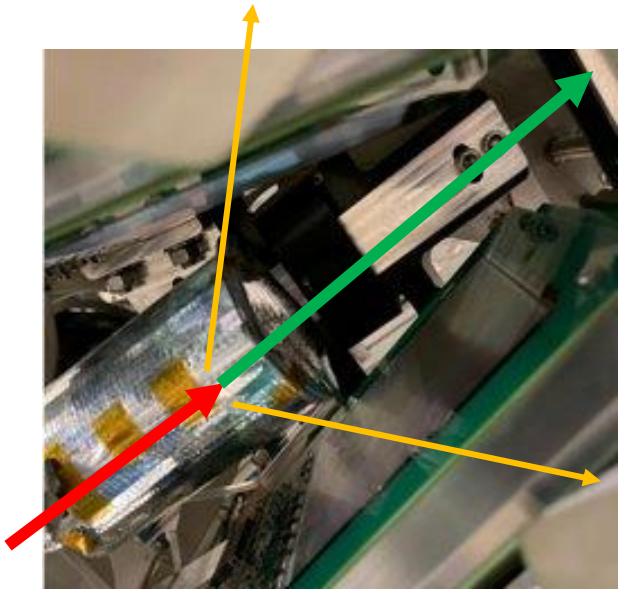

5cm thick LiH_2 target

Califa calorimeter and γ-rays detection

QFS reaction e.g. (*p,pn*) and (*p,2p*) in LiH_2

Complete measurement in inverse kinematics (E,**p**):

- **Incoming nuclei**;
- **γ-rays and light particles emitted from the target**;

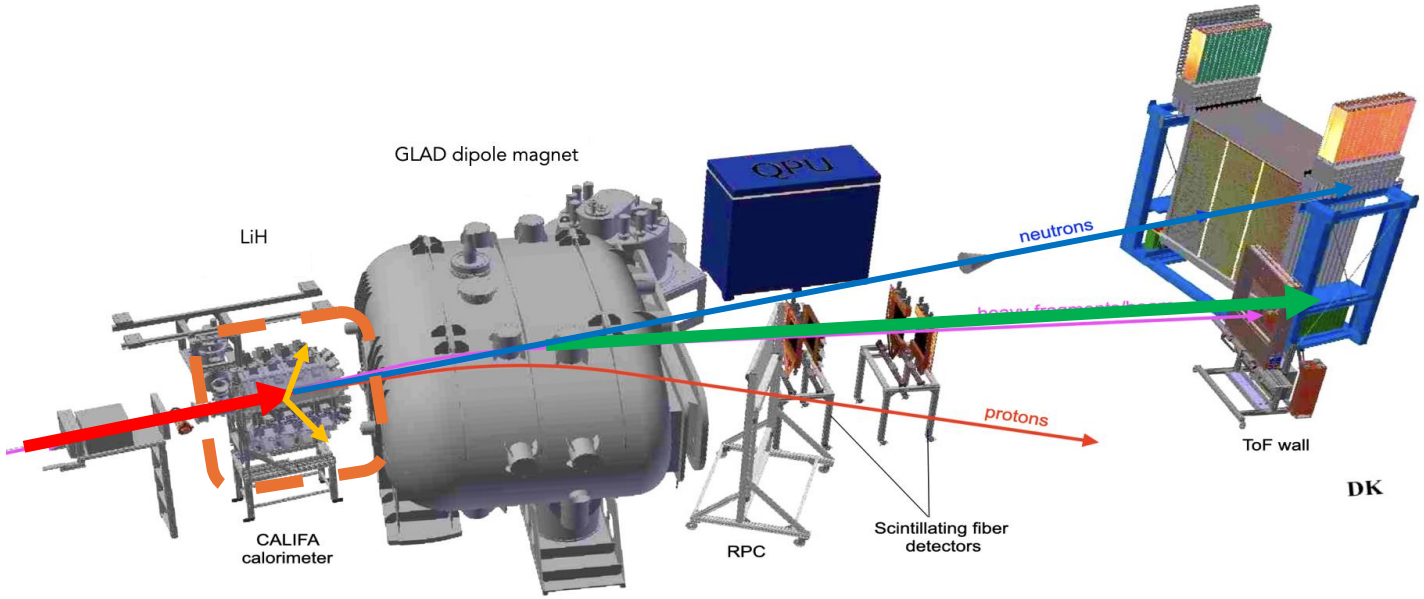

CALIFA ($\theta,\varphi,\Delta E$)

1504 CsI crystals,
480 crystals with two gains

Resolution at 1 MeV about 46.2 keV (β = 0.77)

γ-rays detection efficiency at 1MeV of 43.5(14) %

Detection of the light particles emitted from the target

QFS reaction e.g. (*p,pn*) and (*p,2p*) in LiH_2

Complete measurement in inverse kinematics (E,**p**):

- **Incoming nuclei**;
- **γ-rays and light particles emitted from the target**;

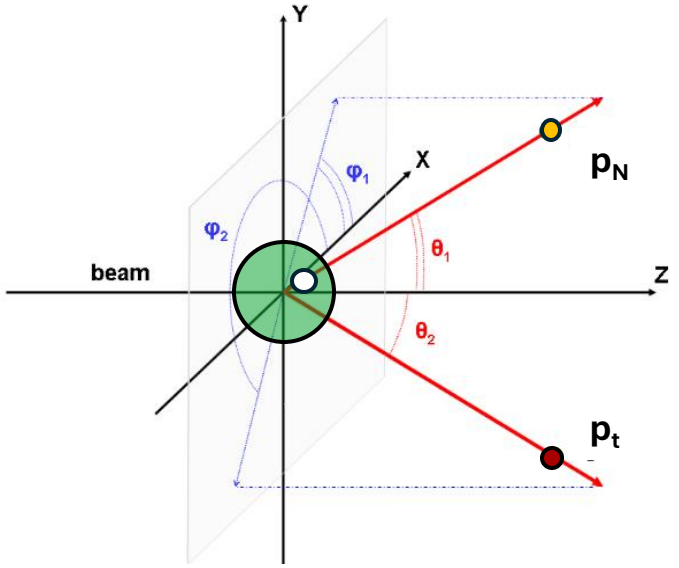

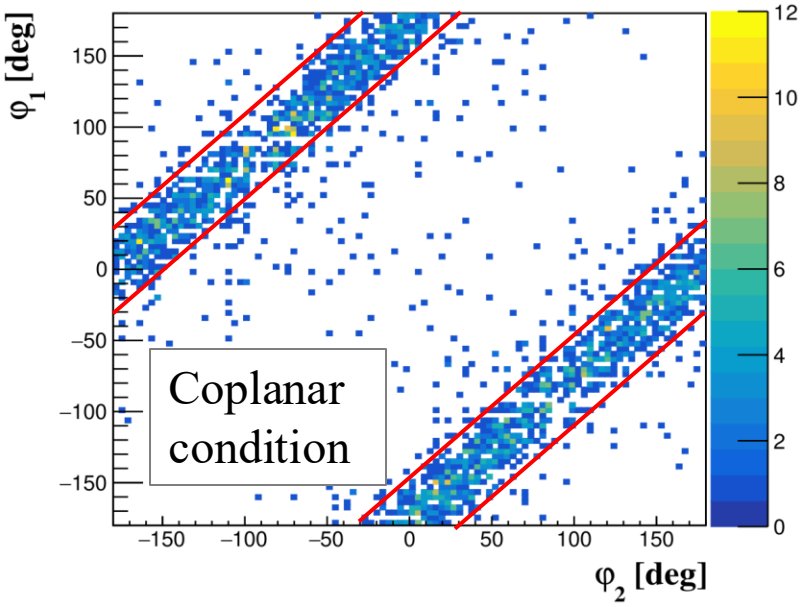

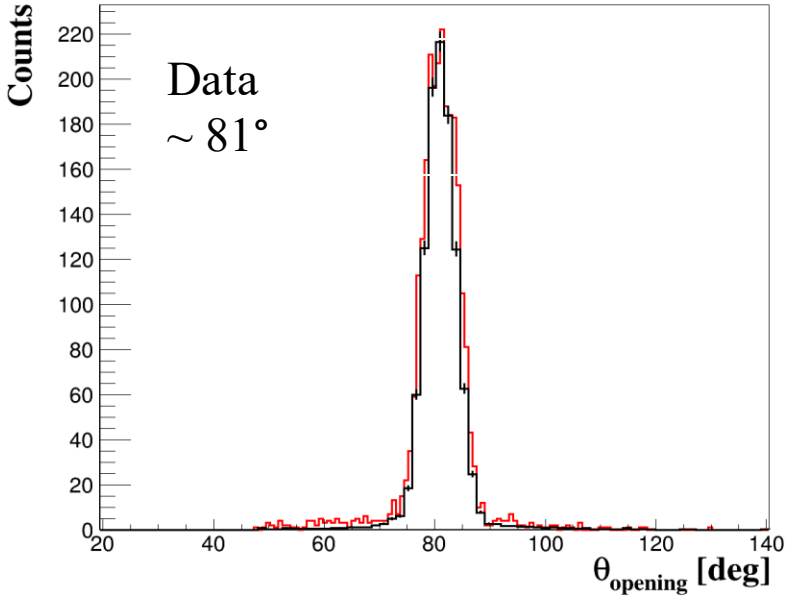

Determination of the fragment charge

QFS reaction e.g. (*p,pn*) and (*p,2p*) in LiH_2

Complete measurement in inverse kinematics (E,**p**):

- **Incoming nuclei**;
- **γ-rays and light particles emitted from the target**;
- **Outgoing fragments**;

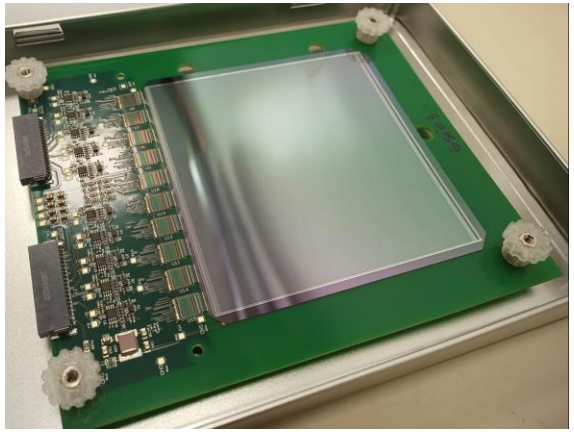

4 in-beam SSDs
("FOOTs")

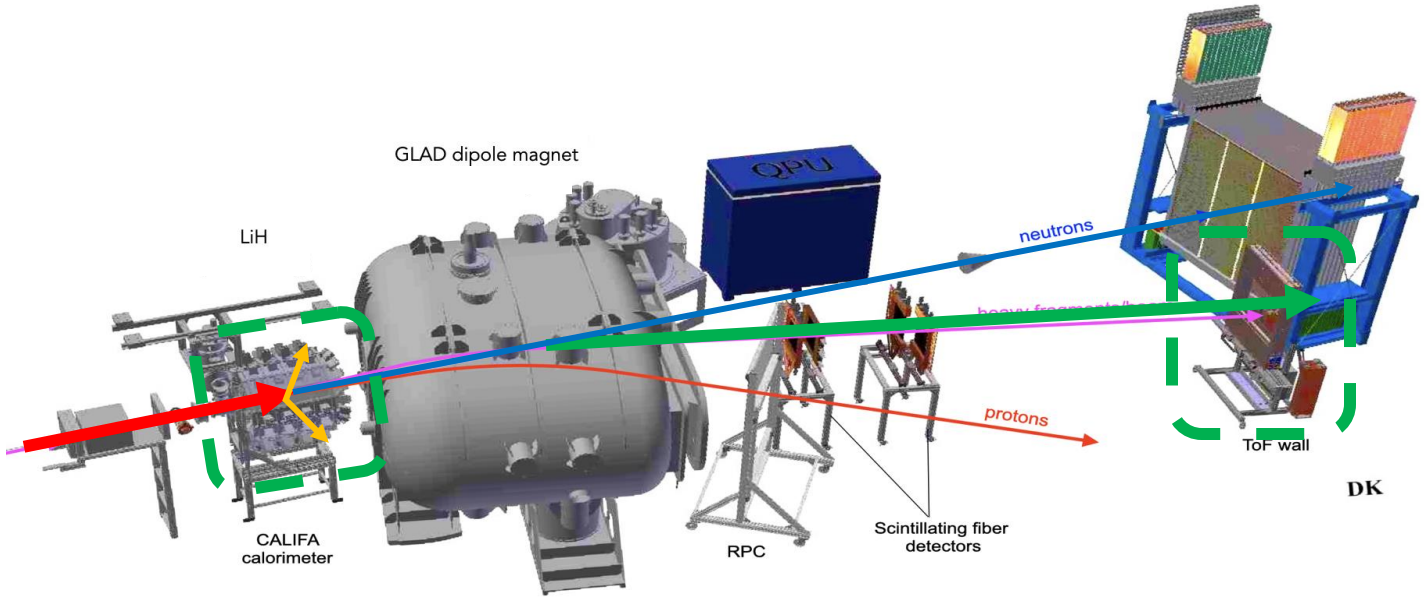

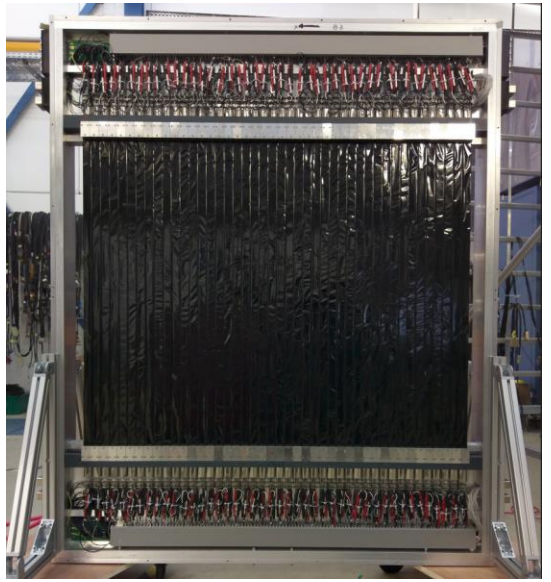

ToFD (x,y,z,ΔE)

Determination of the fragment mass: the ^{22}O(*p*,2*p*) case

QFS reaction e.g. (*p*,*pn*) and (*p*,2*p*) in LiH_2

Complete measurement in inverse kinematics (E,**p**):

- **Incoming nuclei**;
- **γ-rays and light particles emitted from the target**;
- **Outgoing fragments**;

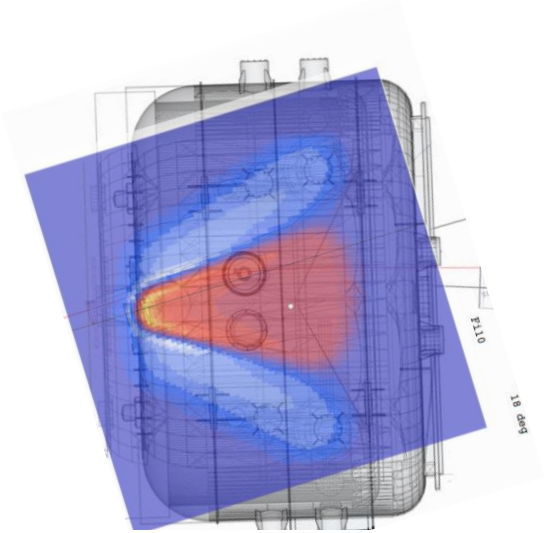

GLAD (field map)

Fibers (x,y,t)

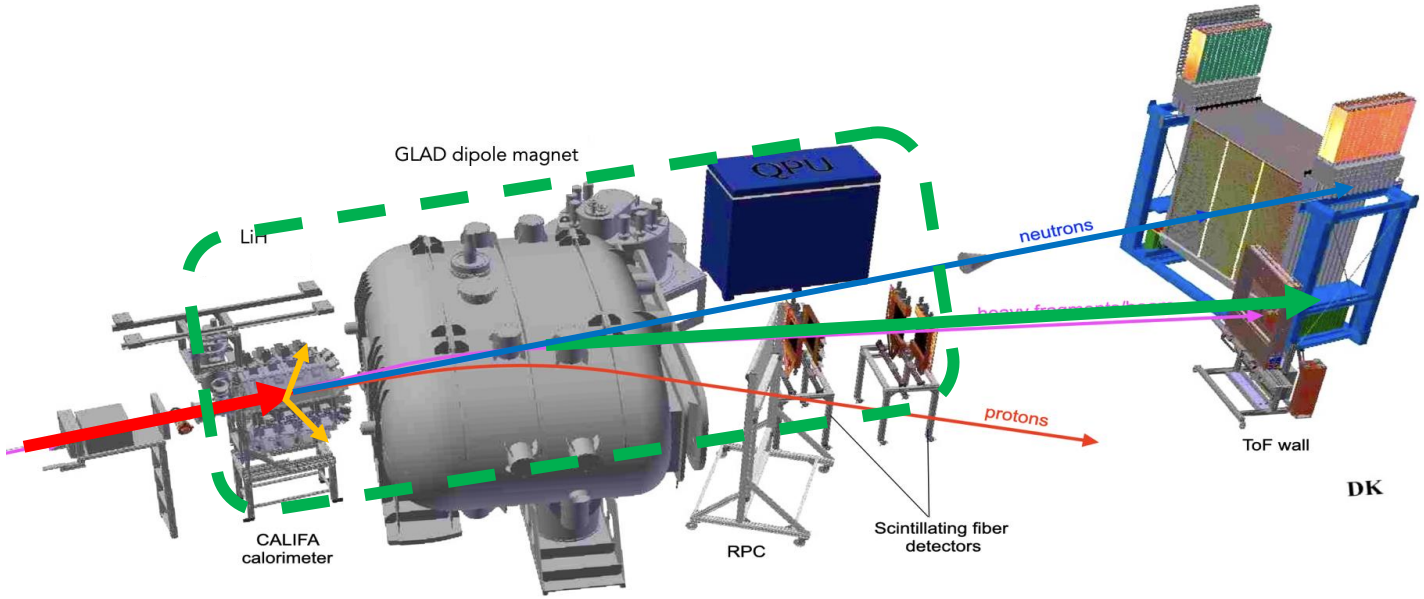

Multi-Dimensional Fit approach (MDF)

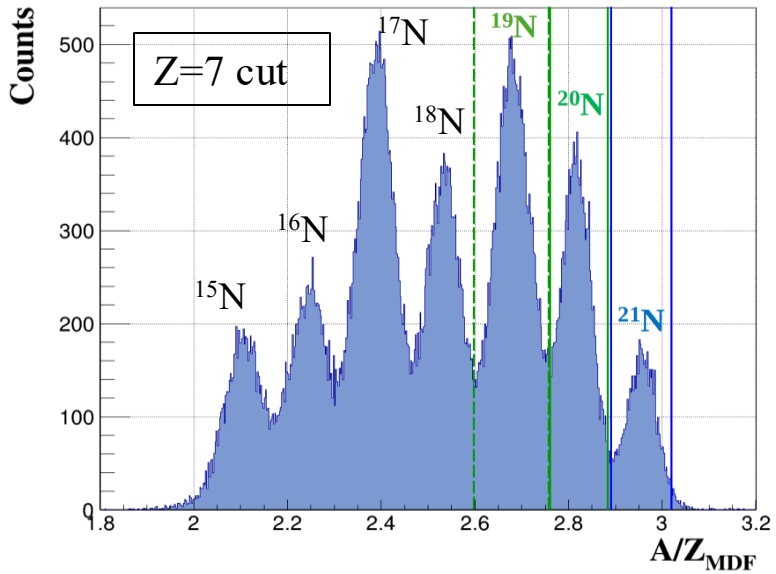

Neutron detection and invariant mass method

QFS reaction e.g. (*p,pn*) and (*p,2p*) in LiH_2

Complete measurement in inverse kinematics (E,**p**):

- **Incoming nuclei**;
- **γ-rays and light particles emitted from the target**;
- **Outgoing fragments**;
- **Neutron(s)**

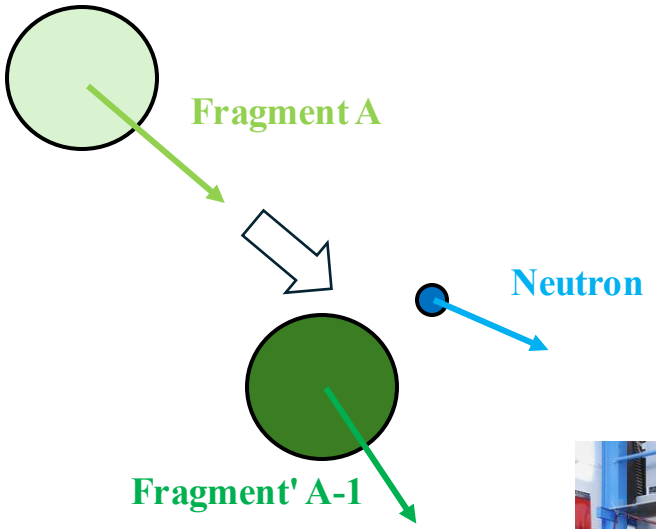

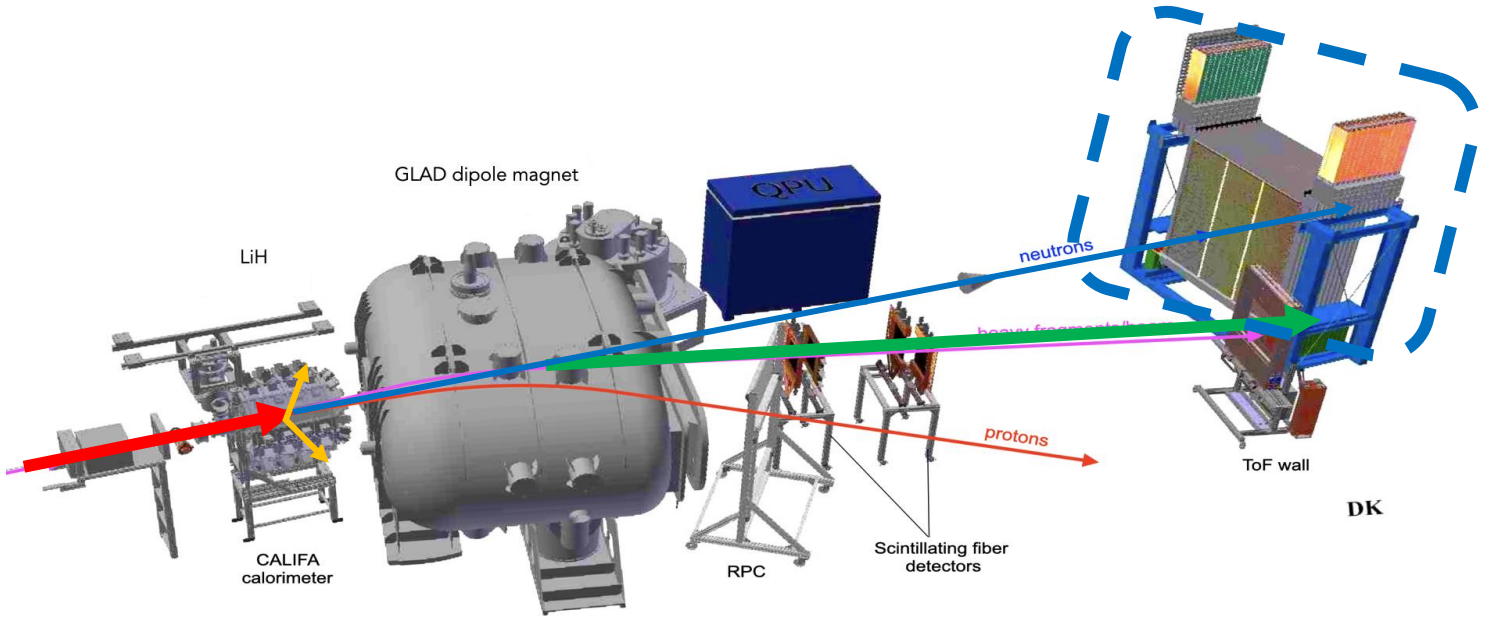

Neuland (x,y,z,t,ΔE)

Neutron detection and invariant mass method

QFS reaction e.g. (*p,pn*) and (*p,2p*) in LiH_2

Complete measurement in inverse kinematics (E,**p**):

- **Incoming nuclei**;
- **γ-rays and light particles emitted from the target**;
- **Outgoing fragments**;
- **Neutron(s)**

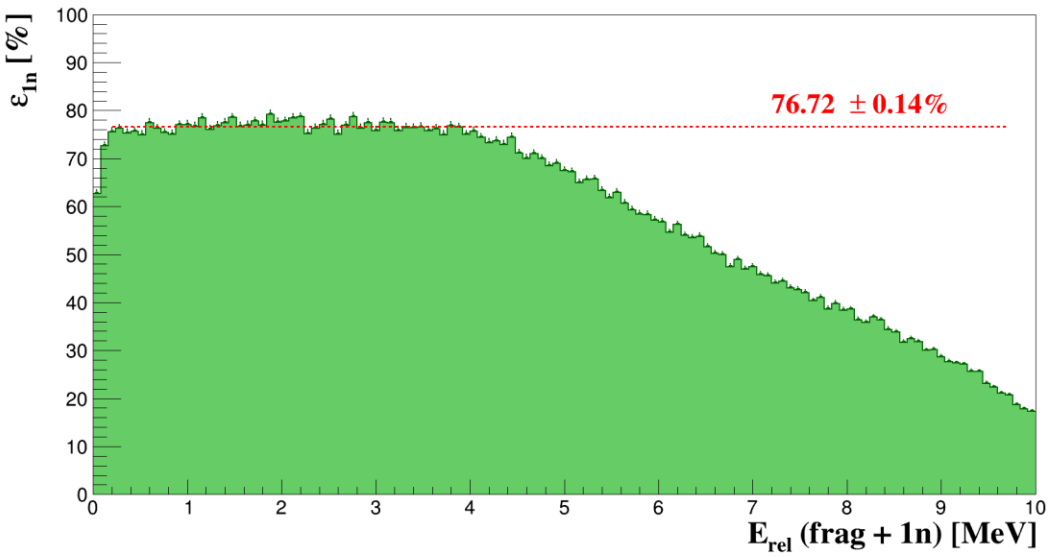

Use of the invariant mass method:

$$M_{inv} = \sqrt{\left(\sum_{i=0}^{N} E_i\right)^2 - \left(\sum_{i=0}^{N} p_i\right)^2}$$

with the energy and momentum of the fragment and neutron(s)

$$E_{rel} = M_{inv} - \sum_{i=0}^{N} m_i$$

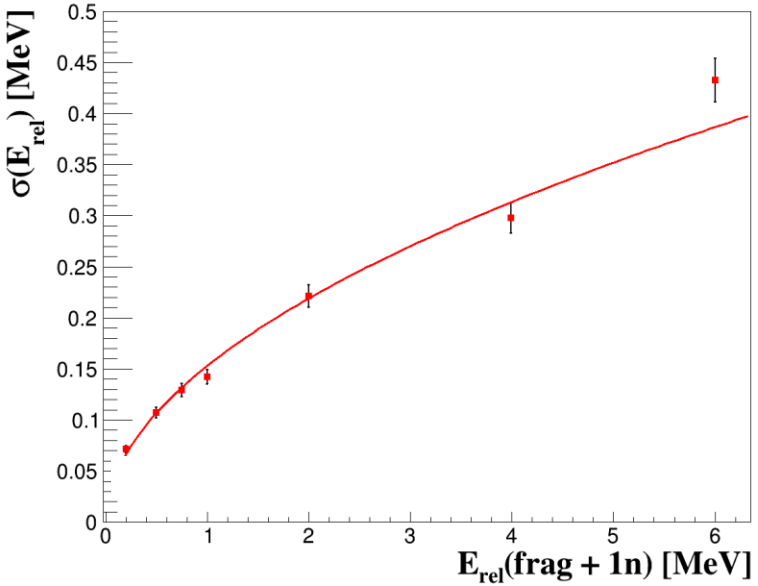

Magicity of the ^{22}O(*N=14*) nucleus through the ^{22}O(*p,pn*)^{21}O$^{(*)}$ reaction

Study of the γ-spectroscopy

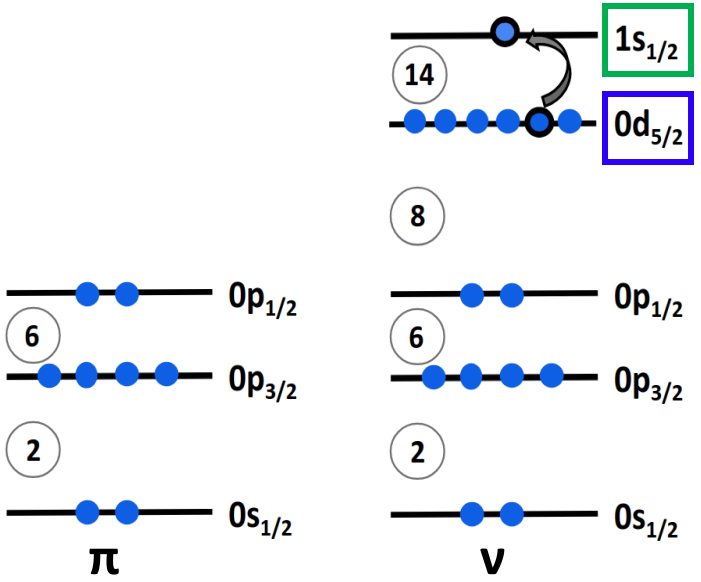

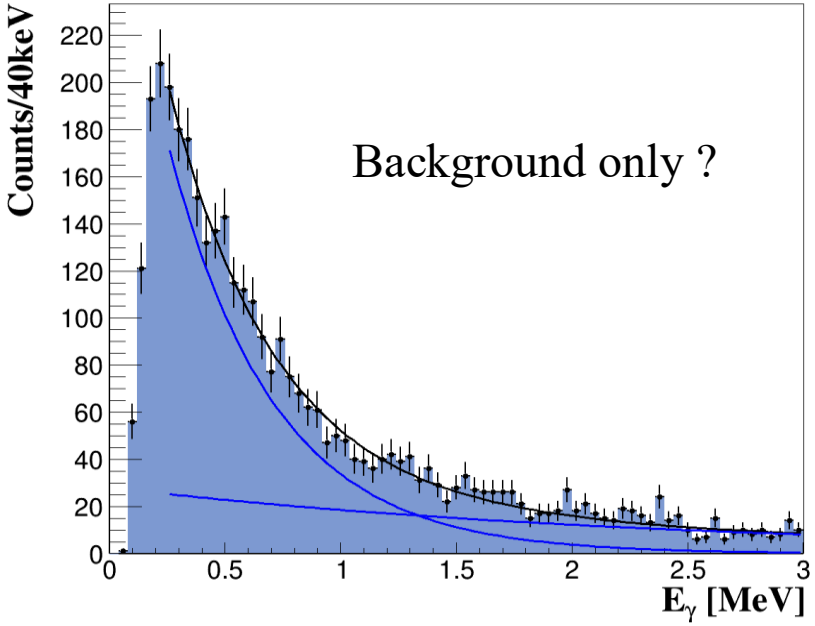

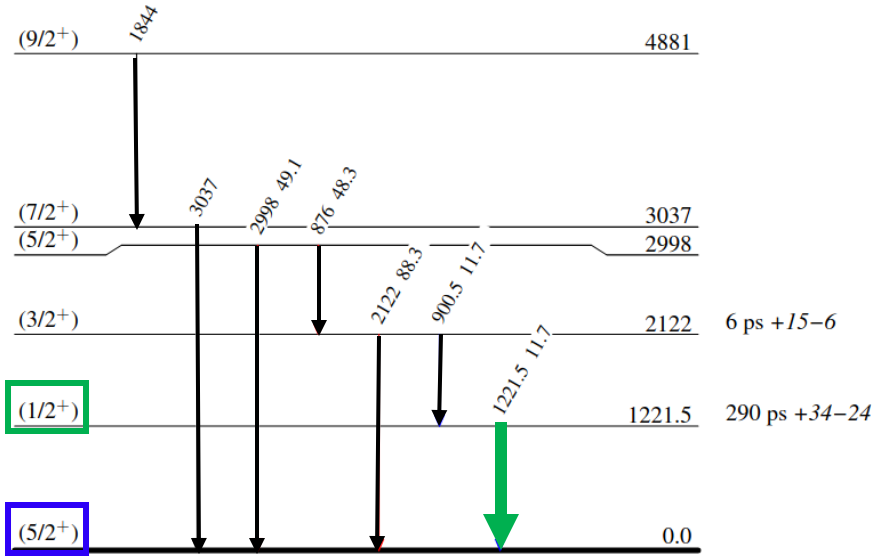

Study of the γ-spectroscopy

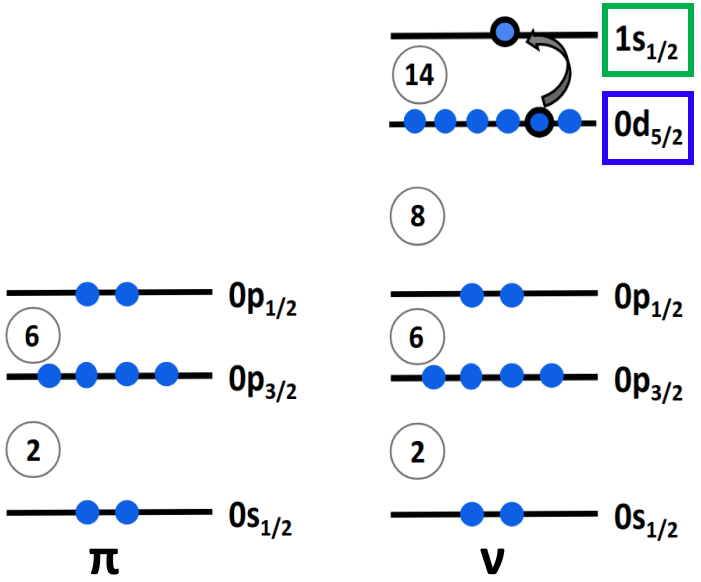

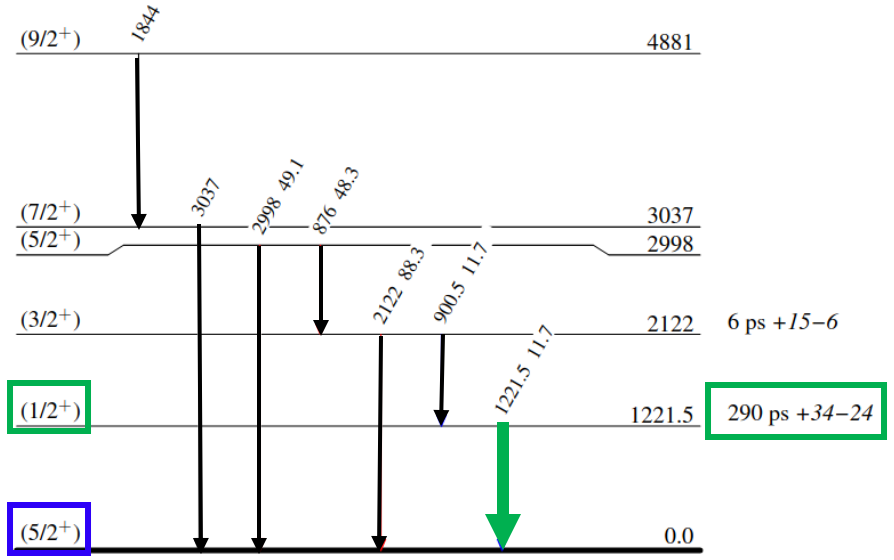

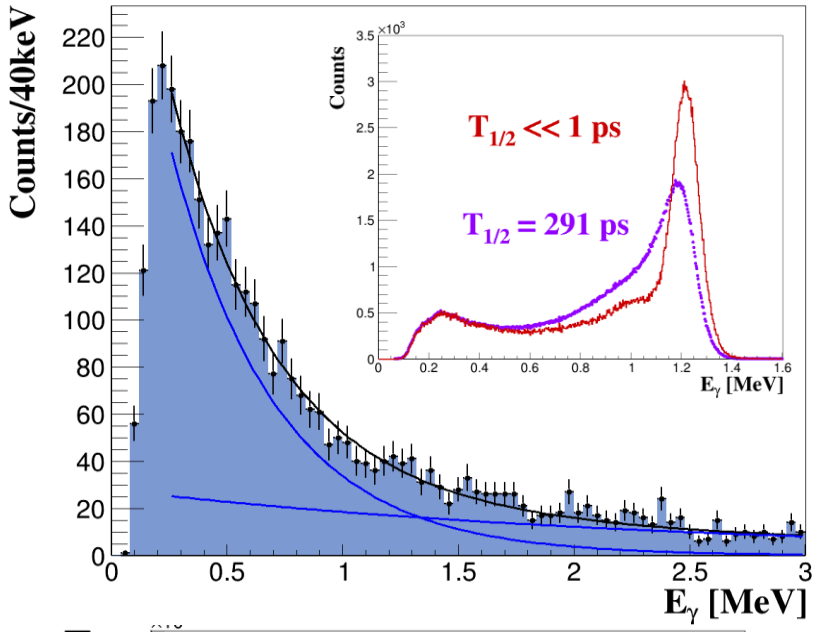

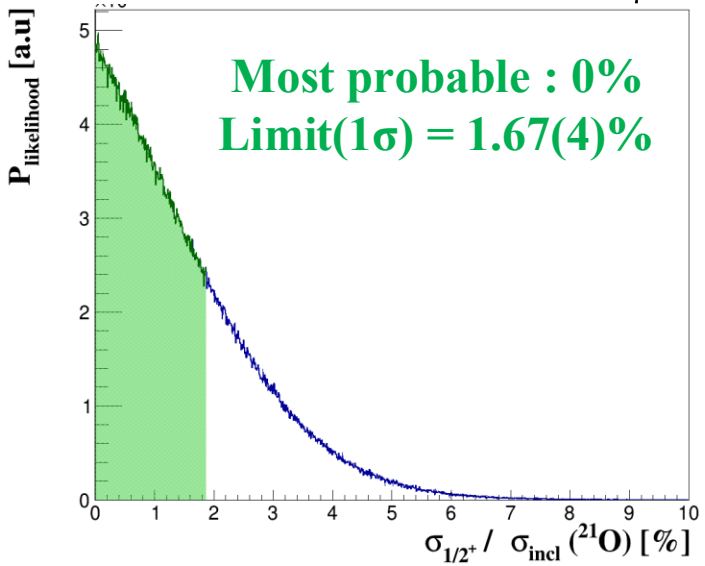

The $1s_{1/2}$ is not or very weakly occupied

Study of the recoil transverse momentum

Recoil momentum distribution :

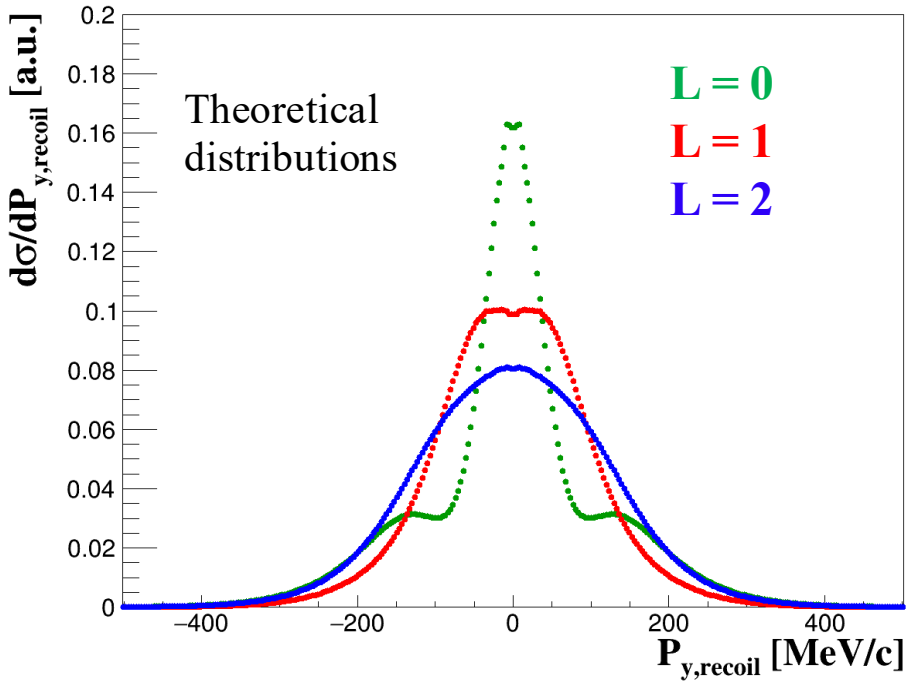

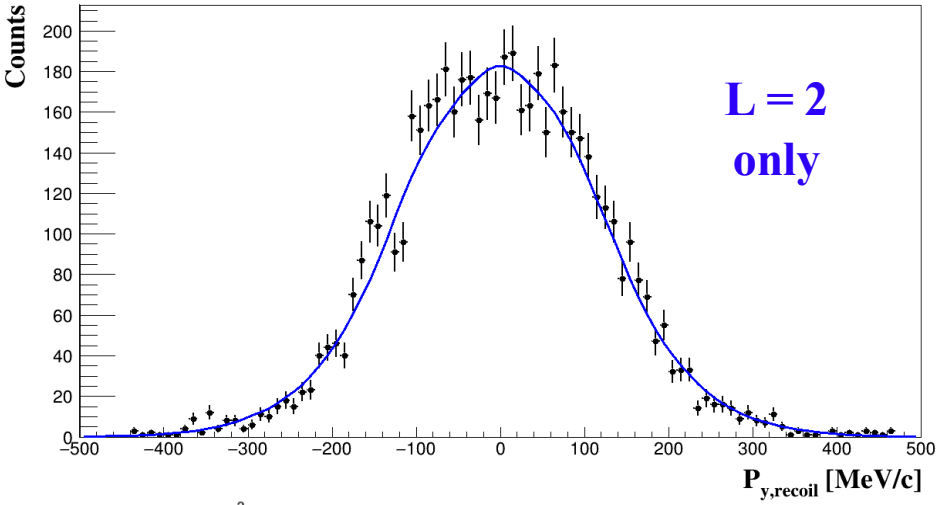

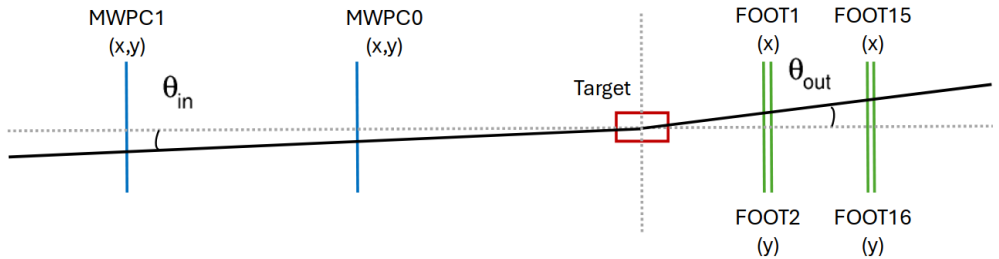

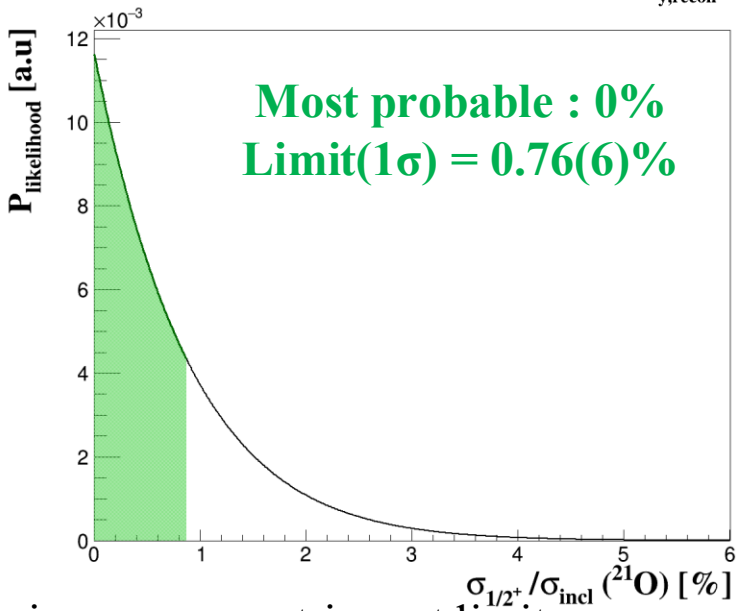

This method confirms what was obtained with γ-rays and gives an even stringent limit.

^{22}O looks more magic than the known doubly magic cases of ^{16}O or ^{14}C, having about 10% neutrons above closed shell.

Determination of the SO splitting $Z=6$ in ^{22}O through the ^{22}O$(p,2p)^{21}$N reaction

Study of $^{22}O(p,2p)^{21}N^* \Rightarrow {}^{21}N + \gamma$

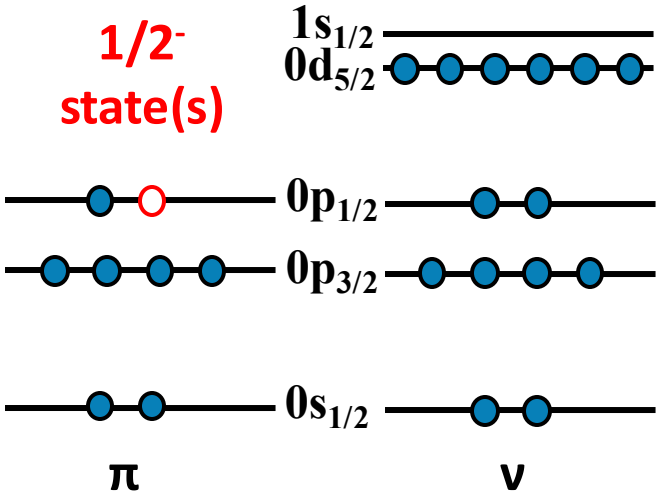

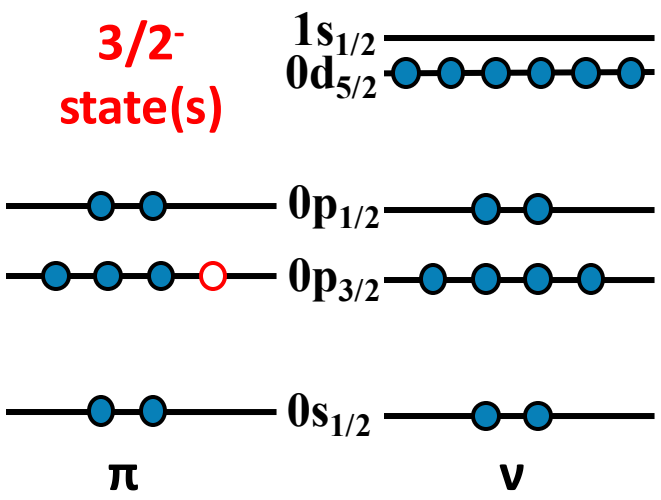

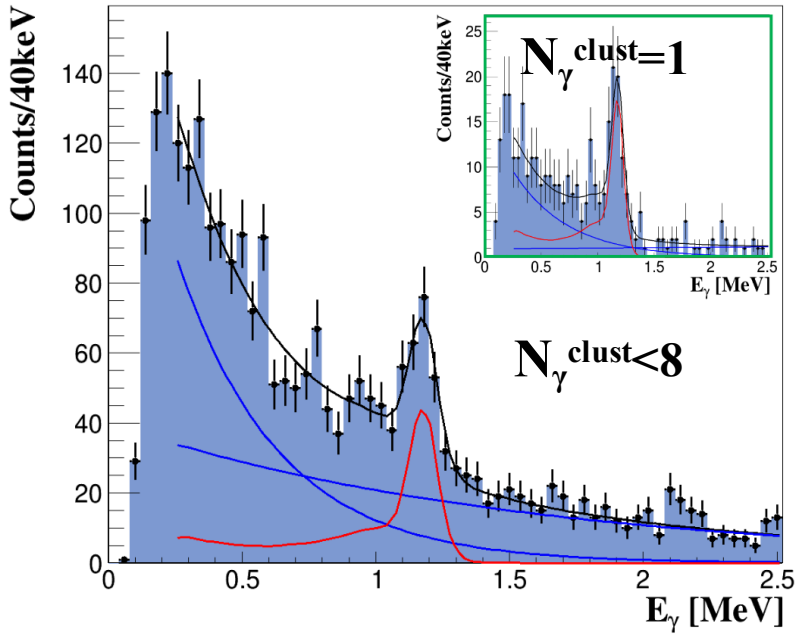

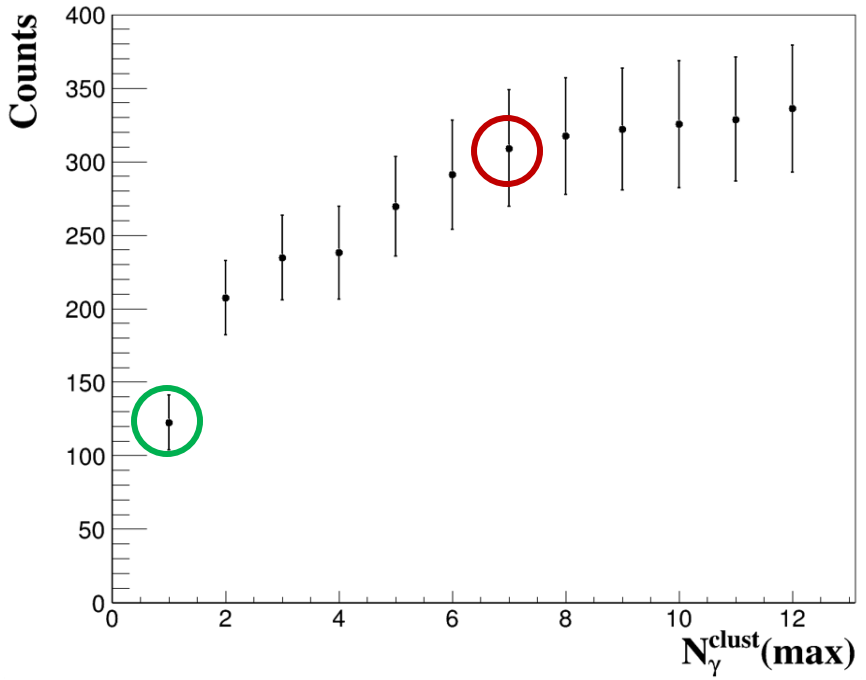

Study of $^{22}O(p,2p)^{21}N^* \Rightarrow {}^{21}N + \gamma$

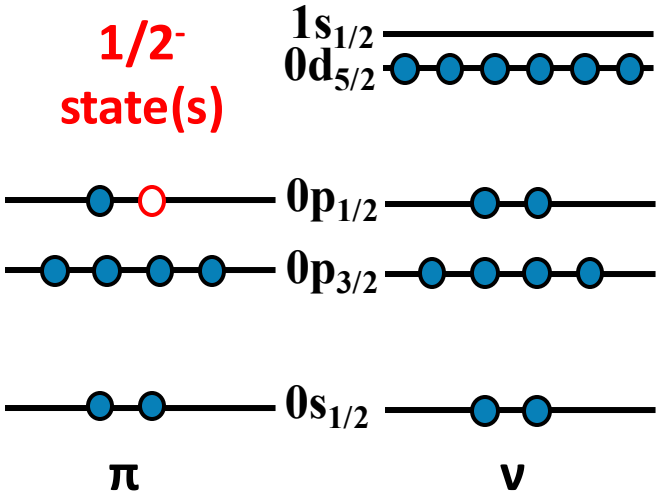

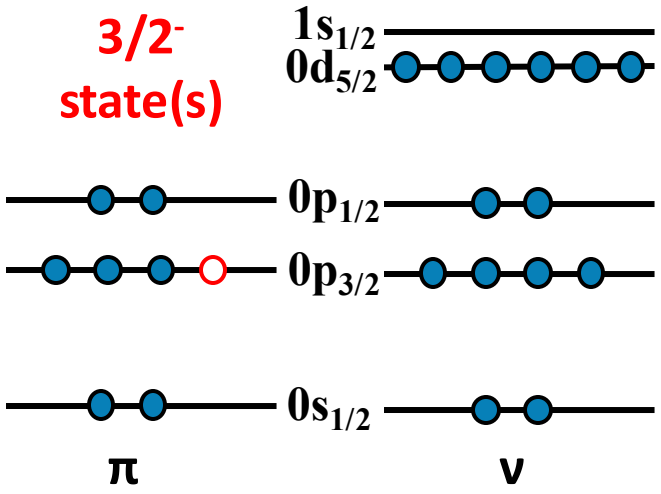

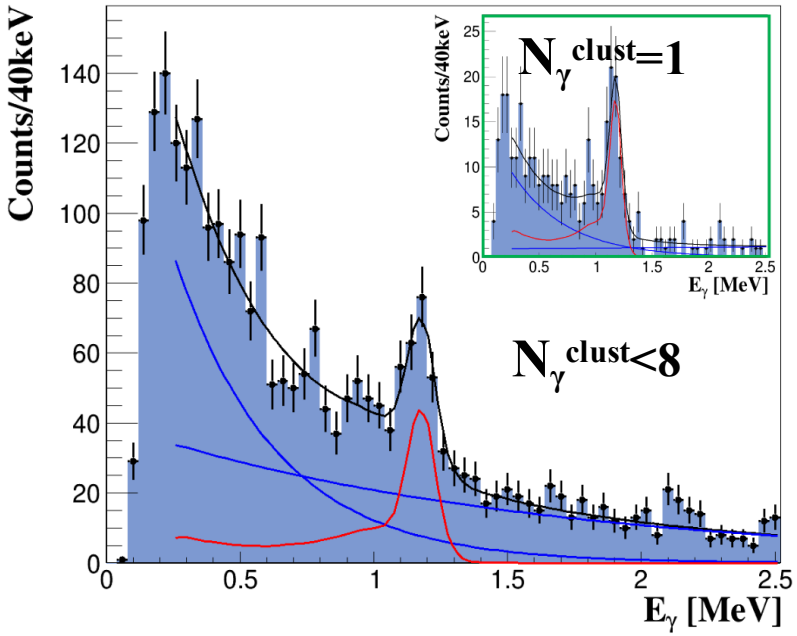

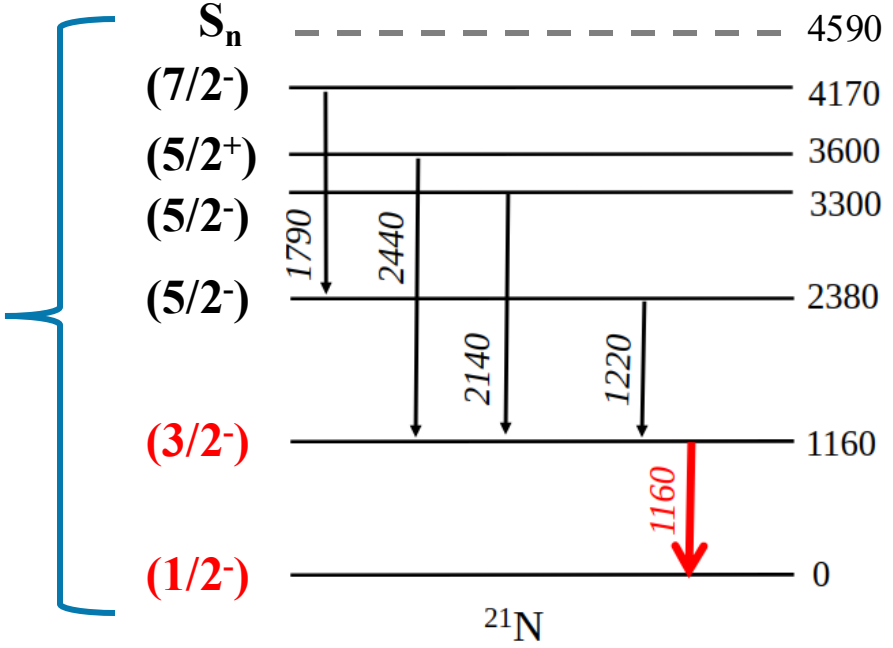

Study of $^{22}O(p,2p)^{21}N^* \Rightarrow {}^{21}N + \gamma$

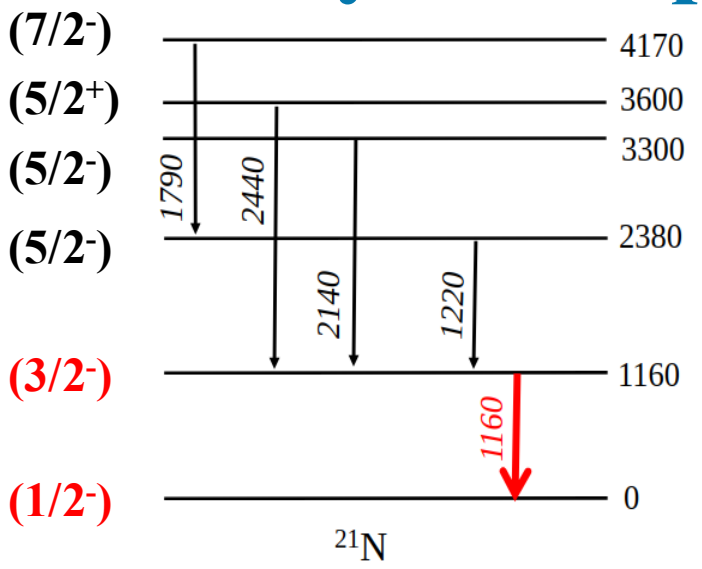

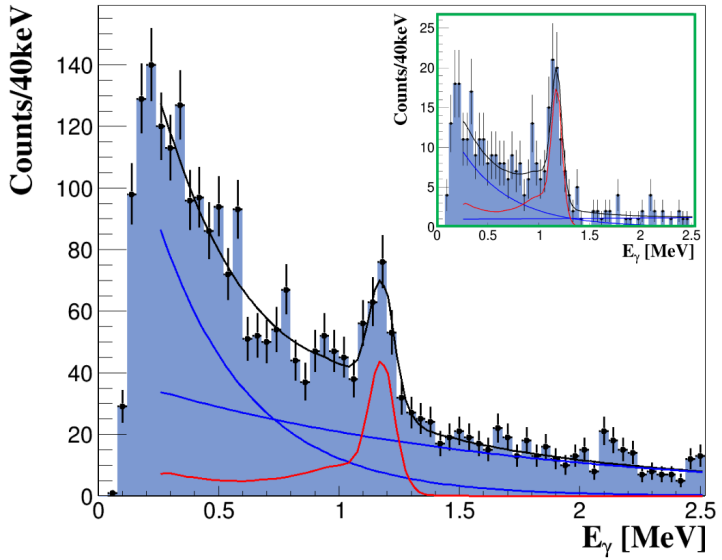

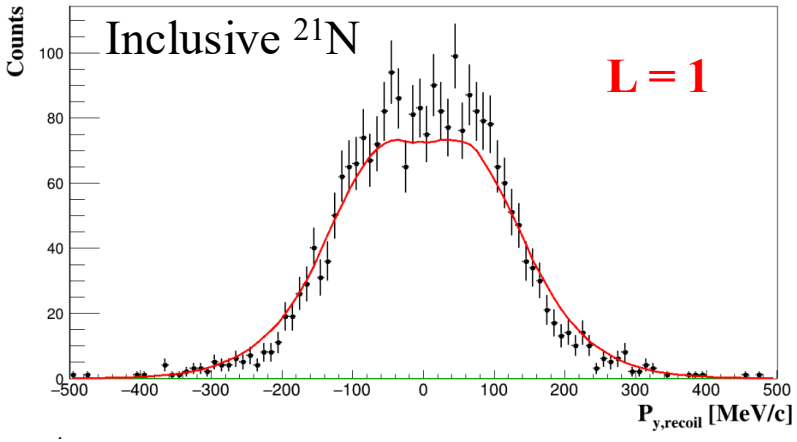

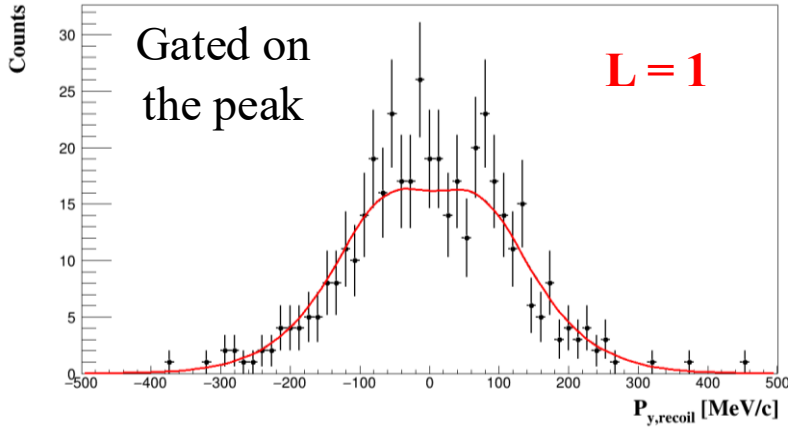

Observation of a peak in the γ-ray energy spectrum corresponding to the decay of the $3/2^-_1$ state.

Study of $^{22}O(p,2p)^{21}N^* \Rightarrow {}^{20}N + 1n\ (+\gamma)$

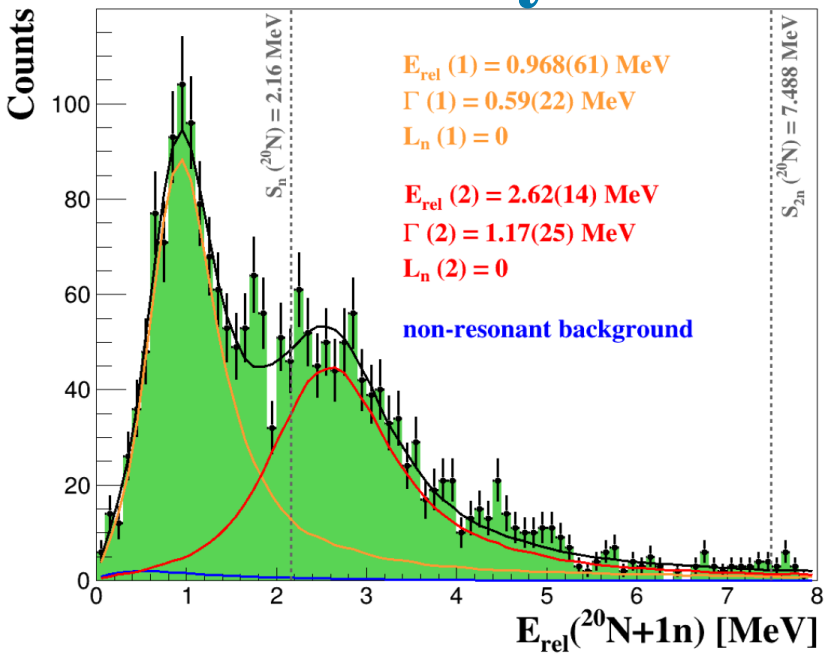

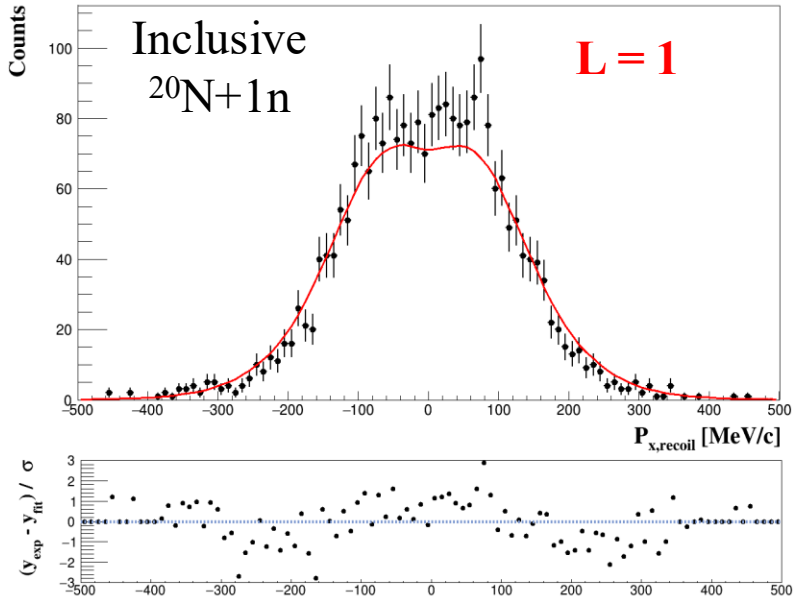

Two resonances fitted with Breit-Wigner functions

Decays from $3/2^-$ in ^{21}N to 2^-_{gs} in ^{20}N ($L_n = 0$)

Only about 5% of events with decays to the excited states of ^{20}N

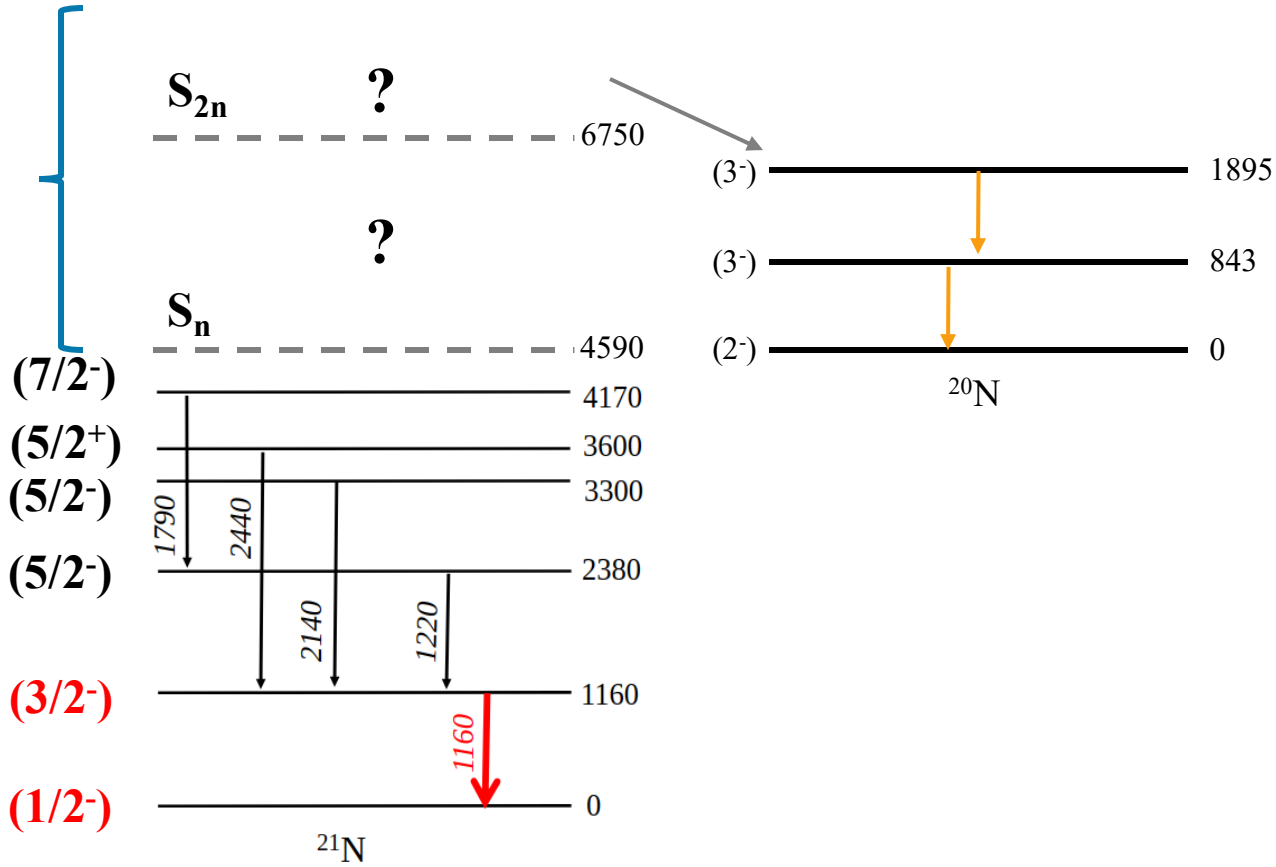

Determination of the *Z*=6 SO splitting in ^{22}O

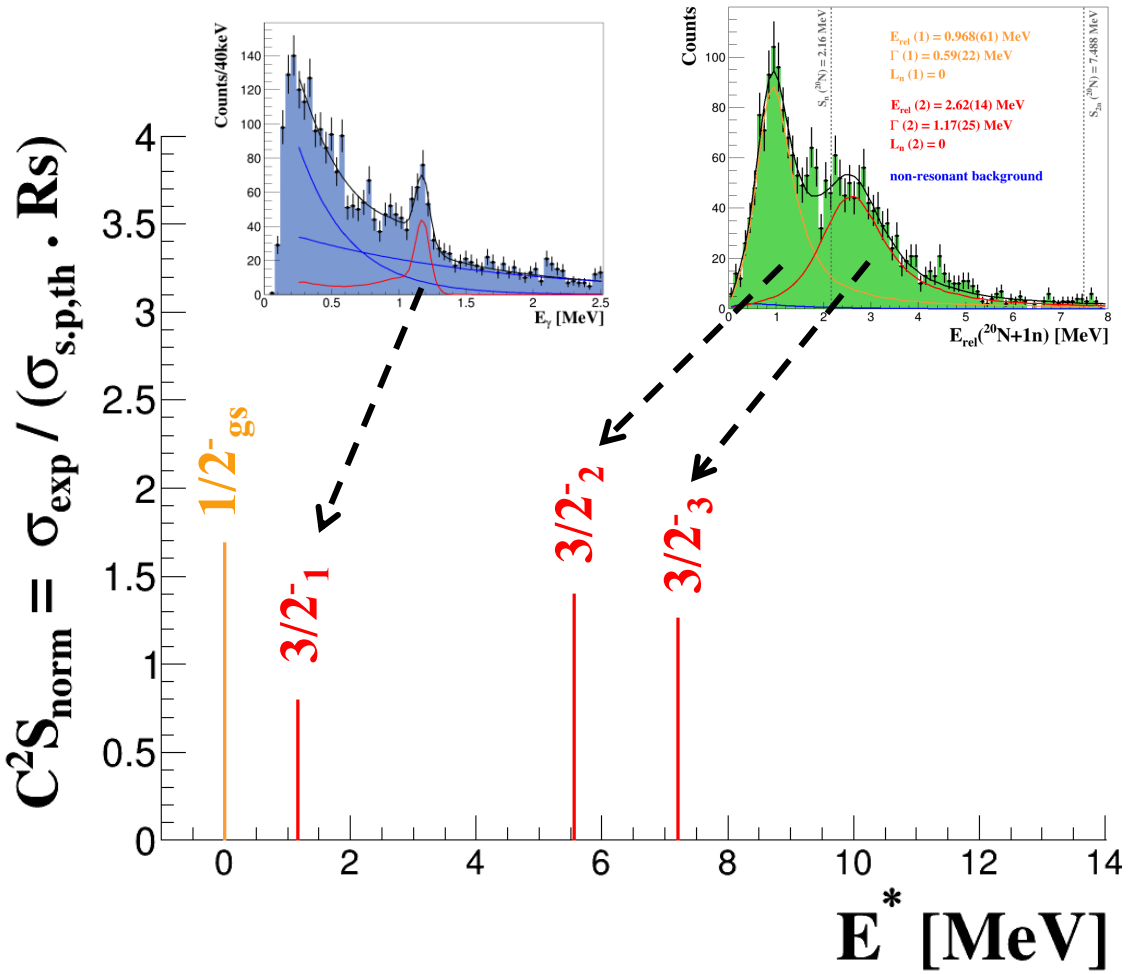

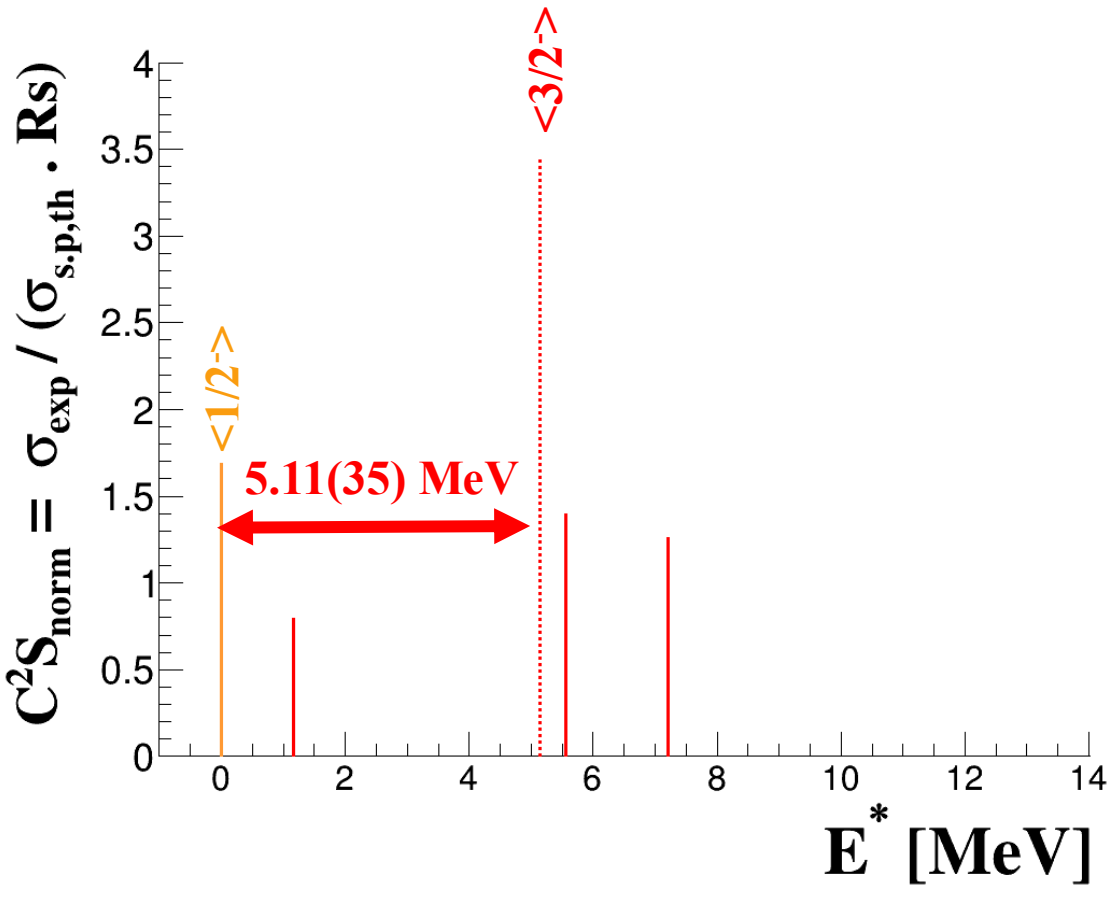

$\sigma(GS) = \sigma_{incl} - \sigma(3/2^-_1)$

Energy centroid = $\Sigma(C^2S \cdot E^*) / \Sigma C^2S$

SO gap : difference between the centroids of SO partners

Evolution of the $Z=6$ gap from ^{16}O to ^{22}O

Reduction of **1.77 MeV** between ^{16}O to ^{22}O

A **much smaller reduction** is estimated from **Mairle's trend** and **Wood-Saxon** (mean-field) calculations.

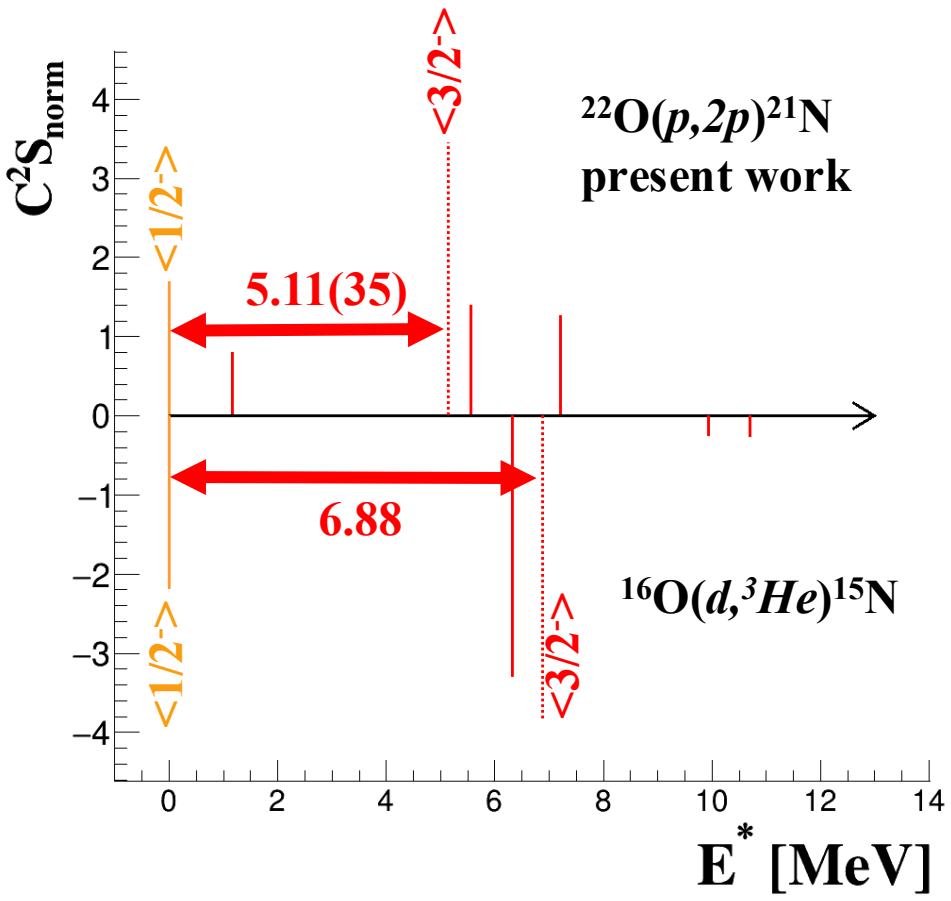

	Exp	WS	Mairle
ΔSO [MeV]	**1.77(35)**	1.006	1.174

Evolution of the *Z*=6 gap from ^{16}O to ^{22}O

Reduction of **1.77 MeV** between ^{16}O to ^{22}O

A **much smaller reduction** is estimated from **Mairle's trend** and **Wood-Saxon** (mean-field) calculations.

Good agreement with the **SM(YSOX)** calculations which includes the monopole terms.

It probably indicates the role of the **tensor force** when filling the $0d_{5/2}$ orbital with 6 neutrons.

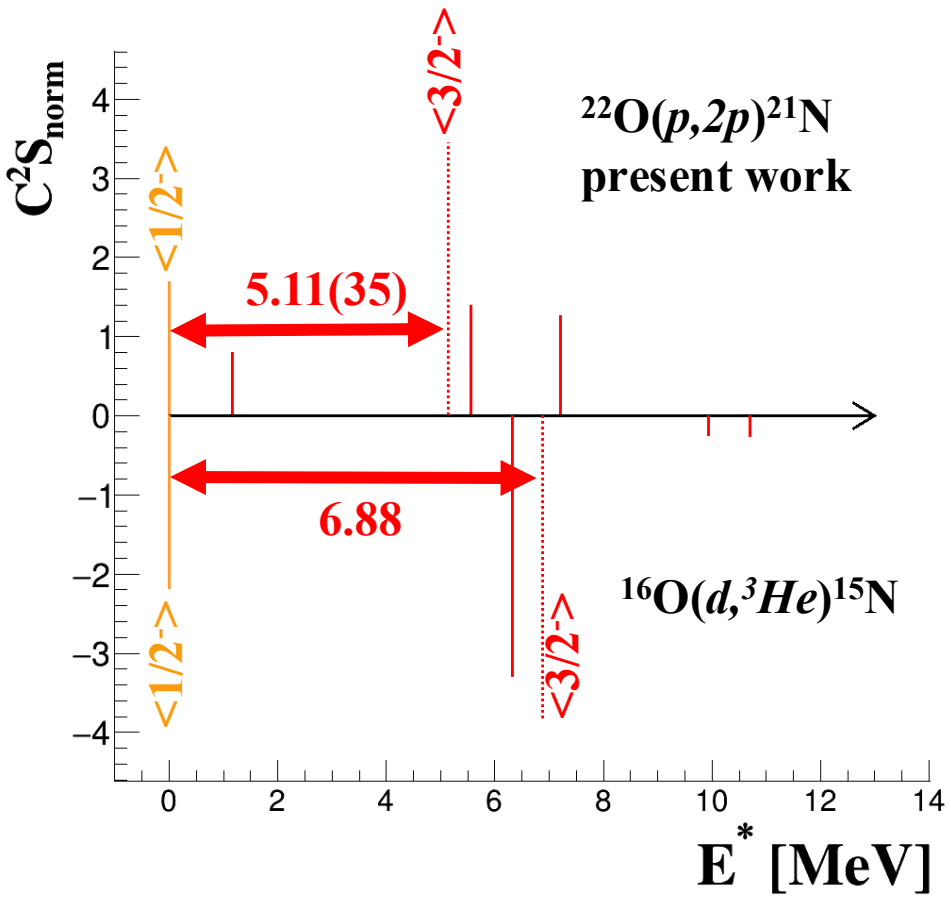

	Exp	WS	Mairle	SM(YSOX)
ΔSO [MeV]	**1.77(35)**	1.006	1.174	1.863

Evolution of the *Z*=6 gap from ^{16}O to ^{22}O

Reduction of **1.77 MeV** between ^{16}O to ^{22}O

A **much smaller reduction** is estimated from **Mairle's trend** and **Wood-Saxon** (mean-field) calculations.

Good agreement with the **SM(YSOX)** calculations which includes the monopole terms.

It probably indicates the role of the **tensor force** when filling the $0d_{5/2}$ orbital with 6 neutrons.

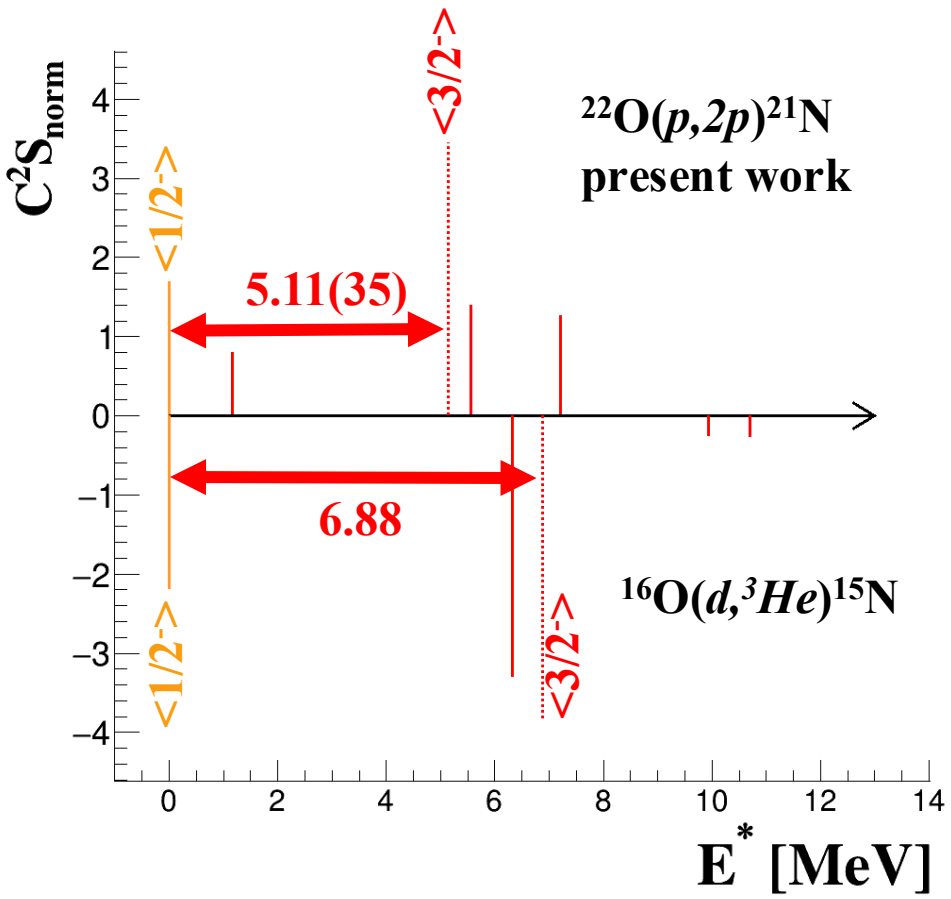

	Exp	WS	Mairle	SM(YSOX)
ΔSO [MeV]	**1.77(35)**	1.006	1.174	1.863

Monopole contributions:
- SO ~ +0.18 MeV
- Tensor ~ -2.76 MeV

Next steps:
- **Decomposition of the SM value into the central, SO and tensor parts;**
- Estimation of the coupling to the continuum, especially in ^{22}O.

Conclusions

^{22}O(*N=14*) magicity and ^{22}O(*p,pn*)

- Better contrainst on the $1s_{1/2}$ neutron occupancy : upper limit(1σ) = 0.76(6)%
- Clear signature of an *N=14* closed subshell
- Identification of a new resonance *(backup slide)*

Size of the *Z=6* gap and ^{22}O(*p,2p*)

- Identification of new resonances
- Evaluation of the SO splitting *Z=6* : 5.11(35) MeV
- Reduction from ^{16}O to ^{22}O : 1.77(35) MeV

Bonus !

Quasi-Free Scattering (QFS)

Direct reaction which requires high beam energy, but can probe deeply bound orbitals.

Selectively populates the final states : probing the initial state of the incoming nucleus

Eikonal approximation (single interaction):
P(nucleon) = -**P** (recoil fragment)

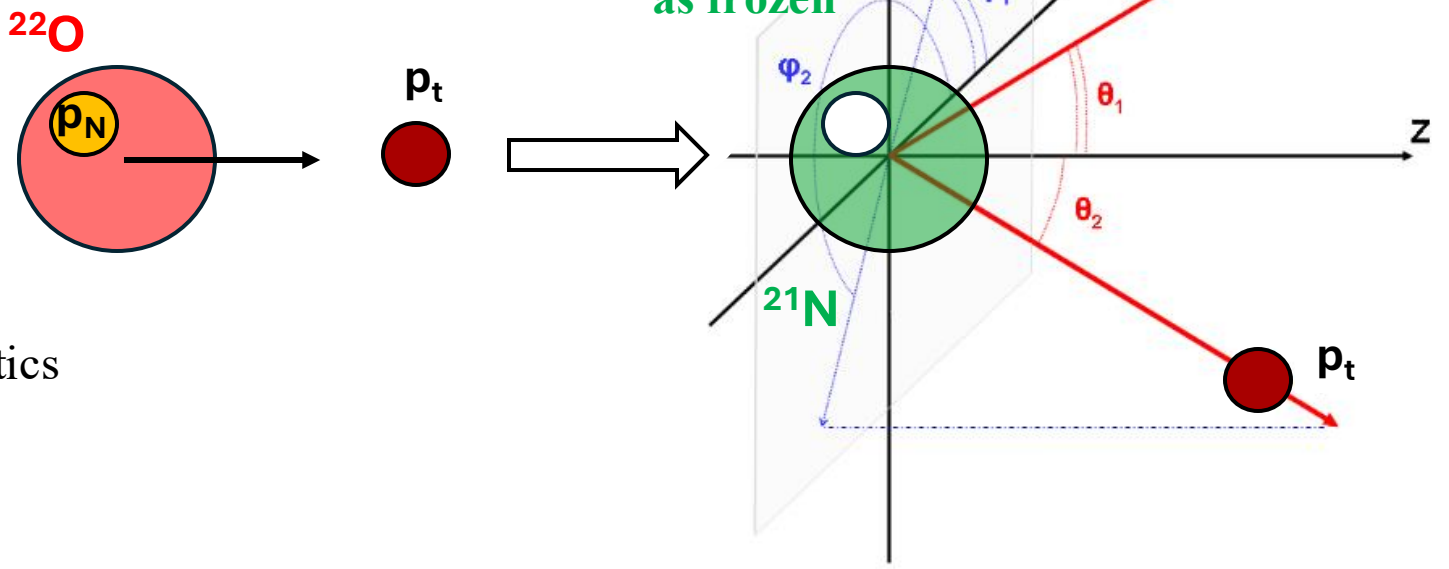

Special features for the kinematics
of the emitted particles:

- emission in the same plan
- opening angle around 80°

Quenching factor for ^{22}O(*p,pn*) and ^{22}O(*p,2p*) reactions

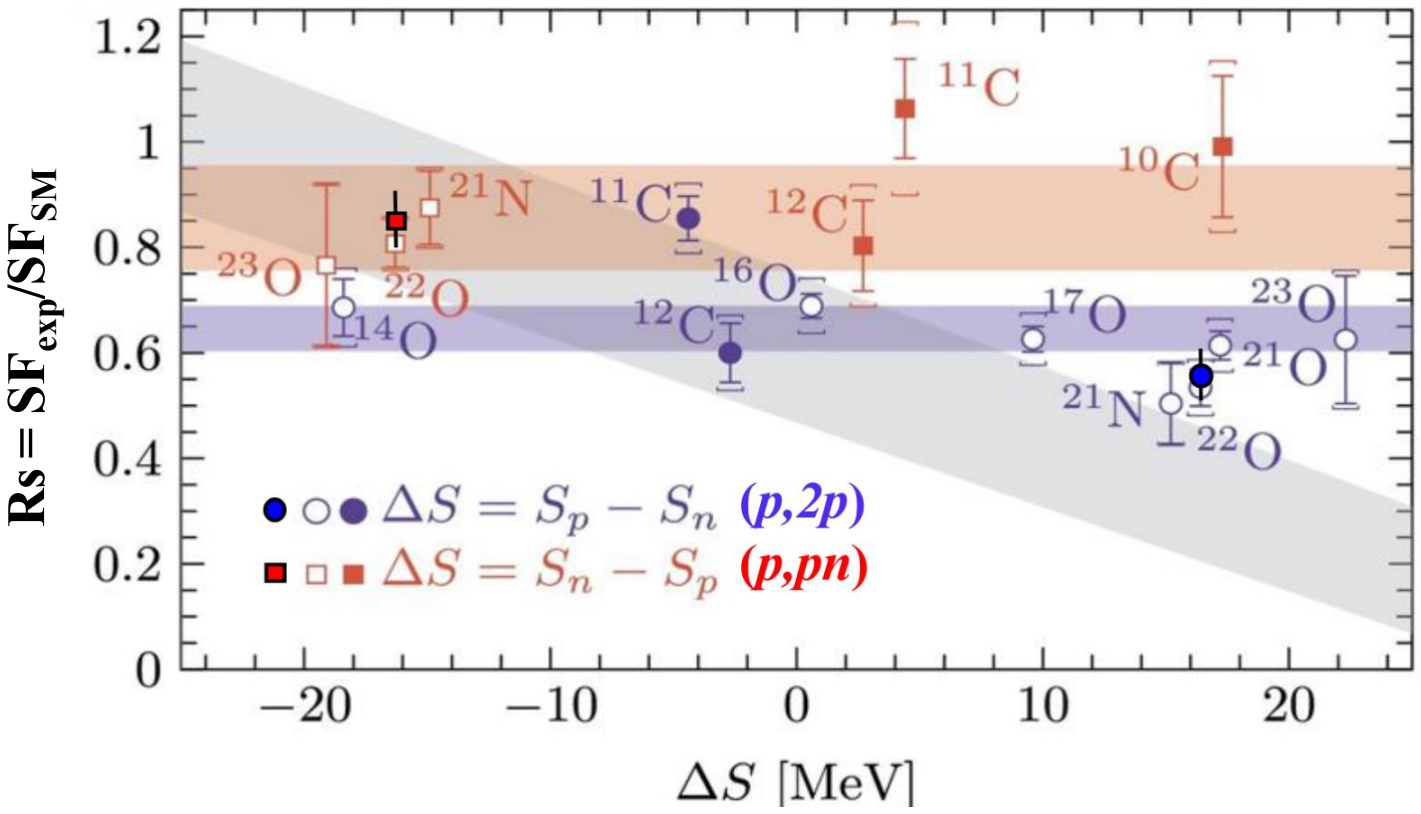

M. Holl et al, PLB (2019)

Values reported in this review:
^{22}O(*p,pn*) Rs = 0.81(5)
^{22}O(*p,2p*) Rs = 0.53(6)
Inclusive measurements with the use of **SM calculations**

Values deduced from the present work:
^{22}O(*p,pn*) Rs = 0.86(2)
^{22}O(*p,2p*) Rs = 0.55(5)
GS => GS exclusive measurements

This confirms the different values between (*p,pn*) and (*p,2p*) reactions

The study of the ^{24}O(*p,pn*) and ^{24}O(*p,2p*) could also contribute to this systematic survey (ΔS = 21.3MeV)

FOOT : energy calibration

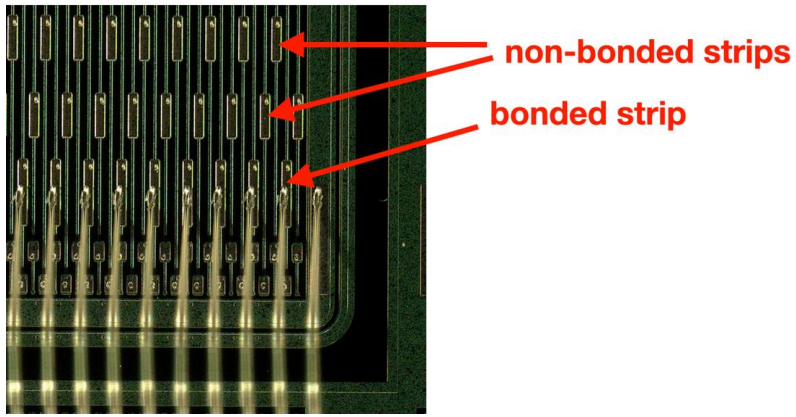

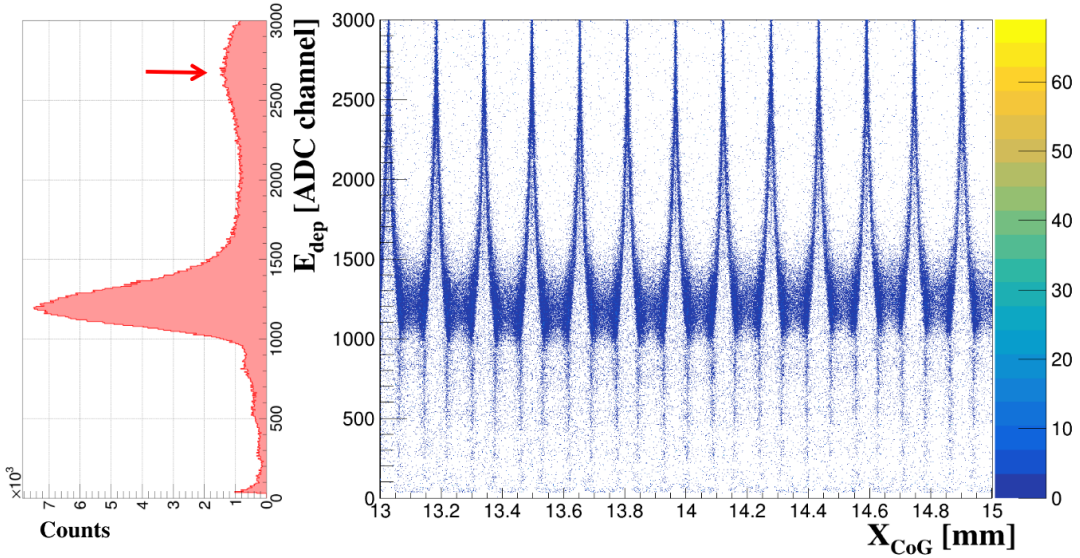

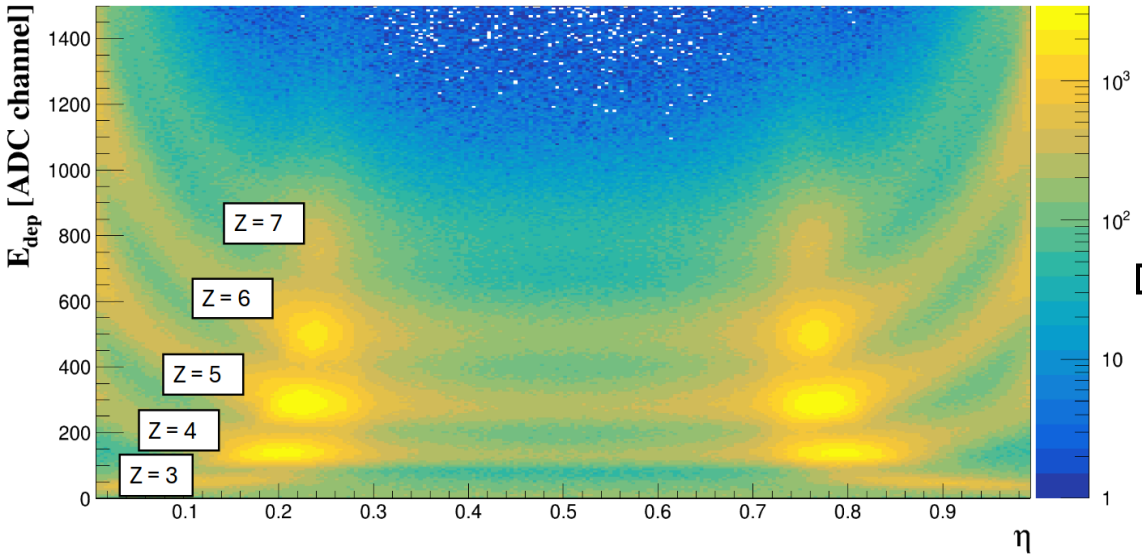

Correction

for Z = 7

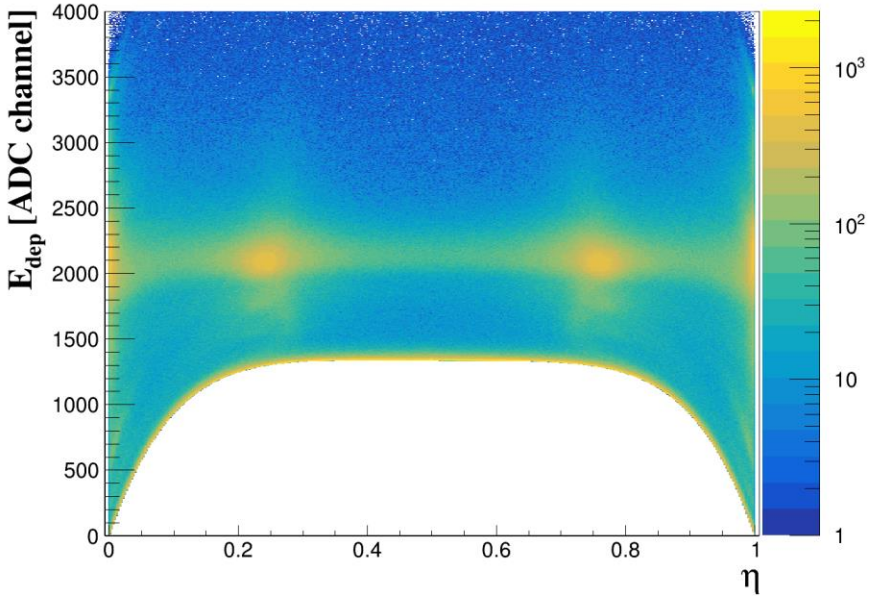

Clustering algorithm for the protons and neutrons

Proton and neutron induced γ-ray showers interacting with the CALIFA crystals

The cluster size used for them in the algorithm should be:
- large enough to capture these additional γ-rays;
- not too large to allow the reconstruction of clusters from γ-ray transitions.

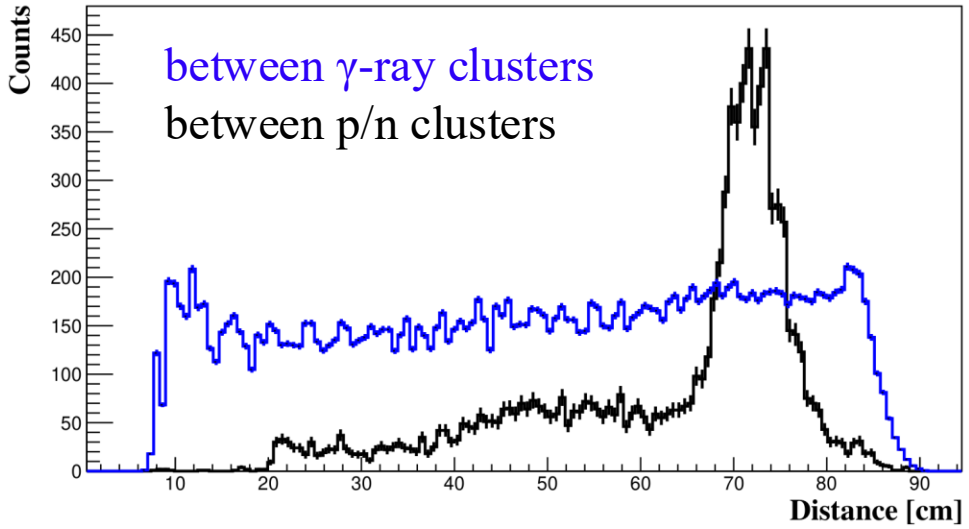

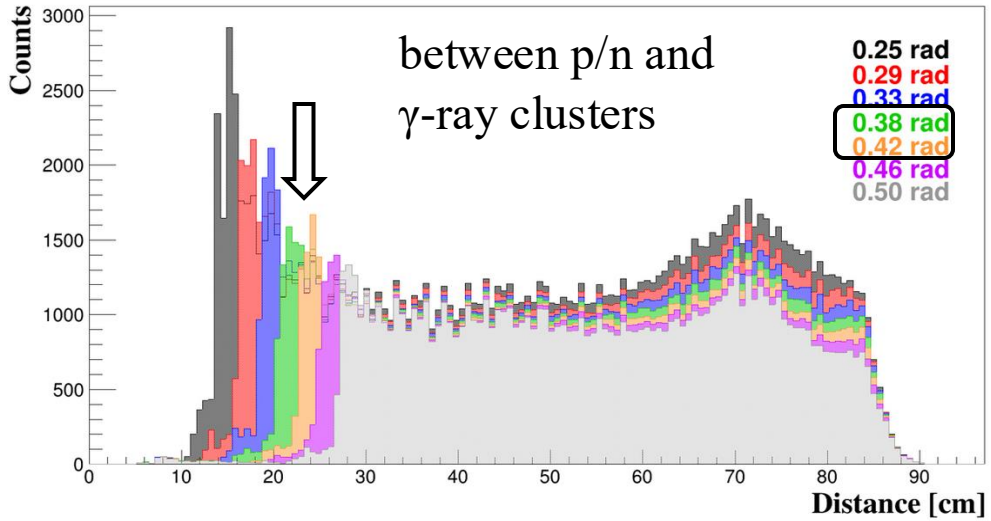

⇨ Optimum ±22.7° (±0.40 rad)

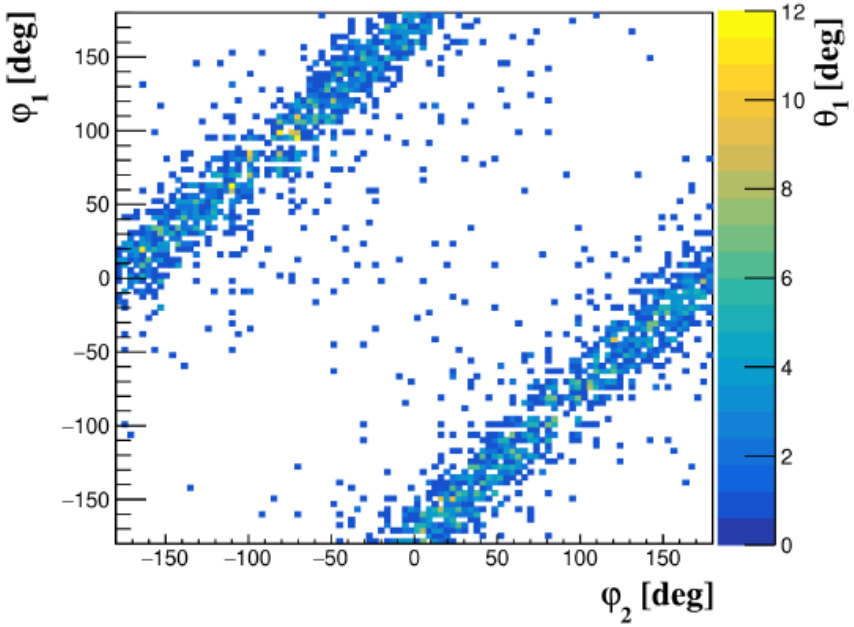

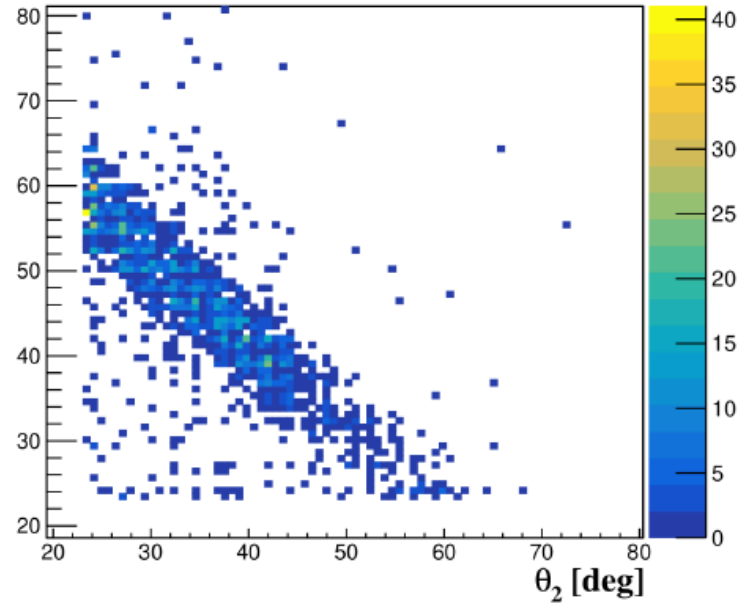

| Δϕ − 180 | < 30° (coplanar condition)

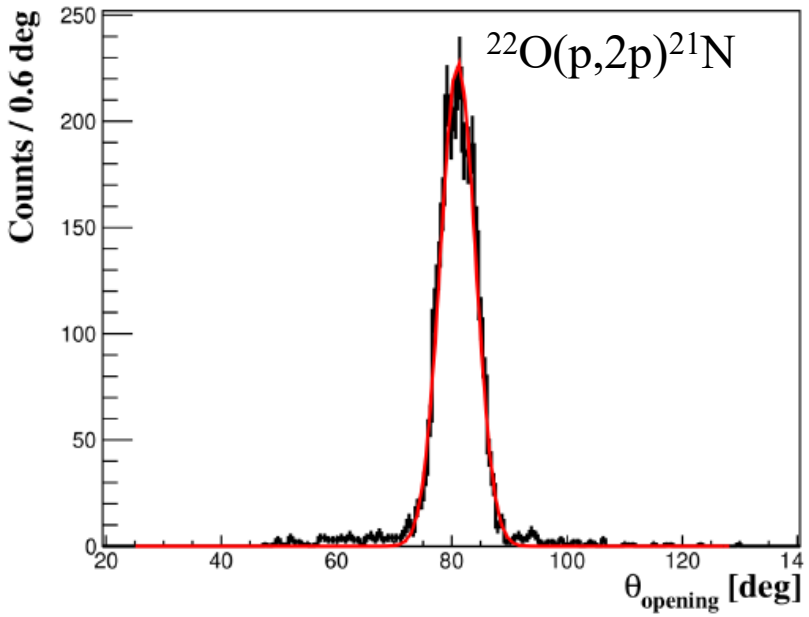

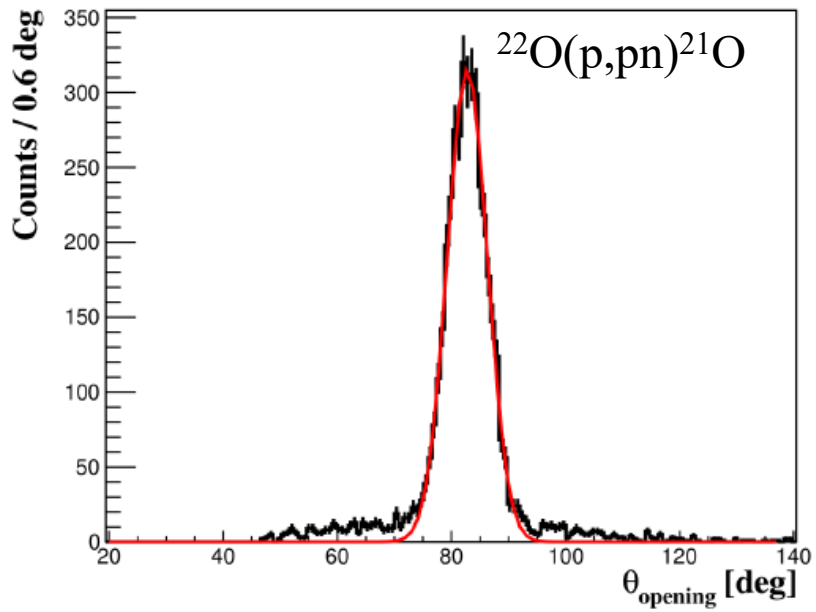

Clustering algorithm for the γ-rays

The source measurements were used to optimize the size of the γ-ray clusters.

The cluster size used for them in the algorithm should be:
- large enough to reconstruct the energy of the incident γ-rays;
- not too large to avoid the sum of the energy deposited by different γ-rays.

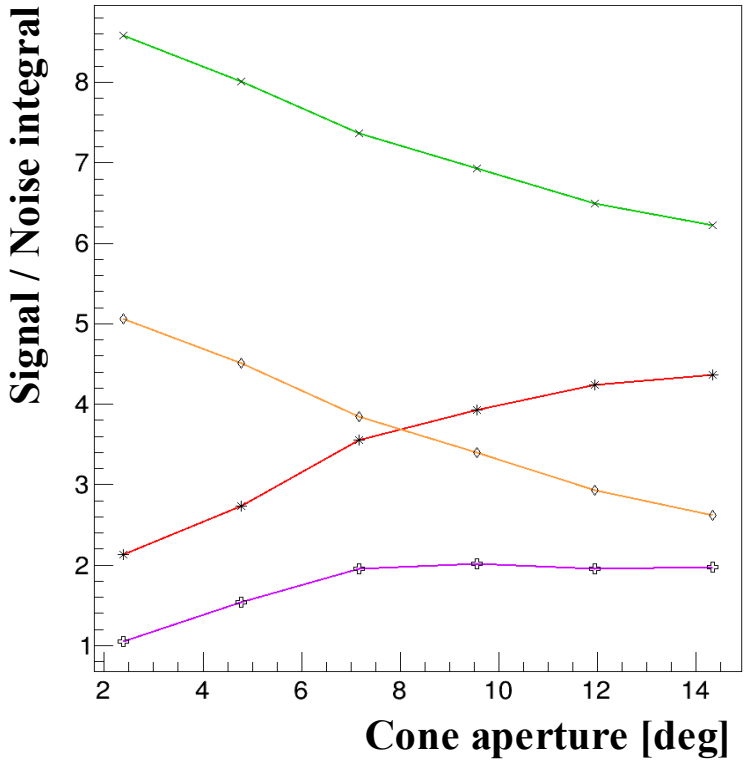

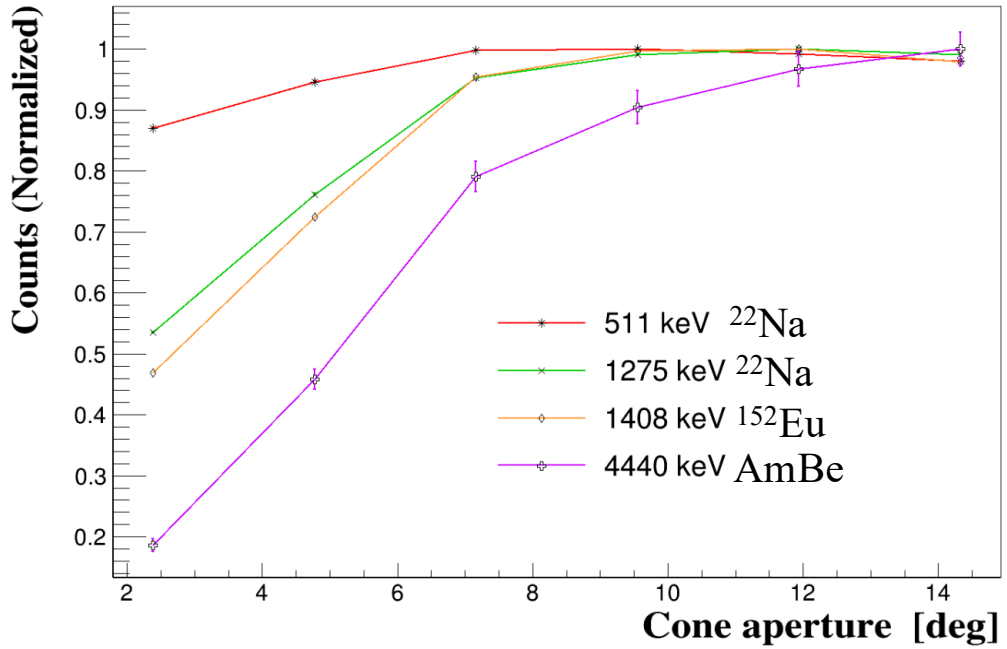

⇨ In this case, the signal-to-noise ratio is not a good indicator.

Clustering algorithm for the γ-rays

The source measurements were used to optimize the size of the γ-ray clusters.

The cluster size used for them in the algorithm should be:
- large enough to reconstruct the energy of the incident γ-rays;
- not too large to avoid the sum of the energy deposited by different γ-rays.

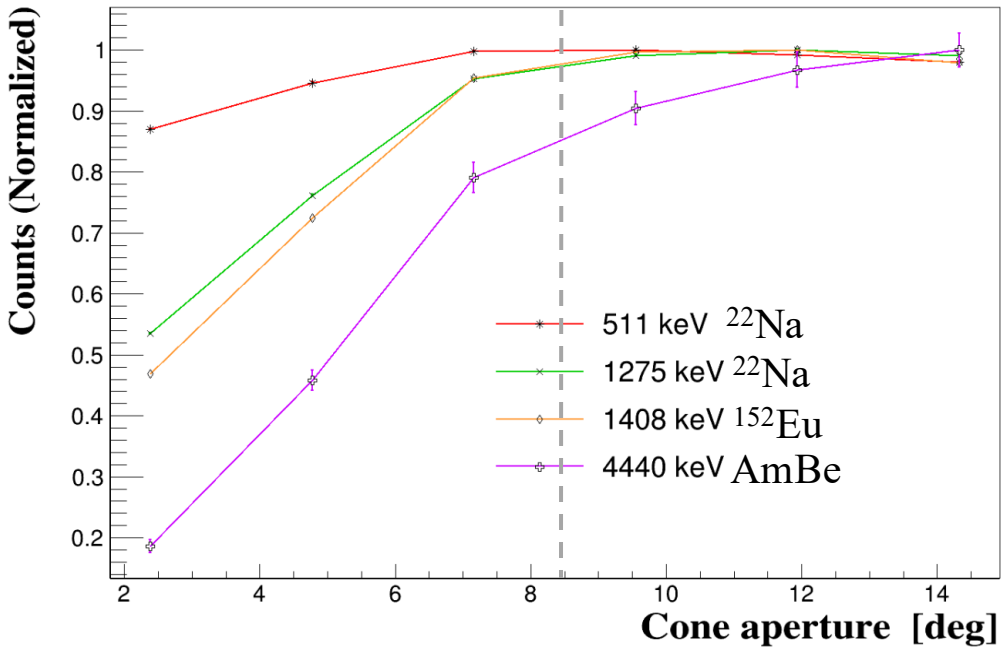

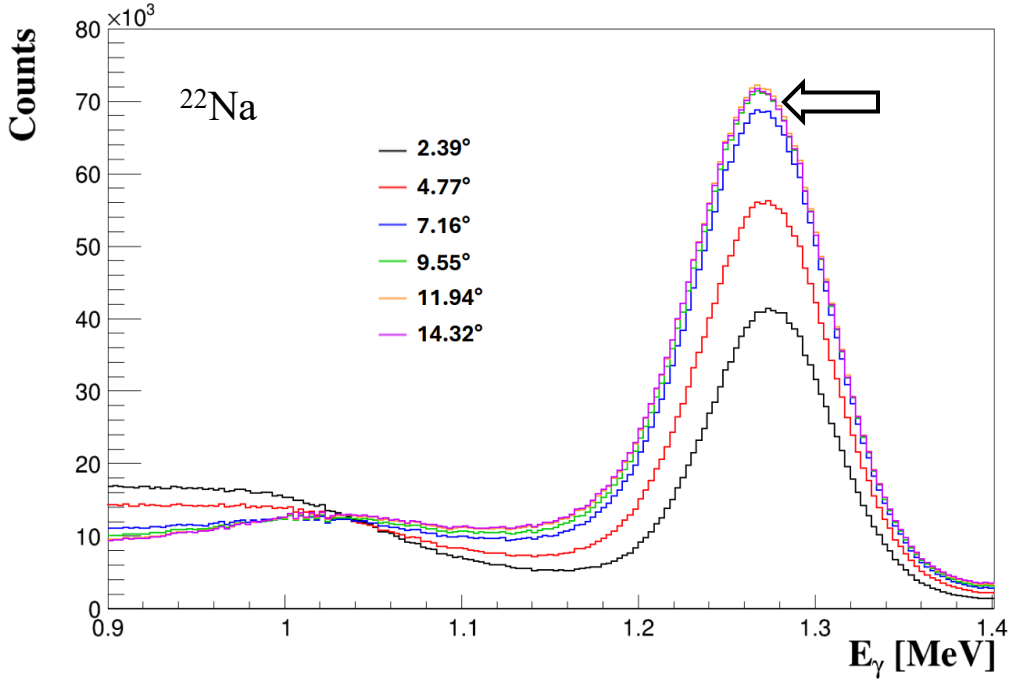

⇨ Optimum ±8.4°

Examples of events in CALIFA

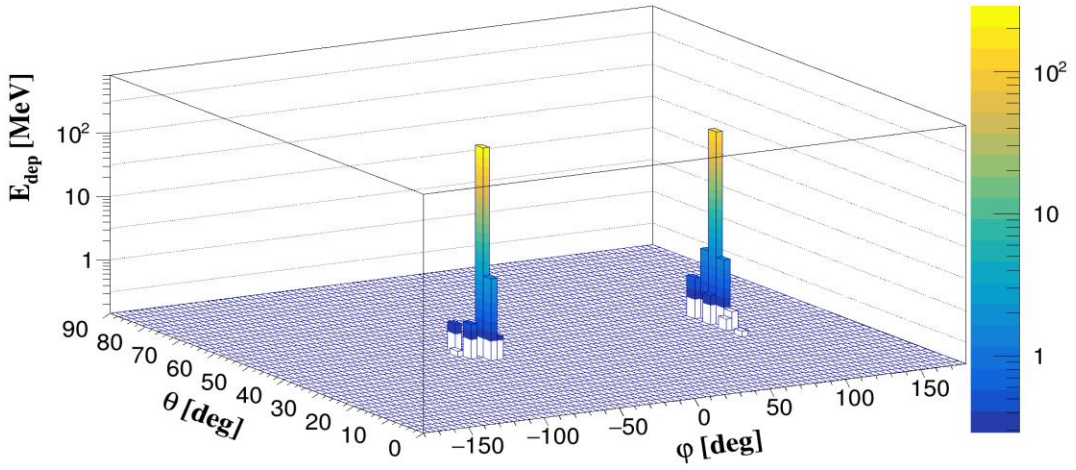

Event from channels where no γ-ray transition is expected, e.g. $^{24}F(p,2p)^{23}O$, no bound excited state in ^{23}O

Only two groups of crystals : seems good !

Examples of events in CALIFA

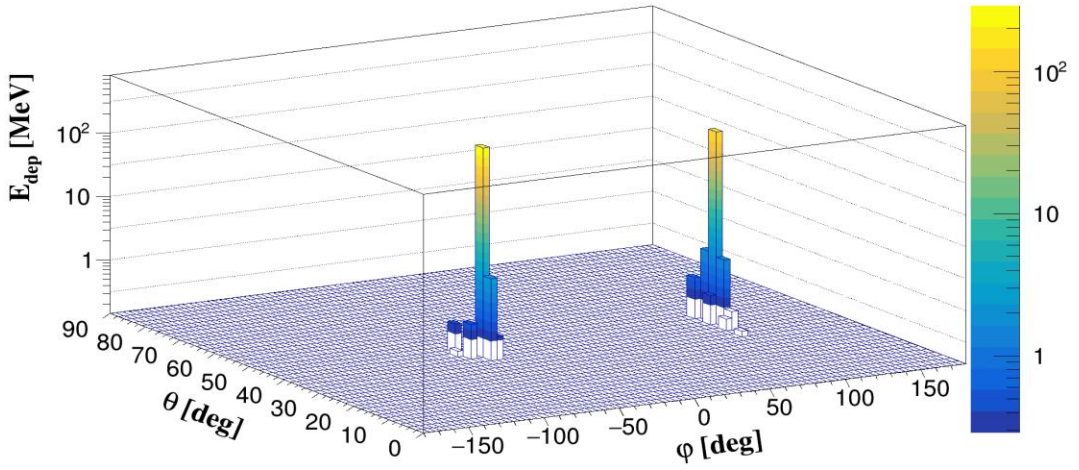

Event from channels where no γ-ray transition is expected, e.g. ^{24}F(p,2p)^{23}O, no bound excited state in ^{23}O

Only two groups of crystals : seems good !

Events from the same channels, but ... many crystals collected energy.

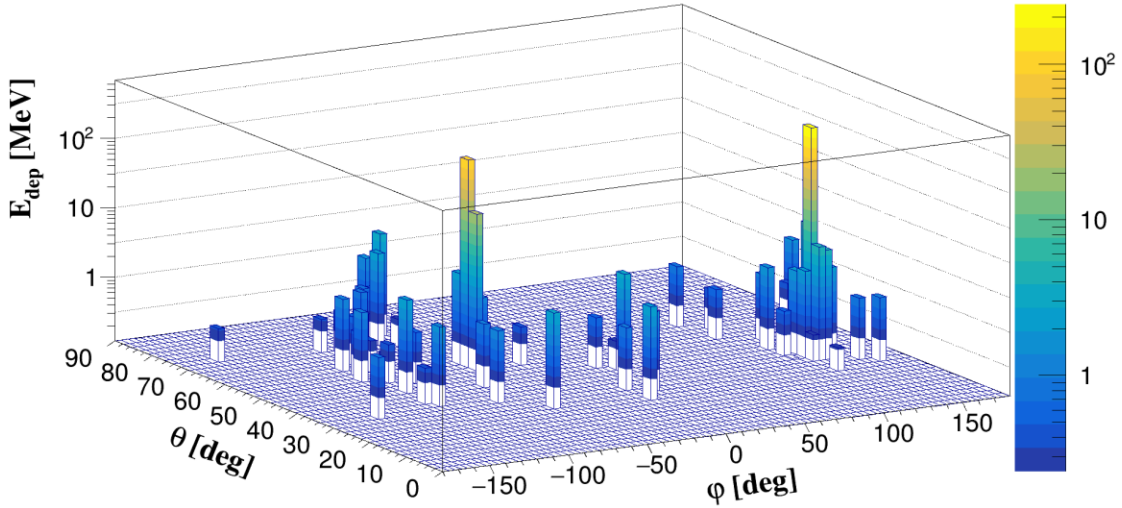

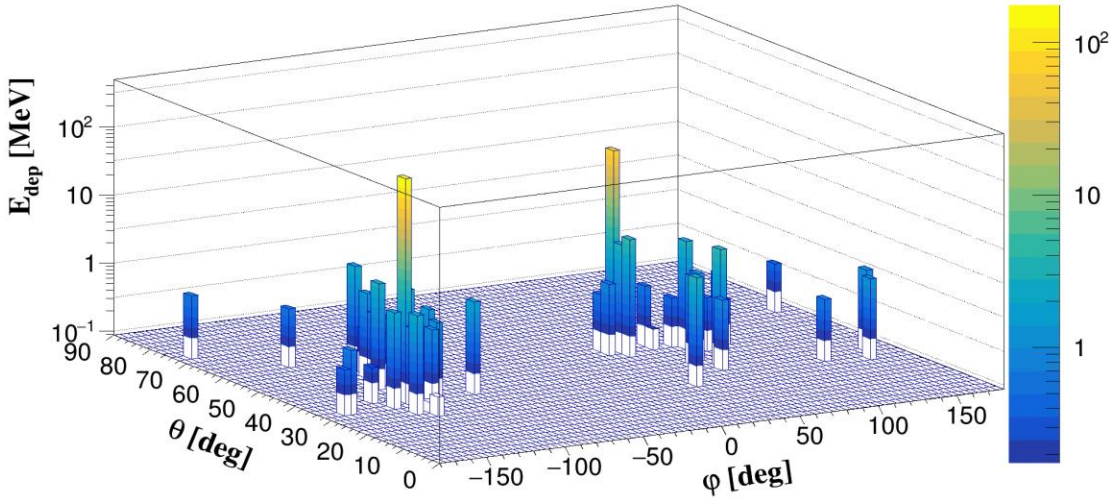

Clustering algorithm for the CALIFA array

Use of the algorithm with an example from **(*p*,*2p*)** reaction:

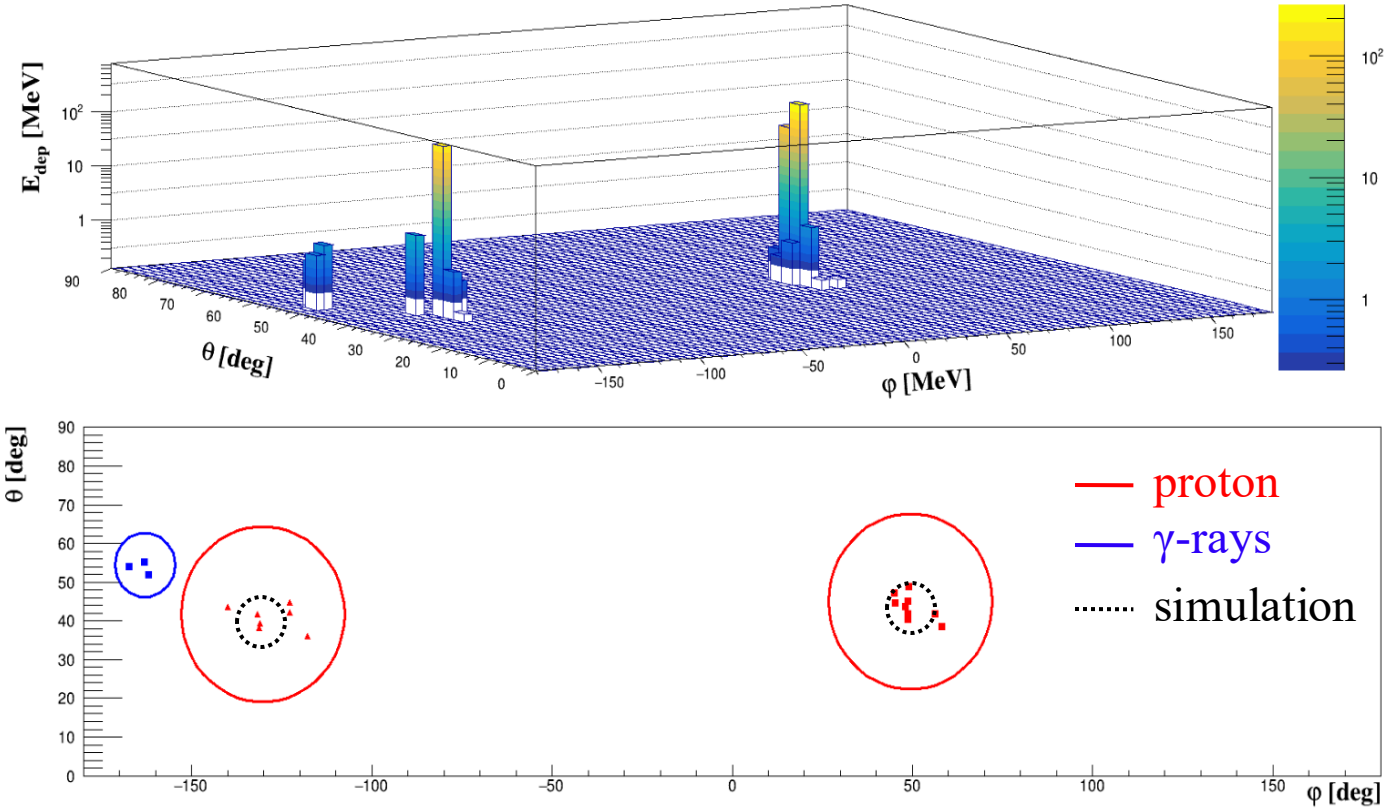

Threshold on E_{dep} = 20 MeV to separate :
- "particle" clusters (> 20MeV)
- "gamma" clusters (<< 20MeV)

Simulations underestimate the size of the "particle" clusters (dashed circle)

Clustering algorithm for the CALIFA array

Use of the algorithm with an example from **(*p*,*pn*)** reaction:

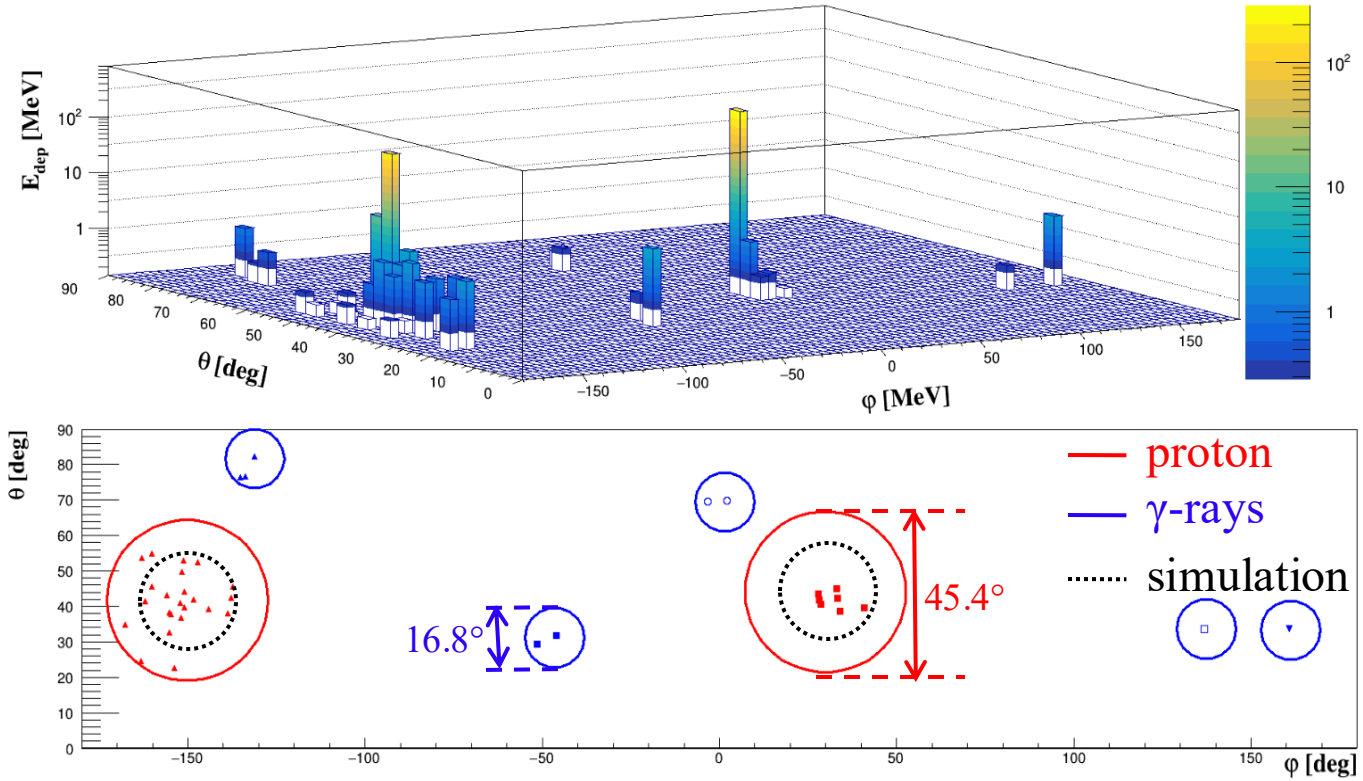

A larger cone aperture is required for the neutron clusters

Threshold on E_{dep} = 20 MeV to separate :
- "particle" clusters (> 20MeV)
- "gamma" clusters (<< 20MeV)

Simulations underestimate the size of the "particle" clusters (dashed circle)

Size optimization of the "particle" clusters performed with the $^{22}O(p,pn)^{21}O$ reaction

Clustering algorithm for the CALIFA array

Use of the algorithm with an example from **(*p*,*pn*)** reaction:

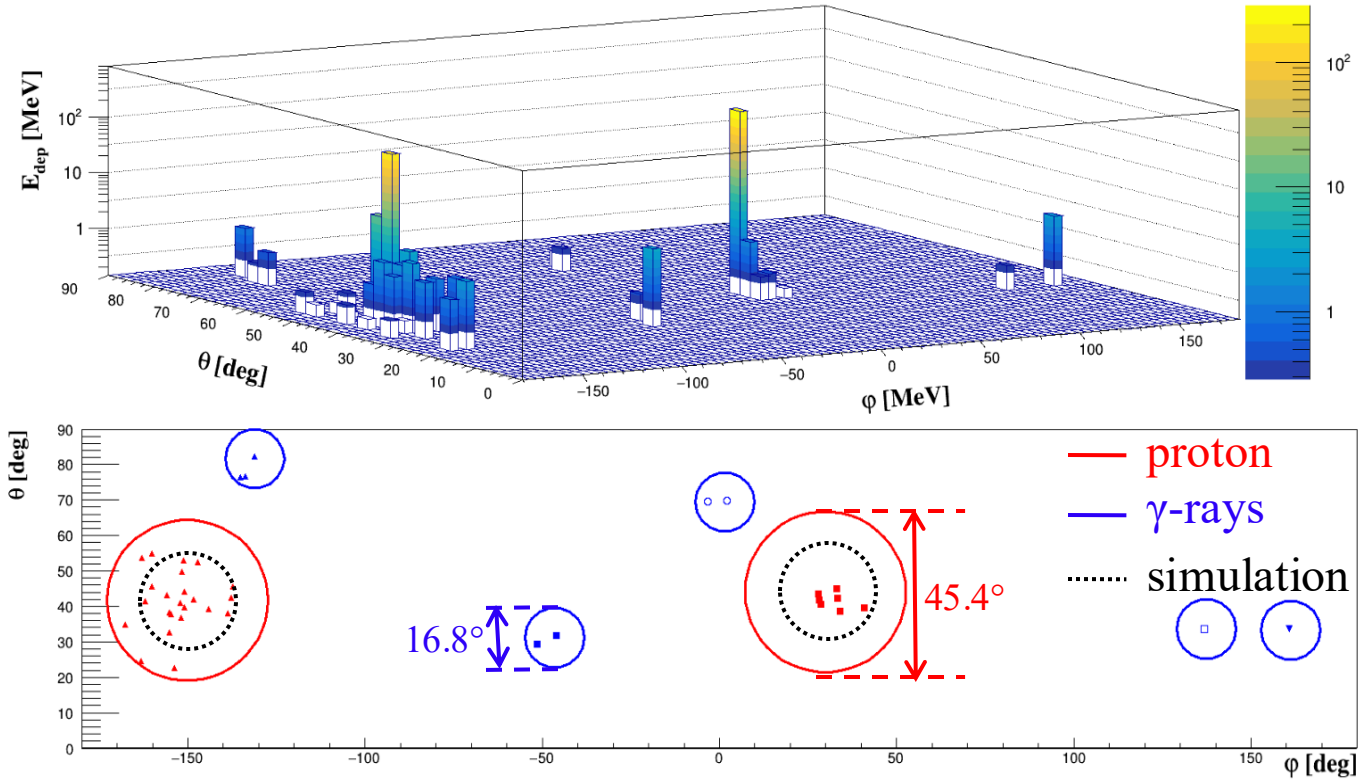

γ-rays detection efficiency curves

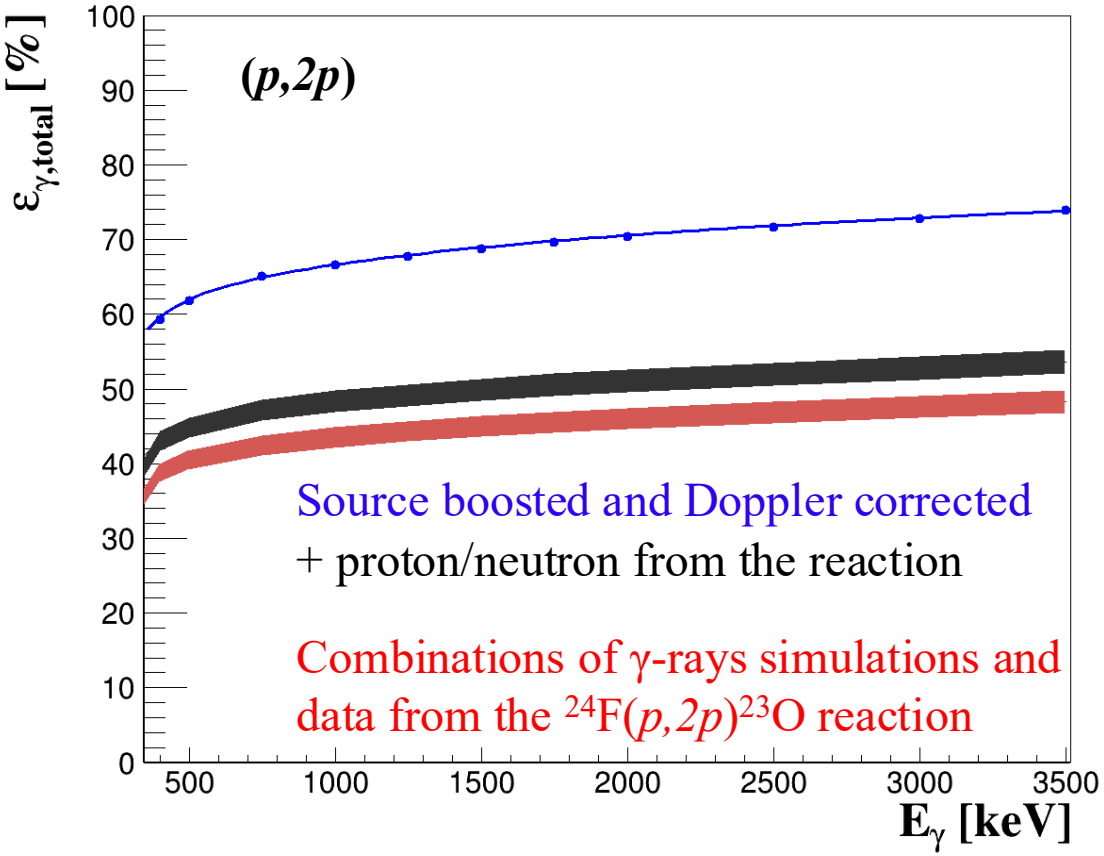

Large reduction of the γ-rays detection efficiency due to the cut in the CALIFA acceptance and the high γ-rays multiplicity.

Clustering algorithm for the CALIFA array

Use of the algorithm with an example from ***(p,pn)*** reaction:

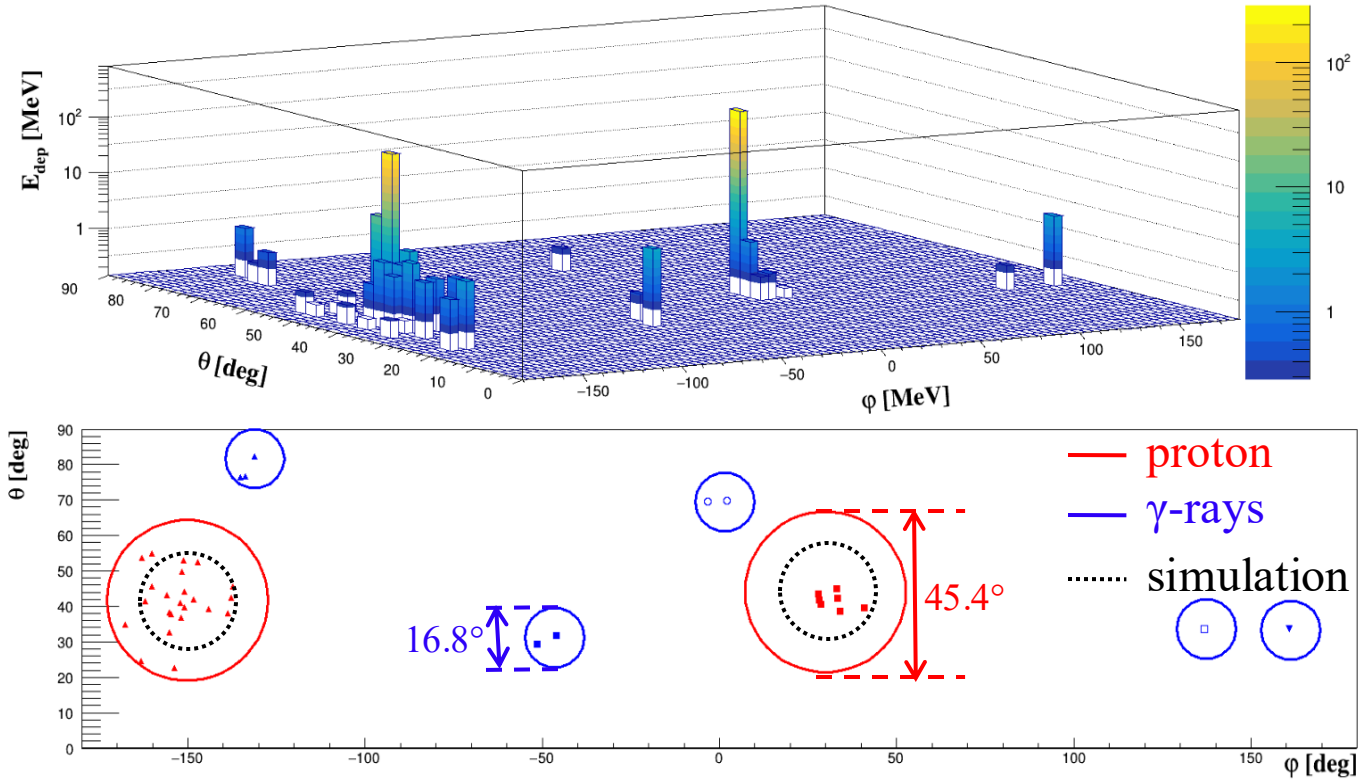

γ-rays detection efficiency curves

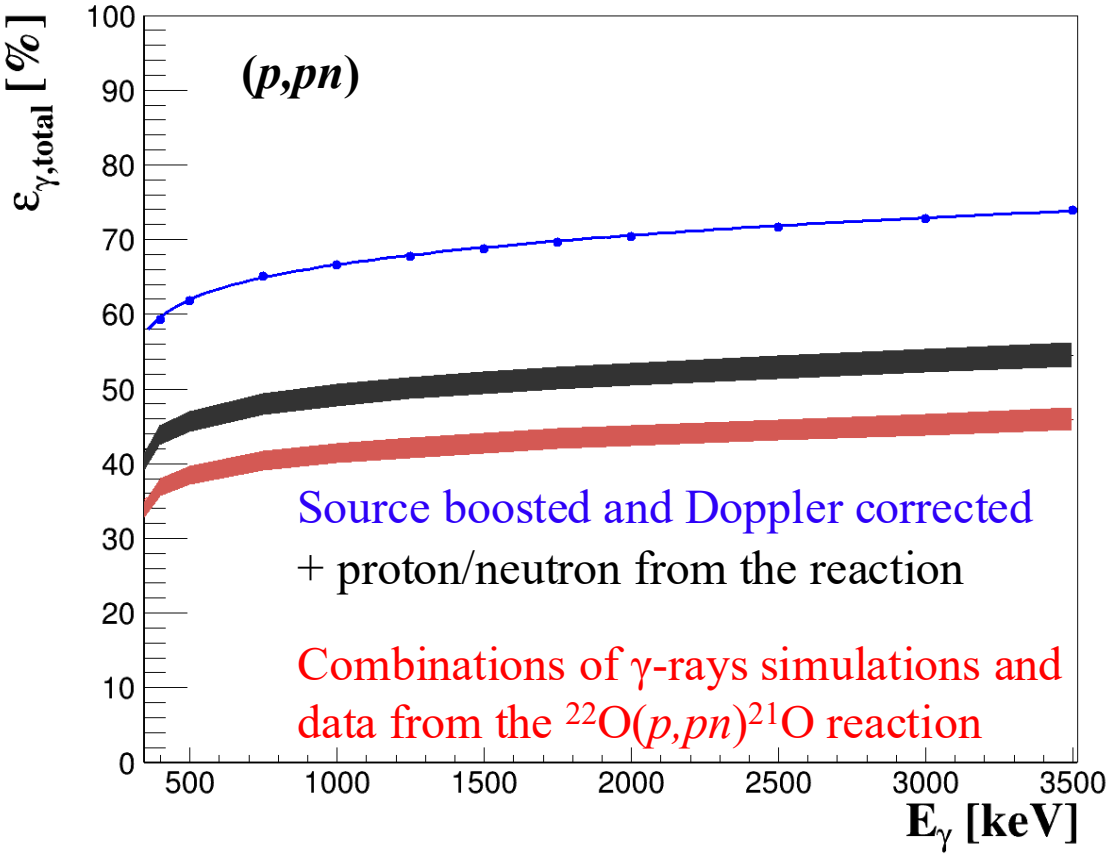

Large reduction of the γ-rays detection efficiency due to the cut in the CALIFA acceptance and the high γ-rays multiplicity.

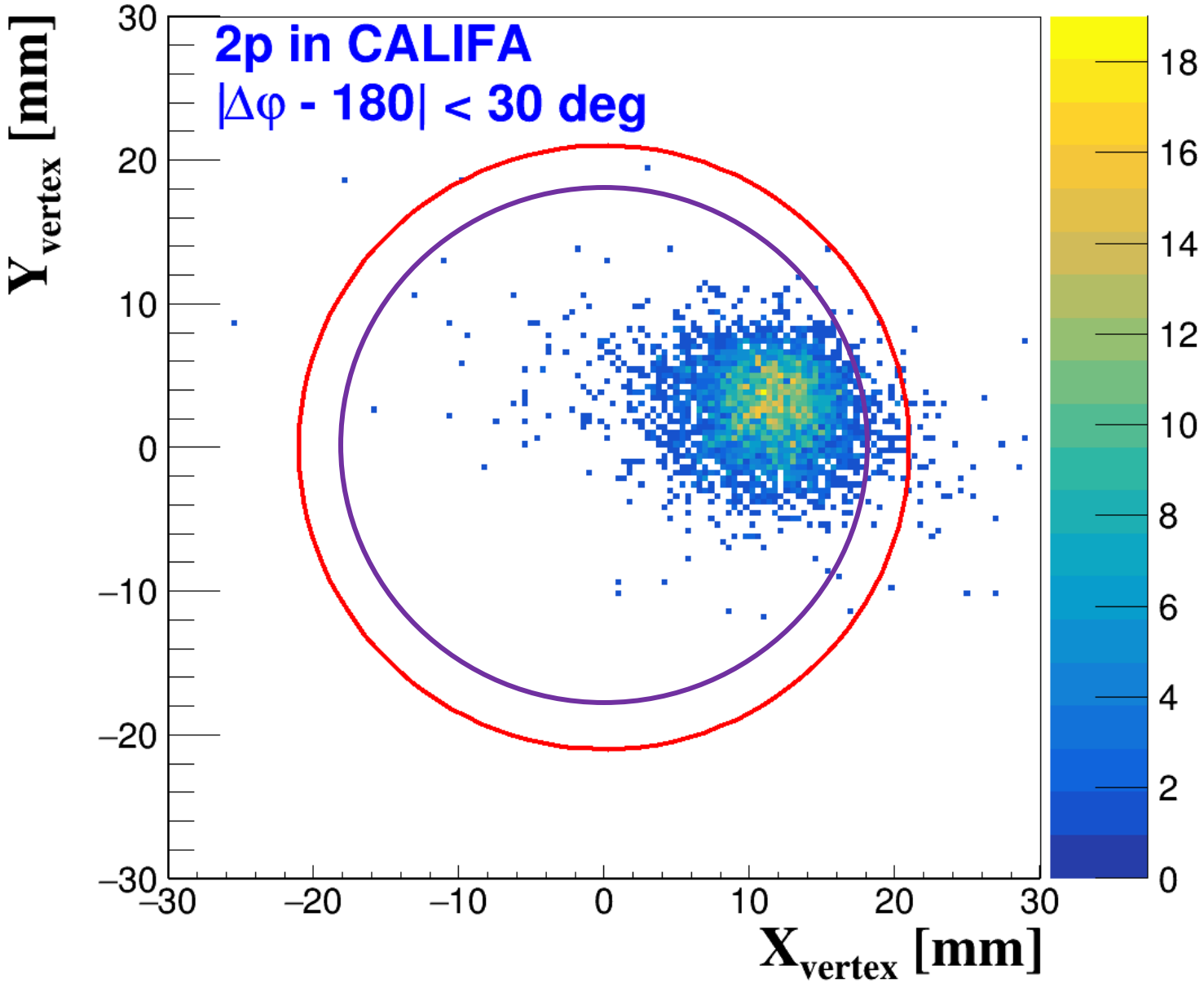
2p in CALIFA
|Δφ - 180| < 30 deg
Y vertex [mm]
X vertex [mm]
30
20
10
0
−10
−20
−30
18
16
14
12
10
8
6
4
2
0

NeuLAND : Efficiency determination

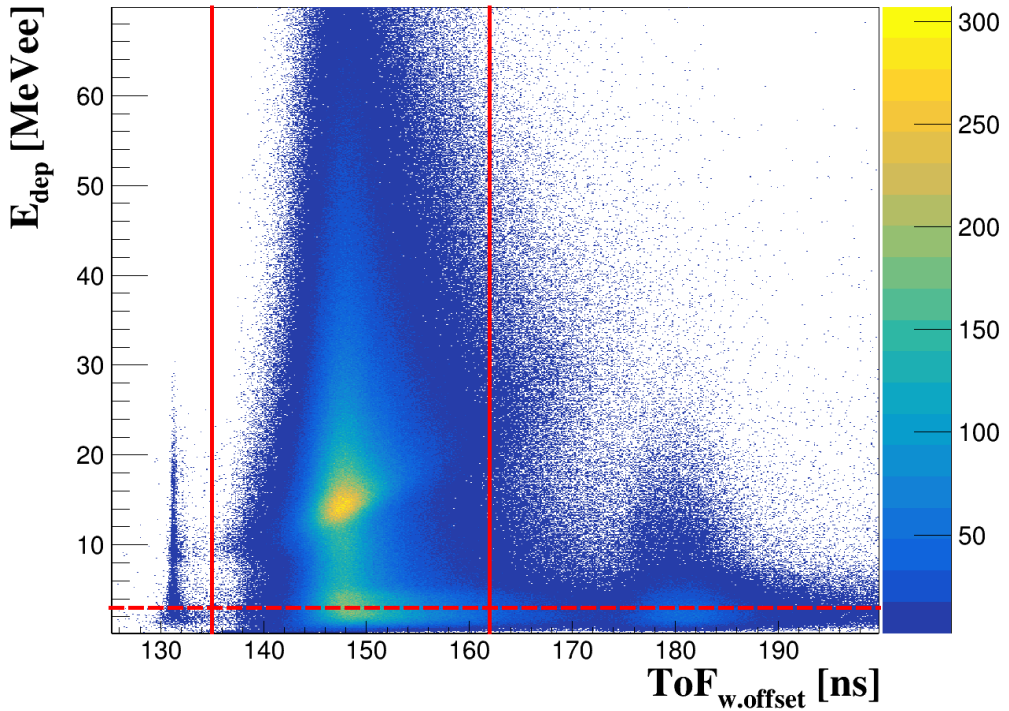

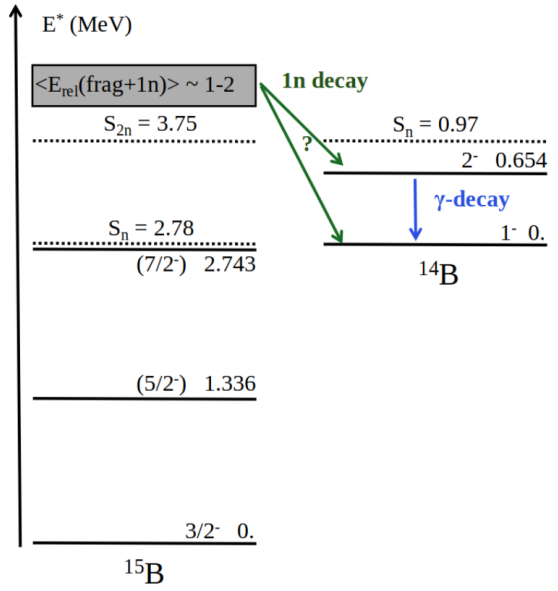

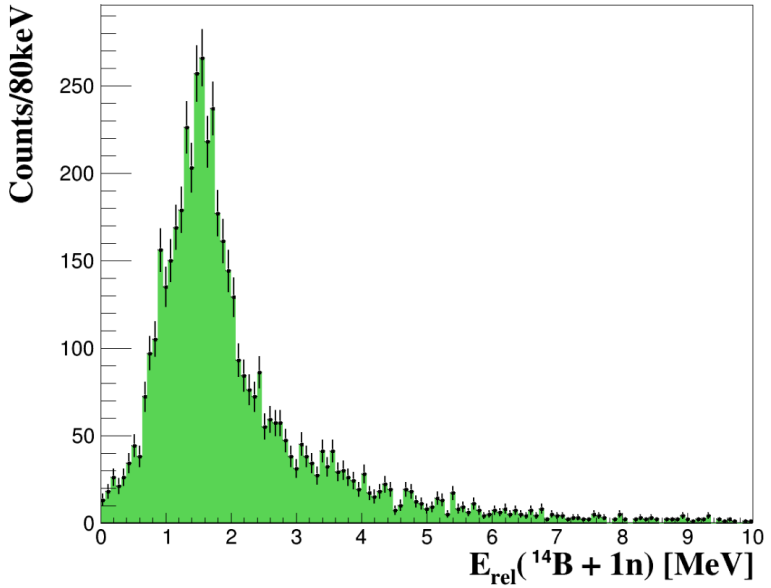

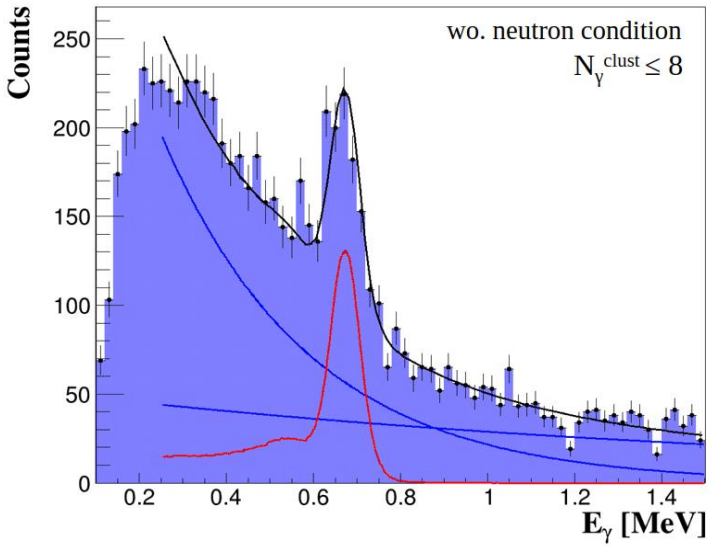

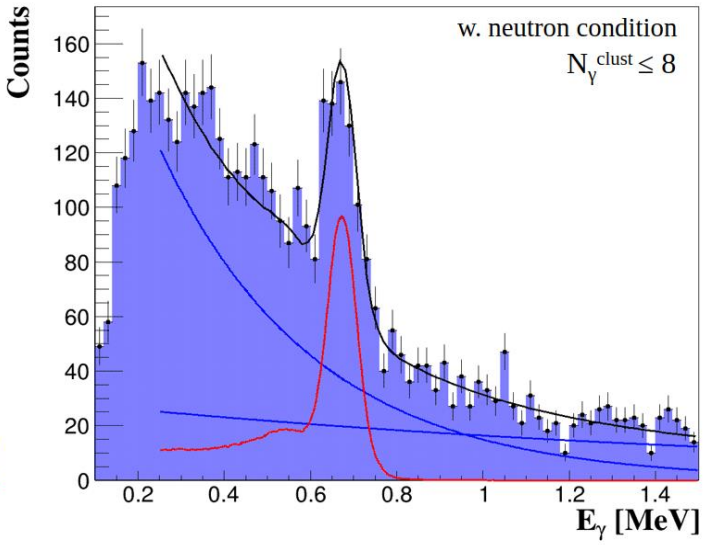

Bound states of the ^{21}N

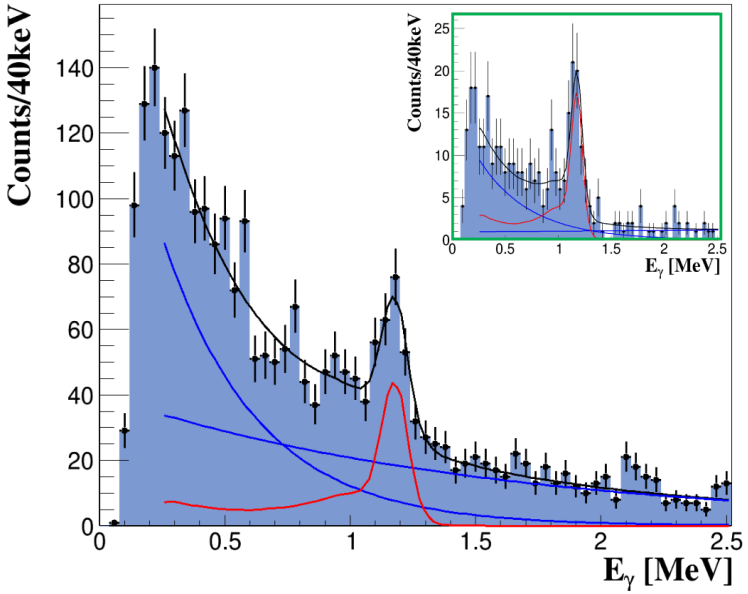

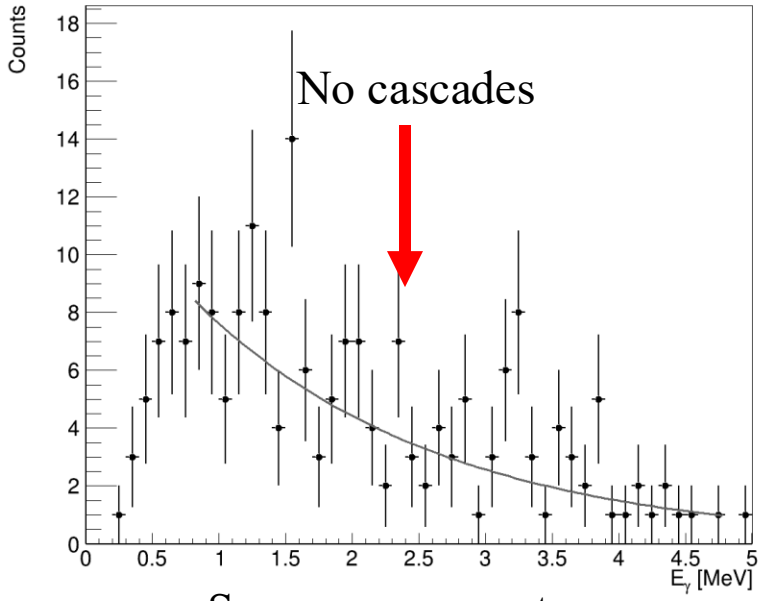

Sum energy spectrum

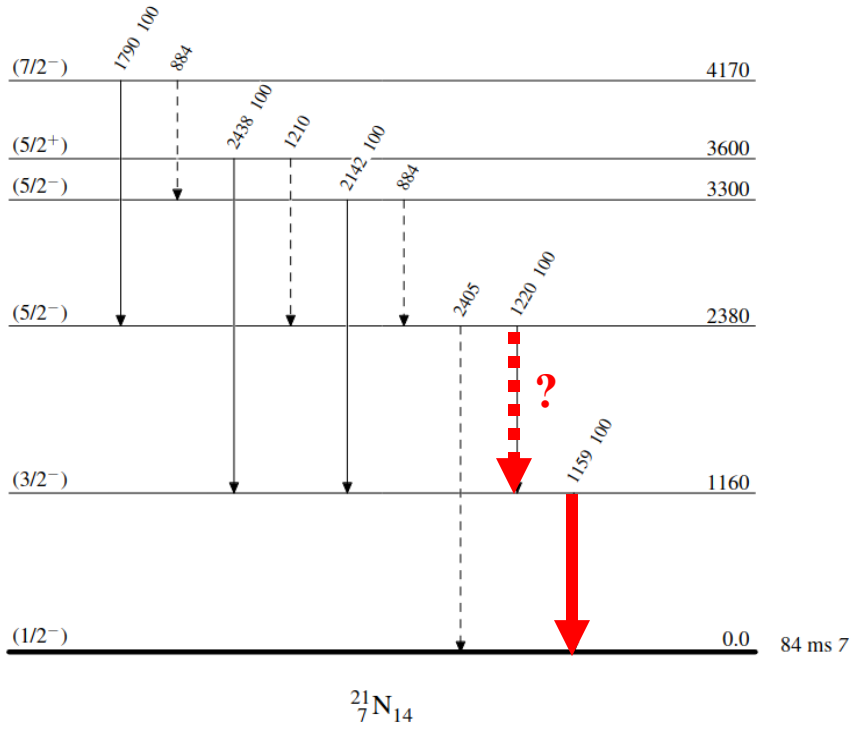

Level scheme from ENSDF

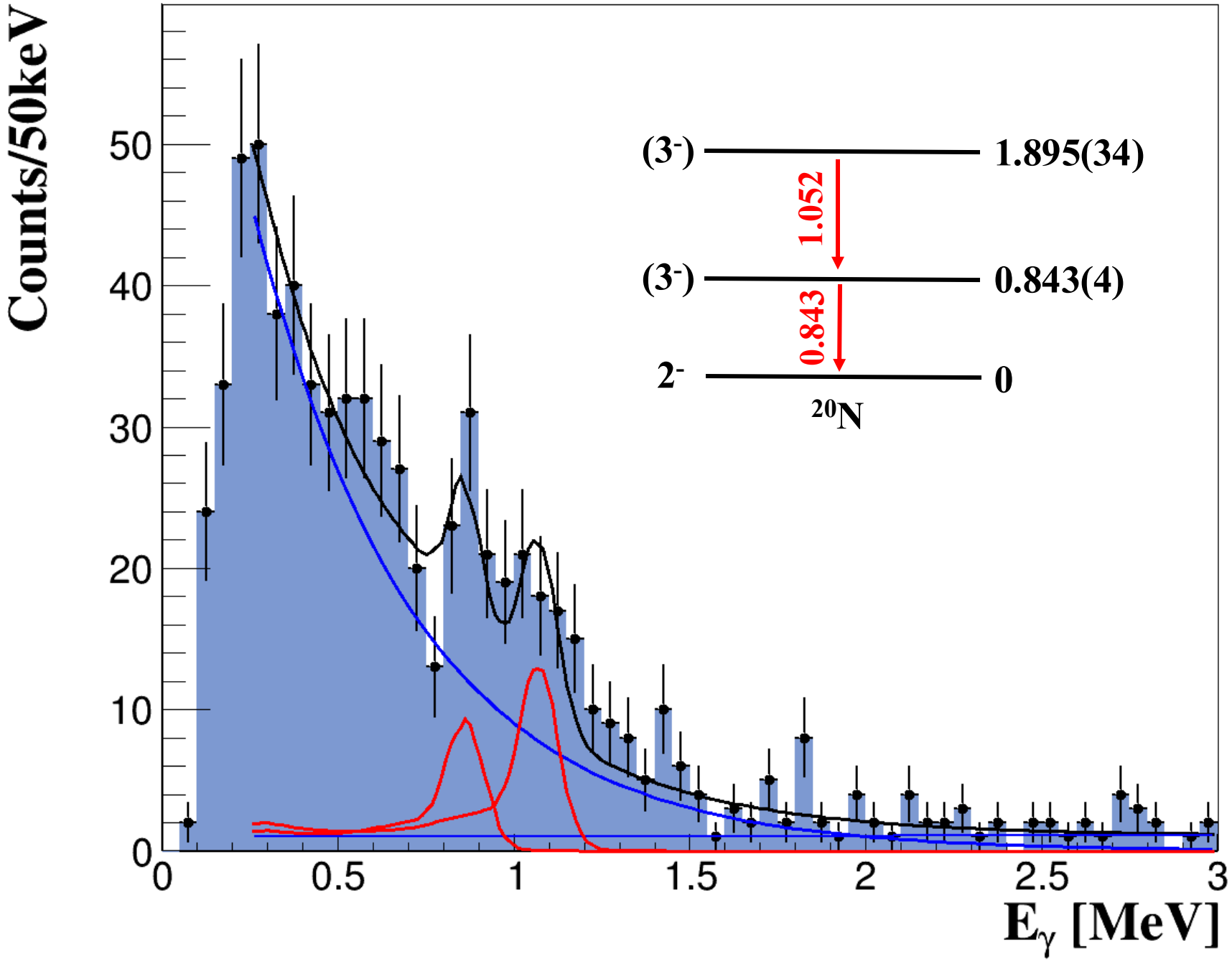
Counts/50keV
50
40
30
20
10
0
0
0.5
1
1.5
2
2.5
3
E_γ [MeV]
(3^-)
1.895(34)
1.052
(3^-)
0.843(4)
0.843
2^-
0
^{20}N

Two-neutrons spectroscopy

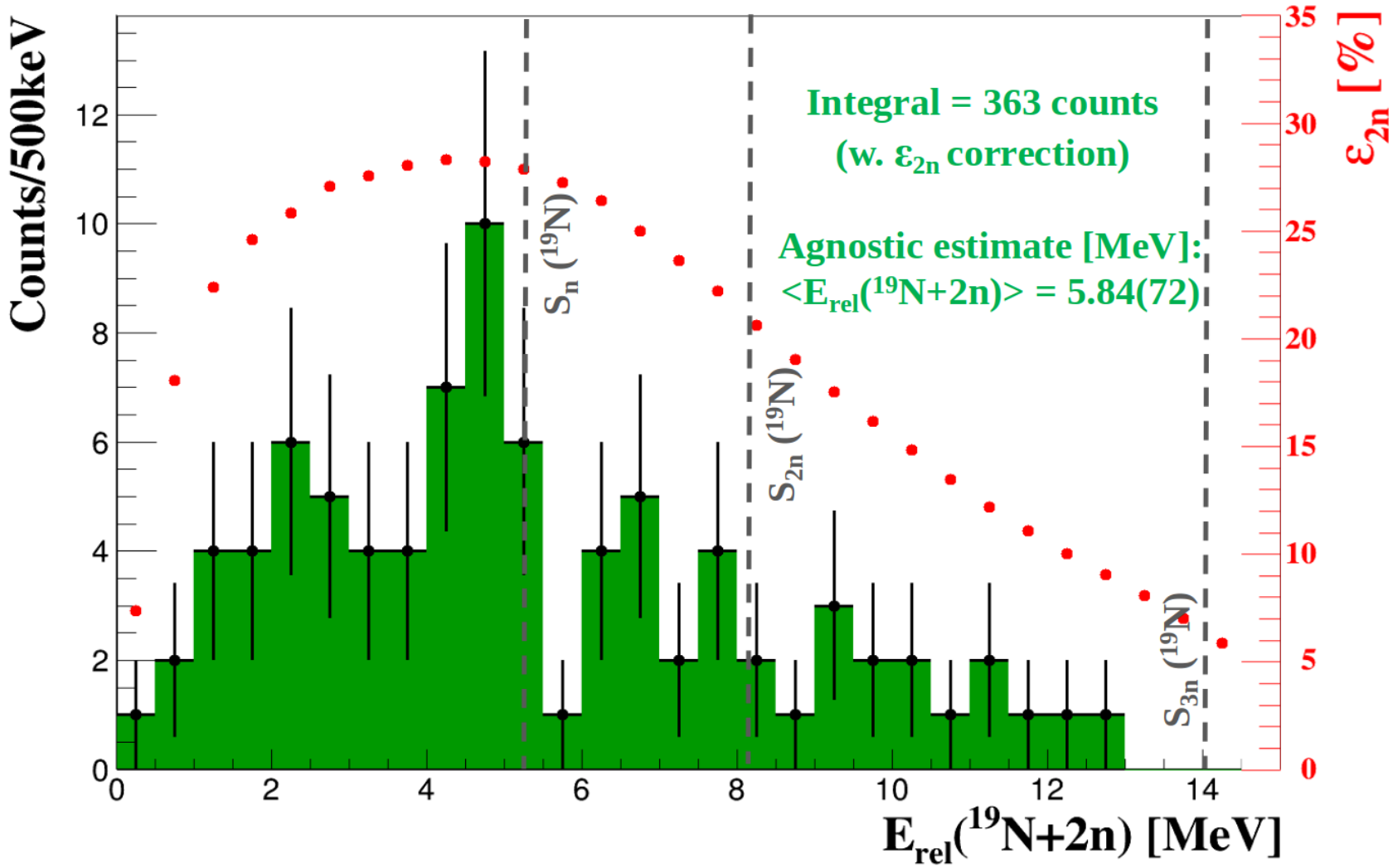

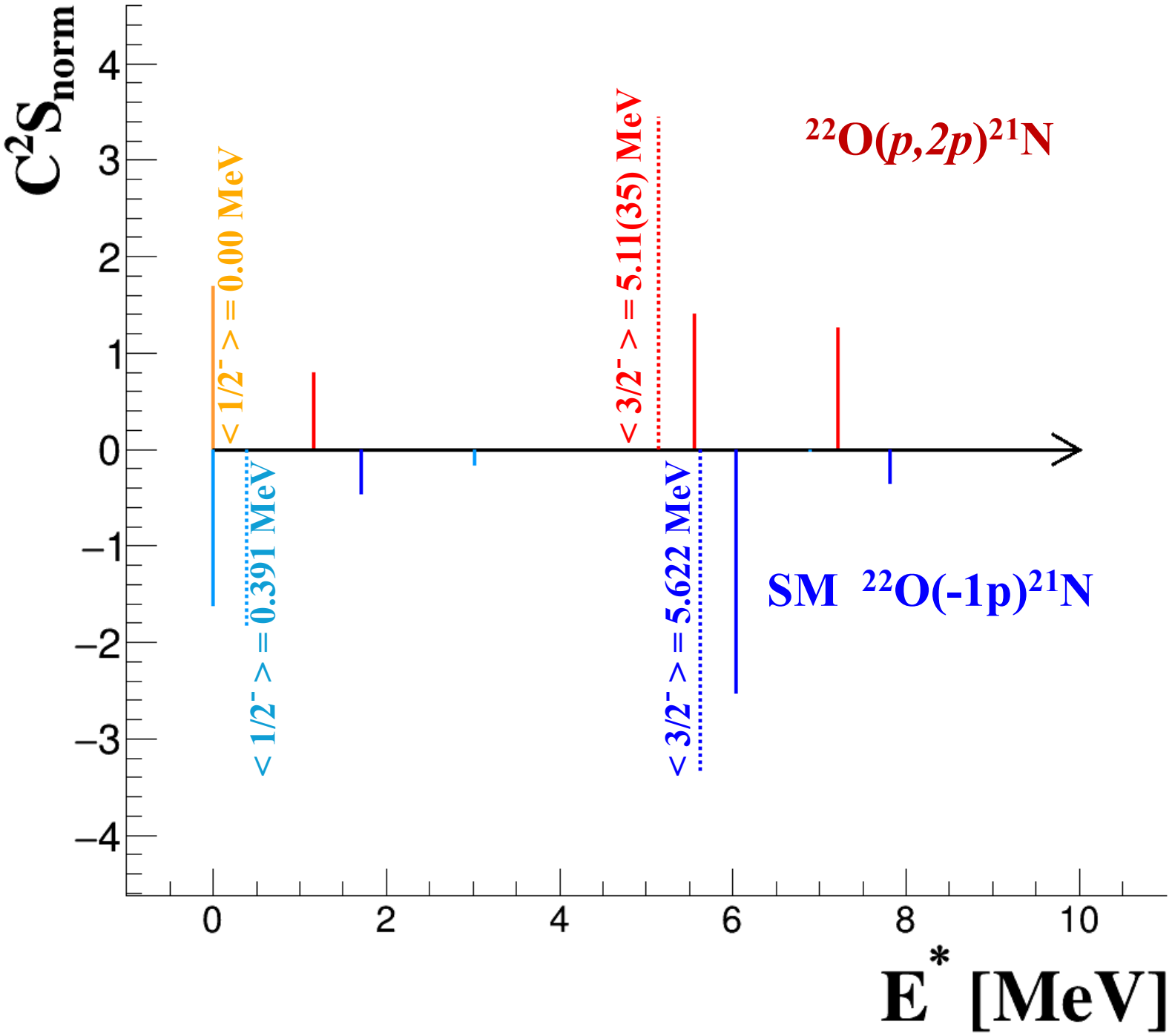
C^2S_{norm}
4
3
2
1
0
−1
−2
−3
−4
0
2
4
6
8
10
E^* [MeV]
$^{22}O(p,2p)^{21}N$
< 1/2⁻ > = 0.00 MeV
< 1/2⁻ > = 0.391 MeV
< 3/2⁻ > = 5.11(35) MeV
< 3/2⁻ > = 5.622 MeV
SM $^{22}O(-1p)^{21}N$

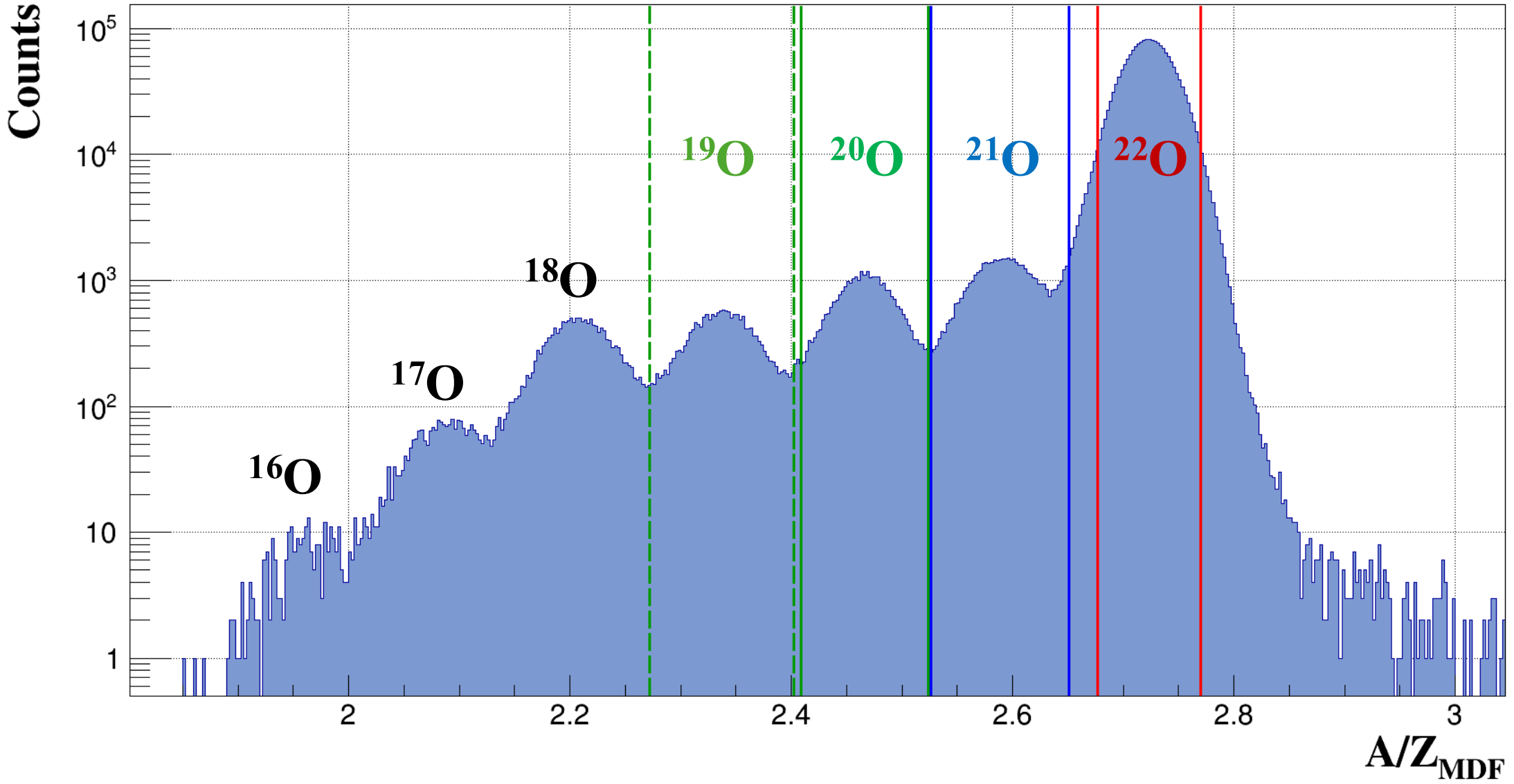
Counts
10^5
10^4
10^3
10^2
10
1
^{16}O
^{17}O
^{18}O
^{19}O
^{20}O
^{21}O
^{22}O
2
2.2
2.4
2.6
2.8
3
A/Z$_{MDF}$

Unbound states of the ^{21}O

Fitted relative energy spectrum (up to 2 MeV)

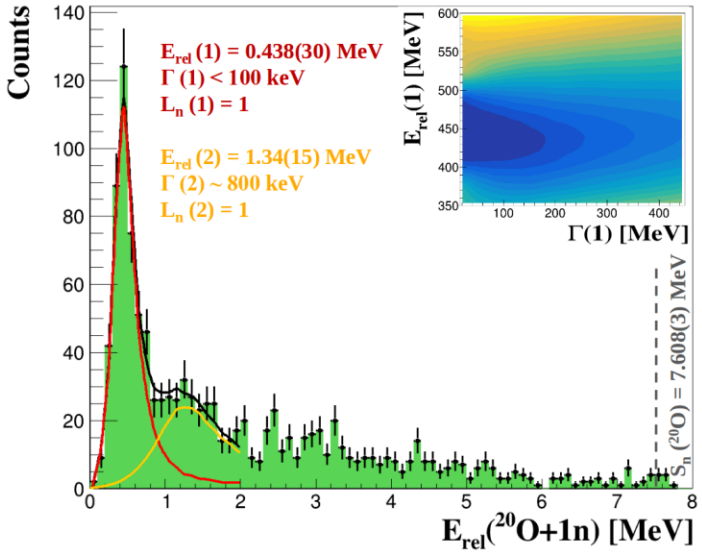

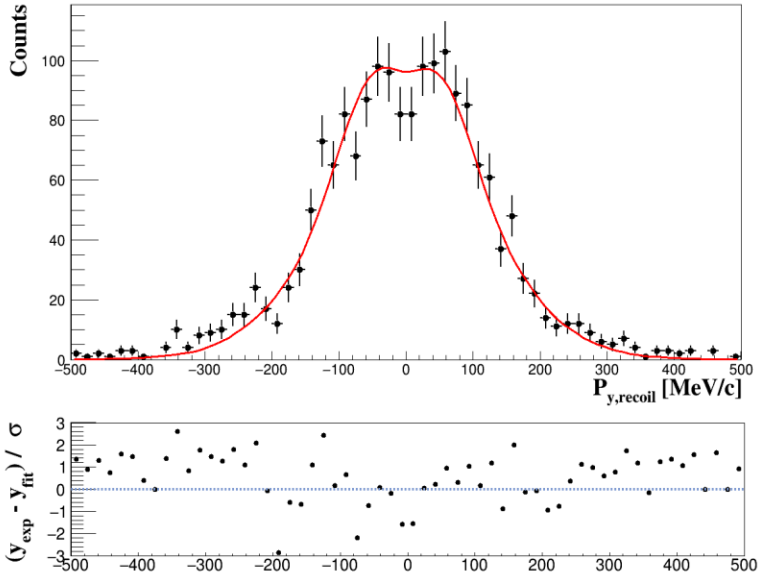

$P_{y,recoil}$ distribution in coincidence

γ-ray energy spectrum in coincidence

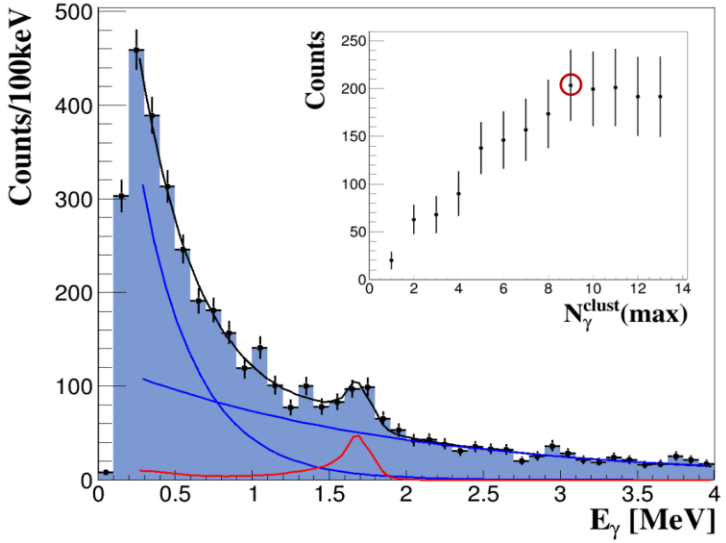

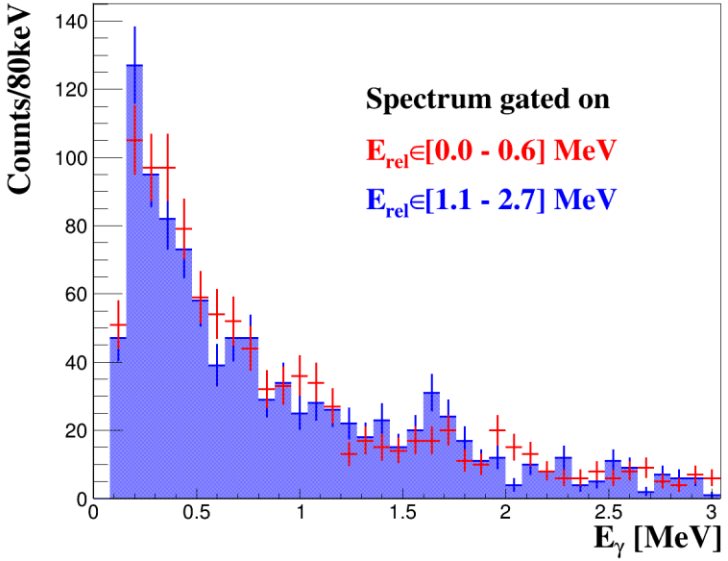

Same with two gates